

Université de Montréal

Characterization of Bacterial Ultrastructure Involved in Storage Granule Formation and DNA Segregation

Par

Fakih Doaa

Département de Biochimie et Médecine Moléculaire

Faculté de Médecine

Thèse présentée

en vue de l'obtention du grade de Philosophiae doctor (Ph.D.)

en Biochimie et Médecine moléculaire

August 2021

© Doaa Fakih, 2021

Résumé

Projet I :

Les endospores représentent un état de dormance des bactéries leur permettant de résister à des conditions extrêmes et de persister pendant des années. La formation d'endospores a façonné l'évolution puisqu'elle se produit exclusivement chez les Firmicutes. Plusieurs études ont rapporté la formation d'endospores chez des espèces en dehors des Firmicutes, en particulier chez deux espèces de Protéobactéries, *Rhodobacter johrii* et *Serratia marcescens*, et une espèce d'Actinobactéries, *Mycobacterium marinum*. Le fait d'identifier les endospores en dehors des Firmicutes pourrait affecter la forme de l'arbre de vie et aiderait dans notre lutte contre les agents pathogènes humains. Par conséquent, nous avons visé d'étudier l'endosporulation chez ces trois espèces en utilisant des approches avancées d'imagerie et d'analyse, y compris la microscopie corrélative alliant la microscopie optique et électronique (CLEM), la tomographie de cryo-électron (cryo-ET) et la lipidomique. Nous avons utilisé la bactérie sporulante bien caractérisée *Bacillus subtilis* comme contrôle positif de la sporulation. L'examen de *R. johrii*, *S. marcescens* et *M. marinum* en utilisant CLEM et cryo-ET a montré que les objets à phase brillante ne ressemblaient à aucun stade de l'endosporulation. Les cryo-tomogrammes ont montré que les objets à phase brillante chez *S. marcescens* étaient des débris cellulaires agrégés de cellules mortes, alors qu'ils présentaient des structures granulaires typiques des cellules bactériennes chez les *R. johrii* et *M. marinum*. L'analyse lipidomique chez *R. johrii* a identifié les structures granulaires comme des granules de stockage potentiels enrichis en triacylglycérides (TAG). Nous pensons que les TAG peuvent fournir une source d'énergie pour résister à l'épuisement des nutriments. Des approches biochimiques et bioinformatiques supplémentaires ont soutenu nos conclusions selon lesquelles *R. johrii*, *S. marcescens* et *M. marinum* sont des bactéries non sporulantes.

Projet II :

Les plasmides jouent un rôle vital dans la propagation des gènes de résistance au sein et entre les espèces bactériennes. Par conséquent, il est essentiel de comprendre les systèmes bactériens impliqués dans le transfert et la maintenance des plasmides pour mieux aider dans notre

lutte contre la propagation de la résistance aux antibiotiques. Dans cette thèse de doctorat, nous avons cherché à caractériser l'opéron *alp7ARC*, en utilisant l'homologue de l'actine bactérienne Alp7A pour séparer le plasmide pLS20 codant pour la résistance à la tétracycline dans *B. subtilis*. La stabilité du plasmide s'est avérée dépendante de l'opéron *alp7ARC*, indiquant un rôle essentiel dans la ségrégation plasmidique. Nos résultats préliminaires sur Alp7A ont montré qu'il s'assemble dans une nouvelle nanostructure tubulaire plutôt que des filaments, suggérant un nouveau mécanisme de ségrégation de l'ADN par Alp7A. Nous avons également étudié la structure d'Alp7A *in vivo* en utilisant une combinaison d'approches, notamment la biologie moléculaire, la Cryo-ET et la fLM. Nous avons également utilisé la CLEM pour localiser Alp7A dans des cellules entières à une résolution macromoléculaire. En outre, nous avons étudié la structure et la fonction d'Alp7A *in vitro* en transfectant *B. subtilis* et *E. coli* avec diverses constructions plasmidiques incorporant des mutations dans le gène d'Alp7A. Nous avons déployé différentes méthodes pour la purification de la protéine Alp7A, y compris la séparation par chromatographie, et le fractionnement au sulfate d'ammonium. J'ai discuté des divers défis que nous avons rencontrés dans ces expériences, tels que la contamination, l'instabilité de la protéine Alp7A et l'épaisseur bactérienne. Enfin, j'ai proposé des approches expérimentales alternatives qui aideraient à étudier le mécanisme de ségrégation des plasmides par Alp7ARC.

Mots-clés : Endospores; Firmicutes; *Rhodobacter johrii*; *Serratia marscescens*; *Mycobacterium marinum*; *B. subtilis* ; Alp7ARC ; Microscopie optique et électronique (CLEM), Tomographie de cryo- électron (cryo-ET); Lipidomique

Abstract

Project I:

Endospores represent a dormant state of bacteria that allows them to withstand extreme conditions and persist for years. Endospore formation has shaped evolution, whereby it exclusively occurs in Firmicutes. Several studies have reported endospore formation in species outside of Firmicutes, particularly in two species of Proteobacteria, *Rhodobacter johrii* and *Serratia marcescens*, and one species of Actinobacteria, *Mycobacterium marinum*. Identifying endospores outside of Firmicutes would affect the shape of the tree of life and aid in our fight against human pathogens. Therefore, we aimed to investigate endosporulation in these three species using advanced imaging and analytical approaches, including correlative light and electron microscopy (CLEM), cryo-electron tomography (cryo-ET), and lipidomics. We used the well-characterized sporulating bacterium *Bacillus subtilis* as a positive control of sporulation. Examination of *R. johrii*, *S. marcescens*, and *M. marinum* using CLEM and cryo-ET showed that phase-bright objects did not resemble any stages of endosporulation. Cryo-tomograms revealed that the phase-bright objects in *S. marcescens* were aggregated cellular debris of dead cells, whereas they displayed granular structures typical of bacterial cells in *R. johrii* and *M. marinum*. Lipidomic analysis in *R. johrii* identified the granular structures as potential storage granules enriched with triacylglycerides (TAGs). We speculate that TAGs may provide an energy source to withstand the nutrient depletion. Additional biochemical and bioinformatics approaches supported our conclusions that *R. johrii*, *S. marcescens*, and *M. marinum* are non-sporulating bacteria.

Project II:

Plasmids play a vital role in the spread of resistance genes within and across bacterial species. Therefore, it is essential to understand the bacterial systems involved in the transfer and maintenance of plasmids to better aid in our fight against the spread of antibiotic resistance. In this doctorate, we aimed to characterize the *alp7ARC* operon, employing the bacterial actin homolog Alp7A to segregate the tetracycline resistance-encoding plasmid pLS20 in *B. subtilis*. The stability of the plasmid was shown to be dependent on the *alp7ARC* operon, indicating an essential role in plasmid segregation. Preliminary results on Alp7A showed that it assembles into a novel tubular

nanostructure rather than filaments, suggesting a novel mechanism for DNA segregation by Alp7A. We further studied the structure of Alp7A *in vivo* using combination of approaches, including molecular biology, cryo-ET, and fLM. We also used CLEM to localize Alp7A in whole cells to a macromolecular resolution. Besides, we investigated the structure and function of Alp7A *in vitro* by transfecting *E. coli* with various plasmid constructs and purification by several methods, including affinity chromatography and ammonium sulfate precipitation. I discussed the diverse challenges we encountered in these experiments, such as bacterial thickness, contamination, and Alp7A protein instability. Finally, I proposed alternative experimental approaches for investigating the mechanism of plasmid segregation by Alp7ARC.

Keywords: Endospores; Firmicutes; *Rhodobacter johrii*; *Serratia marcescens*; *Mycobacterium marinum*; *Bacillus subtilis*, Alp7ARC; Cryo-electron tomography; Correlative light and electron microscopy; Whole cell lipidomic analysis; EDX, Storage granule, Plasmid Segregation

Table des matières

Résumé	i
Abstract.....	iii
Table des matières	v
Liste des tableaux	ix
Liste des figures.....	xi
Liste des sigles et abréviations	xiii
Acknowledgements	xv
1 Introduction	1
1.1 Overview of sporulation and storage granule formation in bacteria	1
1.1.1 Bacteria.....	1
1.1.2 Classification of bacteria.....	2
1.1.3 Evolution of sporulation.....	4
1.1.4 Exospores	5
1.1.5 Endospores	5
1.1.6 Storage granules	15
1.1.7 Types and functions of storage granules	16
1.2 Bacterial Cytoskeletal Proteins and DNA Segregation.....	19
1.2.1 Bacterial cytoskeleton	19
1.2.2 Bacterial tubulin homologs	21
1.2.3 Intermediate filament-like proteins in bacteria	22
1.2.4 Actin-like proteins in bacteria	23
1.2.5 Other members of the bacterial cytoskeleton	26
1.2.6 Plasmid segregation in bacteria.....	26

1.2.7	Plasmid segregation mechanisms.....	27
1.2.8	Alp7A	29
1.2.9	Polymerization and function of Alp7A in bacteria	30
1.3	Justification of methods used for the detection of bacterial ultrastructure	32
1.3.1	Microscopy.....	32
1.3.2	Phenotypic methods	34
2	Objectives and hypothesis.....	37
2.1	Project 1: Characterization of phase-bright objects in members of Proteobacteria and Actinobacteria.....	37
2.2	Project 2: Characterization of Alp7A structure <i>in vivo</i> and <i>in vitro</i>	38
3	Materials and Methods	41
3.1	Project 1: Characterization of phase-bright objects in members of Proteobacteria and Actinobacteria.....	41
3.1.1	Bacterial growth conditions	41
3.1.2	Phase contrast microscopy	41
3.1.3	Cryo-electron tomography (cryo-ET)	42
3.1.4	Correlative light and electron microscopy (CLEM)	42
3.1.5	Scanning electron microscopy (SEM) and energy-dispersive x-ray analysis (EDX)	43
3.1.6	Dipicolinic acid (DPA) detection.....	43
3.1.7	Heat resistance of mature endospores	44
3.1.8	Differential staining of bacterial spores	44
3.1.9	Whole cell lipidomic analysis of <i>R. johrii</i>	45
3.1.10	Detection of genes required for endospore production	45
3.2	Project 2: Characterization of Alp7A structure <i>in vivo</i> and <i>in vitro</i>	46
3.2.1	Plasmid constructs for investigating Alp7A <i>in vivo</i>	46

3.2.2	Cell culture preparation.....	47
3.2.3	SDS-PAGE and Immunoblotting of Alp7A-GFP	47
3.2.4	Fluorescence microscopy of Alp7A-GFP	48
3.2.5	Cryo-ET of Alp7A-GFP and Alp7ARC in <i>B. subtilis</i>	48
3.2.6	CLEM of Alp7A-GFP.....	48
3.2.7	Conventional resin section of Alp7A-GFP for TEM	49
3.2.8	Chemically competent <i>E. coli</i> cells preparation.....	50
3.2.9	Plasmid transformation into <i>E. coli</i> with heat shock method.....	50
3.2.10	Plasmid Expression and purification of Alp7A-His using <i>E. coli</i> Arctic express (DE3) bacterial cells.....	50
3.2.11	Alp7A purification from <i>E. coli</i> DE3 bacterial cells.....	51
3.2.12	Alp7A-GFP-His expression and purification from <i>E. coli</i> C43 (DE3) cells	52
3.2.13	Immunogold labeling of Alp7A-GFP-His.....	53
4	Results	55
4.1	Project 1: Characterization of phase-bright objects in members of Proteobacteria and Actinobacteria.....	55
4.1.1	Detection of phase-bright objects in the three bacterial species	55
4.1.2	Cryo-electron tomography (cryo-ET) showed lack of spore-like structures in the three bacterial cultures with phase-bright objects	56
4.1.3	Phase-bright objects in <i>R. johrii</i> and <i>M. marinum</i> resemble the structure of storage granules under CLEM.....	60
4.1.4	Scanning electron microscopy (SEM) and energy-dispersive x-ray analysis (EDX)	62
4.1.5	Proteobacteria and Actinobacteria do not possess phenotypic features of endospores	64
4.1.6	The <i>R. johrii</i> cells contain lipid storage granules.....	68

4.1.7	<i>R. johrii</i> lacks essential genes of sporulation	70
4.2	Project 2: Characterization of Alp7A structure <i>in vivo</i> and <i>in vitro</i>	72
4.2.1	SDS-PAGE validated the of Alp7A in <i>B. subtilis</i> strains	72
4.2.2	Cryo-ET of <i>B. subtilis</i> showed potential filamentous structure of Alp7A	74
4.2.3	CLEM and LR white resin sections validated the filamentous structure of Alp7A-GFP in <i>B. subtilis</i> strain 3267	76
4.2.4	Purification and visualization of Alp7A from <i>E. coli</i> Arctic Express (DE3) cells	78
4.2.5	Purification and EM imaging of Alp7A-GFP-His from <i>E. coli</i> (DE3) cells..	81
4.2.6	Purification of Alp7A from <i>E. coli</i> by ammonium sulfate precipitation and size exclusion chromatography	84
5	Discussion	87
5.1	Project 1: Characterization of phase-bright objects in members of Proteobacteria and Actinobacteria.....	87
5.1.1	<i>M. marinum</i> are unable to sporulate and survive high temperatures	87
5.1.2	Putative storage granules in <i>R. johrii</i> and <i>S. marcescens</i>	88
5.1.3	TAGs as a survival arsenal in <i>R. johrii</i> cells	89
5.1.4	Lack of sporulation genes in <i>R. johrii</i> , and <i>S. marcescens</i>	90
5.1.5	Conclusion.....	90
5.2	Project 2: Characterization of Alp7A structure <i>in vivo</i> and <i>in vitro</i>	91
5.2.1	Alp7A forms filamentous structure in <i>B. subtilis</i>	92
5.2.2	Challenges during Alp7A purification for <i>in vitro</i> studies.....	92
5.2.3	Conclusion and suggestions	93
	Articles and Contributions.....	95
6	References	97

Liste des tableaux

Table 1 - Analytical detection of endospores in bacteria by DPA concentration measurement. ...	64
Table 2 - Bacterial recovery after heat shock.....	65
Table 3 - Whole cell lipidomic analysis on <i>R. johrii</i> with (+) and without (-) storage granules (156).	69
Table 4 - Analysis for presence of endospore formation genes in <i>R. johrii</i> and <i>S. marcescens</i> (156).	71

Liste des figures

Figure 1. –	Anatomy of the bacterial cell.	2
Figure 2. –	A schematic representation of bacterial cell envelope in Gram-positive and Gram-negative bacteria.....	4
Figure 3. –	Bacterial endospore.	7
Figure 4. –	The life cycle of endospore-forming bacteria.	8
Figure 5. –	Micrographs of <i>R. johrii</i> JA192 (T).	11
Figure 6. –	Transmission electron micrograph of <i>Serratia marcescens</i> subsp. <i>sakuensis</i> (strain no. 9; KRED ^T).....	12
Figure 7. –	Fluorescence microscopy and TEM images of <i>M. marinum</i>	15
Figure 8. –	Structure of intracellular lipid storage granules in prokaryotes.	18
Figure 9. –	Superstructures and functions of bacterial cytoskeleton proteins.	20
Figure 10. –	Structural homology between prokaryotic and eukaryotic cytoskeletal intermediate filaments.	22
Figure 11. –	Conserved tertiary structures of bacterial actin and actin.	24
Figure 12. –	Phylogenetic tree of bacterial actin.	25
Figure 13. –	A schematic representation of plasmid partitioning by ParM in <i>E. coli</i>	29
Figure 14. –	Fluorescence microscopy image of Alp7A-GFP in <i>E. coli</i>	30
Figure 15. –	Plasmid retention by Alp7AR in <i>B. subtilis</i>	31
Figure 16. –	Phase-contrast LM of <i>R. johrii</i> , <i>S. marcescens</i> , <i>M. marinum</i> , and <i>B. subtilis</i> cells induced for endospore formation.	56
Figure 17. –	Cryo-ET of <i>R. johrii</i> and <i>S. marcescens</i> reveals a lack of endospores.	58
Figure 18. –	Cryo-electron tomography of <i>M. marinum</i> and <i>B. subtilis</i> showing morphologies of phase bright objects.	58
Figure 19. –	Cryo-tomogram of <i>M. marinum</i>	59
Figure 20. –	Correlative light and electron microscopy (CLEM) images of <i>R. johrii</i>	61
Figure 21. –	Correlative cryo-light and electron microscopy of <i>M. marinum</i>	62
Figure 22. –	Correlative light and scanning electron microscopy in <i>Rhodobacter johrii</i>	63
Figure 23. –	Differential staining of <i>B. subtilis</i> , <i>M. marinum</i> , and <i>R. johrii</i>	68

Figure 24. – SDS-PAGE of Alp7A in *B. subtilis* cells.73

Figure 25. – Expression of Alp7A-GFP in *B. subtilis* strain 3267.74

Figure 26. – Cryo-ET of Alp7A and Alp7A-GFP in *B. subtilis*.76

Figure 27. – Correlative light-electron microscopy (CLEM) of *B. subtilis* strain 3267.....77

Figure 28. – LR white resin sectioning of *B. subtilis* strain 3267 expressing Alp7A-GFP.....78

Figure 29. – Purification and Electron microscopy (EM) of Alp7A-His from *E. coli* Arctic
express (DE3) cells.....80

Figure 30. – Purification of Alp7A-GFP-His from *E. coli* (DE3) cells.82

Figure 31. – EM visualization of Alp7A-GFP-His after purification from *E. coli*.83

Figure 32. – Alp7A purification from *E. coli* (BL21).85

Liste des sigles et abréviations

aa	amino acid
ADP	adenosine diphosphate
Alp	actin like protein
ATP	adenosine triphosphate
<i>B. subtilis</i>	<i>Bacillus subtilis</i>
BtubA	bacterial tubulin α homolog
BtubB	bacterial tubulin β homolog
CLEM	Correlative light and electron microscopy
cm	centimeter
CreS	crescentin
Cryo-ET	cryo-electron tomography
Cryo-ET	Cryo-Electron Tomography
DNA	Deoxyribonucleic acid
Dpa	Dipicolinic acid
<i>E. coli</i>	<i>Escherichia coli</i>
EDX	energy-dispersive x-ray analysis
F-actin	fibrous actin
fLM	fluorescence microscopy
FtsZ	Filamenting temperature-sensitive mutant Z
G-actin	globular actin
GFP	green fluorescent protein
GTP	guanosine triphosphate
IFs	intermediate filaments
IMP	Inner membrane protein
IsM	inner spore membrane
Kbps	kilobase pairs
kDa	kilodalton
LM	light microscopy
LP	lipoproteins
LPS	lipopolysaccharide
LTA	Lipoteichoic acid
<i>M. marinum</i>	<i>Mycobacterium marinum</i>
Mass spec	mass spectrometry
mM	millimolar
Mtb	Mycobacterium tuberculosis

nm	nanometer
NTM	nontuberculous mycobacteria
OM	outer memberane
OMP	outer membrane protein
OsM	outer spore membrane
PG	peptidoglycan
PHAs	polyhydroxyalkanoates
PHBs	polyhydroxybutyrates
<i>R. johrii</i>	<i>Rhodobacter johrii</i>
RNA	Ribonucleic acid
<i>S. marcescens</i>	<i>Serratia marcescens</i>
SEM	scanning electron microscopy
TAGs	triacyclglycerols
TEM	Transmission Electron Microscopy
TubZ	tubulin/FtsZ-like protein
UV	ultra-violet light
WACAs	Walker A cytoskeletal ATPases
WEs	waxesters
WTA	wall teichoic acid
μm	micrometer

Acknowledgements

First, I would like to have this opportunity to thank Dr. Nanci and Dr. Tocheva for being great supervisors who mentored me scientifically and provided tremendous personal support concerning general life lessons.

I want to thank the Tocheva and Nanci labs for being an intellectually creative and stimulating group of people to work with. I am extremely thankful to Driss Lajoie for sharing his expertise in all aspects of biochemistry and cell biology. Great thanks also go for my colleagues Aurélien Fouillen, Katia Pnoce, Dainelys Bello, and Alejandra Rodriguez for their collaboration and help with experiments and scientific discussions, and for their support and being amazing friends during my PhD. I am also thankful to the Pascal and Baron lab members for their collaboration, and for kindly offering reagents, protocols, and help on biochemical principles. Thanks to Dr. Kaustuv Basu at the Facility for Electron Microscopy Research (FEMR) of McGill University for his help in microscope operation.

I am very thankful for my thesis committee members Dr. Oeffinger and Dr. Sygusch for their mentorship and advice throughout my PhD. Many thanks for my doctoral jury members for accepting the task of judging this thesis. I would like to thank the administrative and technical staff, specifically Elaine Meunier, Monique Vasseur and Dr. Linda D'Astous, for their help with administrative matter.

Thanks to Rola, Rania, Driss, Dainelys, Anna, Giovanna, Katia, Renan, Alejandra, Lorea, Amira, Eliza, Adrian, Jaafar, Charline, Ola, Zack, Mellissa, Bastien, Benoit and Sacha. I feel very fortunate coming to Canada and meeting such supportive people. Special thanks to Rola Dali and Driss Lajoie for the support and advice you handed out.

Finally, I would have never come to this point in my life without my parents and brothers' support. I am grateful to my mother for her sincere support and always being there for me.

Thank you all. It would have not been possible to pass my PhD without you!

1 Introduction

1.1 Overview of sporulation and storage granule formation in bacteria

1.1.1 Bacteria

Bacteria constitute one of the primary taxonomic domains of life (1). These single-cell microscopic prokaryotes are considered the most diverse living organisms. They play vital roles in the environment and in both health and disease of humans and other organisms (2). Bacteria live as communities in almost every environment on Earth, expanding from hot springs to frozen snow, and from acidic water to alkaline springs. Bacterial cells are small, typically 1-2 μm in diameter or length. The short generation time of infectious bacteria, less than 30 minutes in some species, accounts for the rapid progression of infectious diseases (2).

Bacterial cells possess a cytoplasm, a cytoskeleton, a plasma membrane, and ribosomes like eukaryotic cells. However, they have features that distinguish them, including nucleoid (genetic material not surrounded by a nuclear membrane), plasmids (circular DNA), the lack of membrane-bound organelles (e.g., endoplasmic reticulum and Golgi apparatus of eukaryotes), a cell wall composed of peptidoglycan, and the flagella (**Figure 1**).

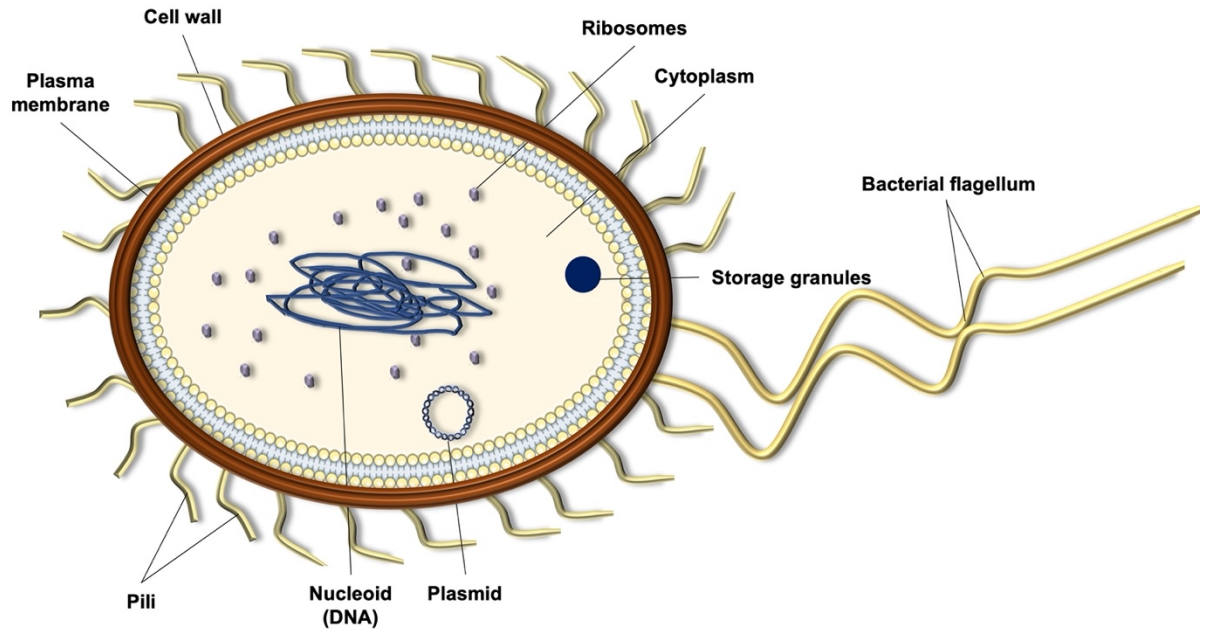


Figure 1. – Anatomy of the bacterial cell. Schematic representation of the internal and external structures of a bacterial cell.

1.1.2 Classification of bacteria

Bacteria are categorized based on their structure into five categories: bacilli (rod-shaped), spirilla (spiral-shape), vibrios (comma-shape), cocci (spherical-shape), and spirochaetes. Bacteria can be classified into Gram-positive and Gram-negative based on their cell wall characteristics. Gram-negative bacteria possess a multi-layered cell envelope made of an outer membrane (OM) surrounding a thin layer of peptidoglycan (PG), and the cell membrane (**Figure 2**) (3). The two membranes delimit a viscous cellular compartment called periplasm. The OM is composed of asymmetric inner and outer leaflets. The outer leaflet of the OM is enriched with phospholipids and glycolipids such as lipopolysaccharide (LPS). In comparison, Gram-positive bacteria possess a thick PG layer and lack an OM (**Figure 2**). Gram-positive bacterial PG ranges between 10-30 PG layers, while that of Gram-negative bacteria is limited to 1-3 layers linked by lipoproteins to the bacterial OM (3). Two types of anionic polymers span the thick PG of Gram-positive bacteria: wall teichoic acids (WTAs) attached to the wall's PG, and lipoteichoic acids (LTAs) attached to the

lipids of the cell membrane (**Figure 2**) (4). These anionic polymers play a fundamental role in the cell envelope and affect the morphology of bacteria. They also play a role in bacterial cell growth and homeostasis. Anionic polymers are involved in the mechanism of antibiotic resistance, making them attractive therapeutic targets for vaccines and antimicrobial drugs (5).

Bacteria react differently with the Gram stain based on their PG thickness. This staining approach is the primary technique used to characterize bacteria based on their wall characteristics. The technique was developed by H. C. Gram in 1884. It relies on the differential ability of bacteria to retain several dyes, such as crystal violet and safranin, before destaining with alcohol. Due to their PG thickness, Gram-positive and Gram-negative retain the stain differently, where Gram-negative bacteria stain pink and Gram-positive stain purple. These color differences can be explained by crystal violet retention by the thick cell wall in Gram-positive bacteria, whereas it is rapidly washed away by alcohol in Gram-negative bacteria due to the thin layer of PG.

Bacteria are further distinguished into two other groups, anaerobic bacteria and aerobic, based on their need for oxygen to survive and grow. While anaerobic bacteria can survive in the absence of oxygen, such as *Bacteroides* found in the large intestines, aerobic bacteria, such as the pathogenic *Pseudomonas aeruginosa*, require oxygen to survive and grow. On the other hand, some bacteria can grow both anaerobically and aerobically and are known as facultative anaerobic bacteria. For example, *Bifidobacteria* are facultative anaerobes that grow and colonize in the newborns' intestines and are transmitted to the infant through vaginal delivery (6).

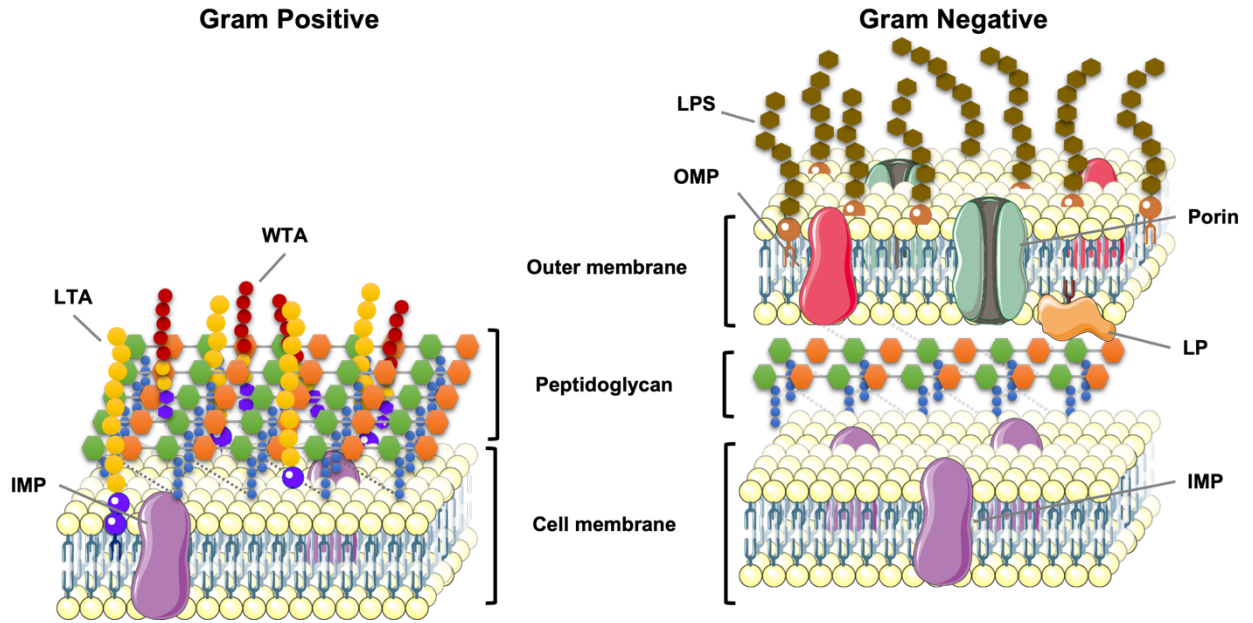


Figure 2. – A schematic representation of bacterial cell envelope in Gram-positive and Gram-negative bacteria.

Gram-positive bacteria possess a membrane and thicker peptidoglycan that contain teichoic acids. Gram-negative bacteria possess an inner membrane, a thin peptidoglycan layer, and an outer membrane. IMP, Inner membrane protein; OMP, outer membrane protein; LP, lipoproteins; LPS, lipopolysaccharide; LTA, Lipoteichoic acid; WTA, wall teichoic acid (5, 7, 8).

1.1.3 Evolution of sporulation

Spores represent a dormant state of bacteria that can persist for hundreds of years (9-11). Different types of bacterial sporulation modes have been documented, all induced by extreme environmental conditions. For example, low nitrogen availability can trigger sporulation in Firmicutes, resulting in the formation of endospores that are resistant to UV radiation, extreme pH, high temperature, and high pressure (12-14). The different types of spores vary morphologically and are encoded by non-homologous pathways (15). For example, members of the phylum Firmicutes form endospores, while *Myxococcus* species and Actinobacteria form fruiting bodies and exospores, respectively (16-18).

1.1.4 Exospores

Exospores are unicellular reproductive structures produced by some species of bacteria under unfavorable conditions. Exospores are formed by budding at the end of the mother cell and are resistant to extreme and unfavorable environmental conditions.

The Gram-positive Actinobacteria are most known to form exospores. Actinobacteria are primarily distributed in ecosystems and are essential in biotechnology and medicine, where they are used to produce more than half of the antibiotics and anti-cancer products. Actinobacteria phylum contains several species that can sporulate by asexual budding (19). Many types of exospores exist in Actinobacteria (19). During exospore formation in Actinobacteria, the growth of mycelia into branching areal hyphae is followed by simultaneous septation and the formation of numerous compartments within the hyphae that eventually mature into chains of exospores (20, 21).

Other bacteria, such as the Gram-negative rod-shaped bacterium *Myxococcus xanthus*, differentiate into ovoid thick-walled exospores that develop as a fruiting body above a colony formed on a flat surface (22). *Myxococcus xanthus* is generally found in animal wastes and soil. Their dormant state is known as myxospore, which is resistant to unfavorable environmental conditions such as heat (23). The fruiting bodies are complex, multicellular organisms that constitute around 10^5 cells. They harbor various shapes depending on the myxobacteria species.

1.1.5 Endospores

Endospore formation is considered a hallmark of the Firmicutes phylum, mainly in the classes Bacilli and Clostridia (12, 13, 24). The two classes harbor bacteria with sporulating and non-sporulating properties.

Clostridium is a Gram-positive genus consisting of rod-shaped bacteria. The genus constitutes anaerobic bacteria that can sporulate and is considered heterogeneous. Members of this

genus are generally found in soil and humans. *Clostridium* genus contains human pathogen species such as *Clostridium botulinum* (*C. botulinum*) and *Clostridium perfringens* (*C. perfringens*). *C. botulinum* is considered one of the most dangerous spore-formers, where it can produce the neurotoxin botulinum under low oxygen levels. The toxin produced by *C. botulinum* is lethal and can cause muscle paralysis and severe food poisoning.

Bacilli are also Gram-positive rod-shaped bacteria found in soil. Members of Bacilli can be either obligate aerobes or facultative anaerobes, and they are facultative endospore-forming bacteria. For example, *Bacillus anthracis* species is a facultative anaerobe that was first demonstrated to cause anthrax by Robert Koch in 1876. This observation was considered one of the first indications that microorganisms can cause specific diseases. The disease is caused by the ingestion or contamination of an open wound with this bacterium's spores from soil or contaminated animal products. The spore of this bacterium can survive in the soil for decades and germinates inside the animal or human host, where it multiplies and can kill the host within a few days or weeks.

1.1.5.1 Endospore structure

Endospores possess a unique structure that makes them resilient to extreme environmental conditions such as heat and ultra-violet (UV) light. An endospore is also resistant to antibiotics. It harbors an outer proteinaceous coat, which protects the endospore from chemical and enzymatic activity. Beneath the coat exists the outer spore membrane (OsM), followed by a thick layer of peptidoglycan, known as the cortex, responsible for protecting the endospore against heat (**Figure 3**). The former consists of modified peptidoglycan, while the latter is speculated to transform into bacterial cell wall after germination when the environmental conditions are convenient. Beneath the inner cortex, an inner spore membrane (IsM) is present, which is considered the main barrier against chemicals in endospores. Finally, the core harbors DNA at the center of the endospore. The core is dehydrated, leading to spore dormancy, and is enriched in dipicolinic acid and calcium ions that represent more than 10% of its dry weight. Also, small acid-soluble proteins (SASPs) are responsible for DNA condensation and play a role in the spore's resistance to UV light. Some endospores also possess an exosporium, which is an outer glycoprotein layer.

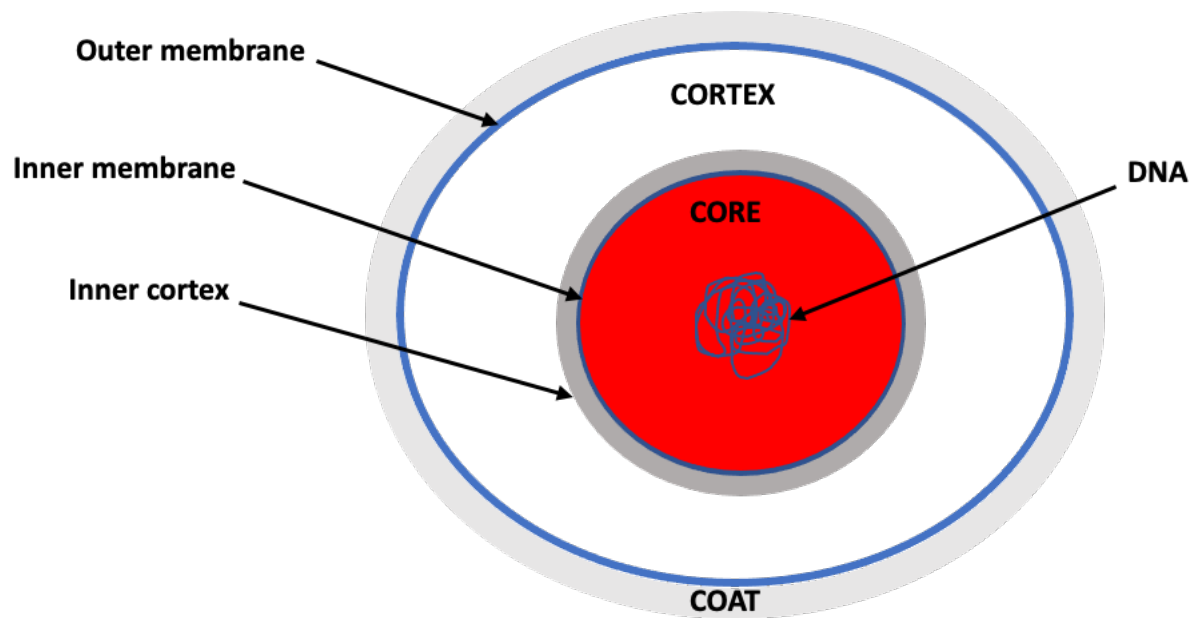


Figure 3. – Bacterial endospore.

Schematic diagram of bacterial spore structure.

1.1.5.2 Stages of sporulation

Sporulation is a complex process controlled by proteins, signaling pathways, and DNA-protein interactions (25, 26). The best-studied sporulation model organism is *B. subtilis*, a fast-growing bacterium that divides by binary fission every 30 minutes under adequate environmental conditions containing enough nutrients. However, under limited conditions, the division process slows down and may take up to 10 hours.

Electron microscopy is considered the optimal visual technique to characterize the stages of sporulation in *B. subtilis* (27). Endospore formation begins with an asymmetric cell division that results in two cells with different fates (28-30). The bigger compartment (mother cell) engulfs the smaller compartment (prespore), and the synthesis of multiple protective layers follows the process. Once layers of the proteinaceous cortex are synthesized, the spore matures and is released by the

lysis of the mother cell (**Figure 4**) (27). A unique characteristic of a mature spore is the replacement of water by dipicolinic acid (DPA) and Ca^{2+} ions. Together with the numerous protective layers, spore dehydration accounts for the resistant properties of endospores (31).

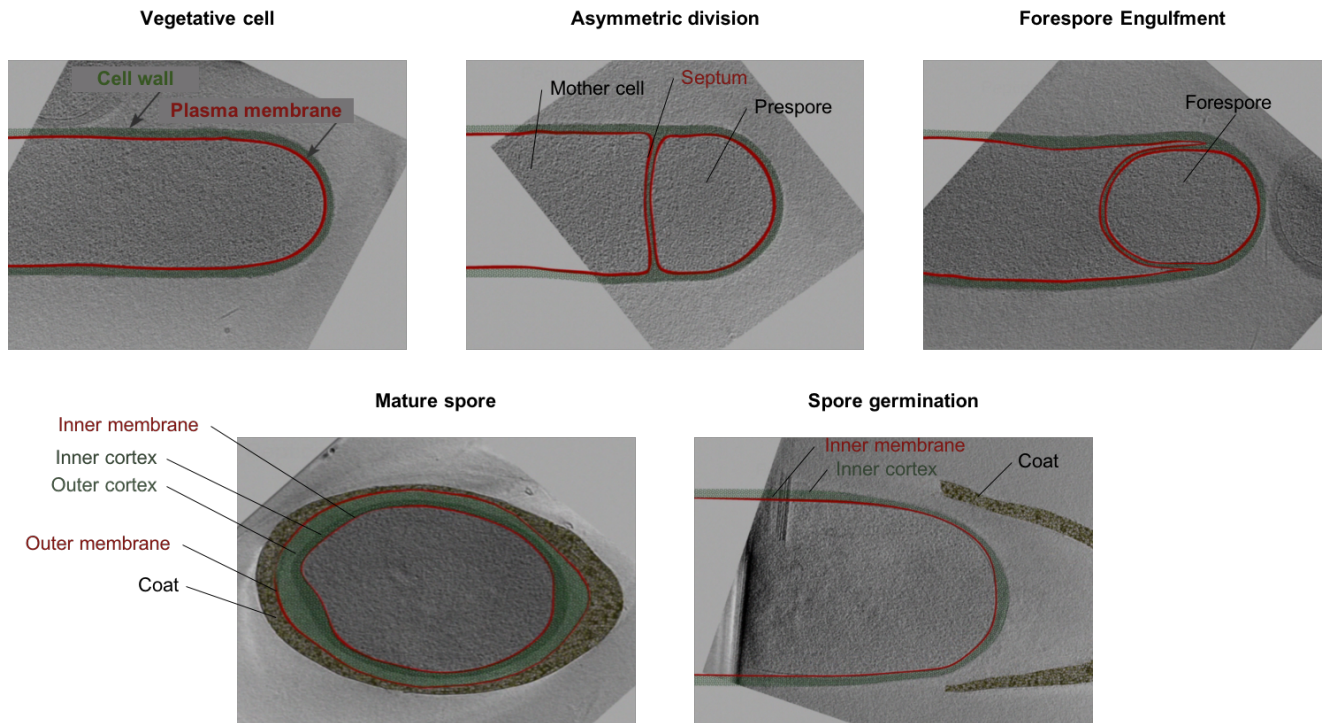


Figure 4. – The life cycle of endospore-forming bacteria.

Cryo-electron tomography (cryo-ET) showing stages of sporulation and germination in *B. Subtilis*. Under unfavorable conditions, sporulation starts with DNA replication and asymmetric division, resulting in the formation of two compartments: the immature prespore (small compartment) and the mother cell (larger compartment). The septum continues to grow, leading to complete engulfment and the formation of a forespore. A protein coat assembles on the mother side of the spore membrane. Dipicolinic acid incorporates into the core of the forespore during this stage. A mature spore is ellipsoidal and is surrounded by multiple protective layers, including the inner membrane, outer membrane, inner cortex, outer cortex, and spore coat. Germination occurs when surrounding conditions become favorable. The process is characterized by opening of the coat and degradation of the outer cortex. The inner cortex of the spore becomes the cell wall of the germinating vegetative cell. Adapted from Tocheva E *et al.*, 2013 (27).

1.1.5.3 Genomic determinants of sporulation

When a bacterial cell is exposed to unfavorable conditions such as low nutrition, harsh chemicals, or extreme temperatures, it adapts to its surroundings by activating a series of adaptation processes that allow it to survive. Hence, sporulation is a tightly regulated process that involves multiple checkpoints that ensure the successful cell division and formation of a mature spore to withstand unfavorable conditions and regerminate under adequate environmental conditions (32).

Sporulation relies on a complex gene regulatory network that involves hundreds of genes involved in the step-by-step endospore formation process, including transcription factors, signaling, and cytoskeleton proteins (13). In *B. subtilis*, sporulation initiation mainly depends on the phosphorylation and activation of the transcription factor Spo0A, which is ultimately achieved through a series of upstream phosphorylation reactions in a response to environmental stress. Particularly, environmental stress activates one of the two histidine kinases, KinA and KinB, which in turn activates a series of phosphorylation reactions through Spo0F, Spo0B, and finally Spo0A. This “phosphorelay” reaction is controlled by specific phosphatases, each of which is responsible for regulating one step of the reaction. The balance between the phosphorylation/dephosphorylation reactions rely on the strength of the environmental signal sensed by other factors within the cells (13).

Activated Spo0A induces the expression of the transcription factor σ^F and its regulators SpoIIAA and SpoIIAB (13). The transcription factor σ^F is responsible for the induction of early genes involved in asymmetric cell division and forespore formation. SpoIIAB acts as an inhibitor that binds σ^F and blocks its activity, whereas SpoIIAA binds to SpoIIAB and prevents its interaction with σ^F . Once the forespore has formed, the downstream cellular program relies on the cell-type-specific activation of four alternative σ subunits of RNA polymerase: σ^F (forespore) and σ^E (mother cells) control early stages before engulfment of the forespore by the mother cell, respectively, whereas σ^G and σ^K are involved at later stages in the forespore and in the mother cell, respectively (33). These factors control the sporulation process through gene expression regulation in association with key signaling pathways in the two cellular chambers (mother cell and future spore).

It has been shown that sporulation in *B. subtilis* involves over 500 genes. Several efforts have been made to map genes involved in sporulation and develop a signature of essential sporulation genes. In their interesting study, Galperin *et al.* (13) have identified several groups of sporulation-specific genes that are conserved among species of bacilli and clostridia. Notably, many of the key regulatory genes of sporulation are conserved among sporulating bacilli and clostridia, whereas those involved in spore morphogenesis (SASPs, spore coat proteins, spore coat polysaccharide biosynthesis proteins and spore germination proteins) varied even between closely related organisms. Such conservation of essential sporulation genes would enable the identification of potential spore-forming bacteria.

1.1.5.4 Putative endospore formation in Proteobacteria

Recent articles have reported sporulation in members of the phylum Proteobacteria such as *Rhodobacter johrii* (*R. johrii*) and *Serratia marcescens* (34, 35). *R. johrii* was discovered in India by Girija *et al.* in 2010. Based on the phylogenetic analysis of the 16S rRNA gene sequence, the characterized strain *R. johrii* JA192(T) was assigned to the *Rhodobacter* genus that contains sixteen different species. *Rhodobacter johrii* is a Gram-negative bacterium that lives in soil, and it harbors 99.9% sequence similarity with the species *Rhodobacter sphaeroides* and 99.8 % with *Rhodobacter megalophilus* JA194(T). Girija *et al.* (35) described endospore production in *Rhodobacter johrii*, strain JA192(T).

The purple non-sulfur bacterium *R. johrii* is a facultative anaerobe with an oval-to-rod cell shape (**Figure 5a**). Girija *et al.* observed *R. johrii* JA192(T) cells as phase bright objects, typically associated with the maturation of an endospore within a mother cell, under phase-contrast microscopy (**Figure 5b**) and could retain malachite green under differential staining, another characteristic of mature endospores (**Figure 5c**). The authors interpreted these findings as evidence that this bacterial species can sporulate. To further support their claims, the authors used transmission electron microscopy (TEM) to image the cells at higher resolution, which showed “endospore-like structures” inside the mother cell of *R. johrii* JA192(T) (**Figure 5d**). Despite these observations, the identified structures lacked some spore features and were observed only in this species of *Rhodobacter*, however, Girija *et al.* concluded that *R. johrii* JA192(T) is a sporulating bacterium.

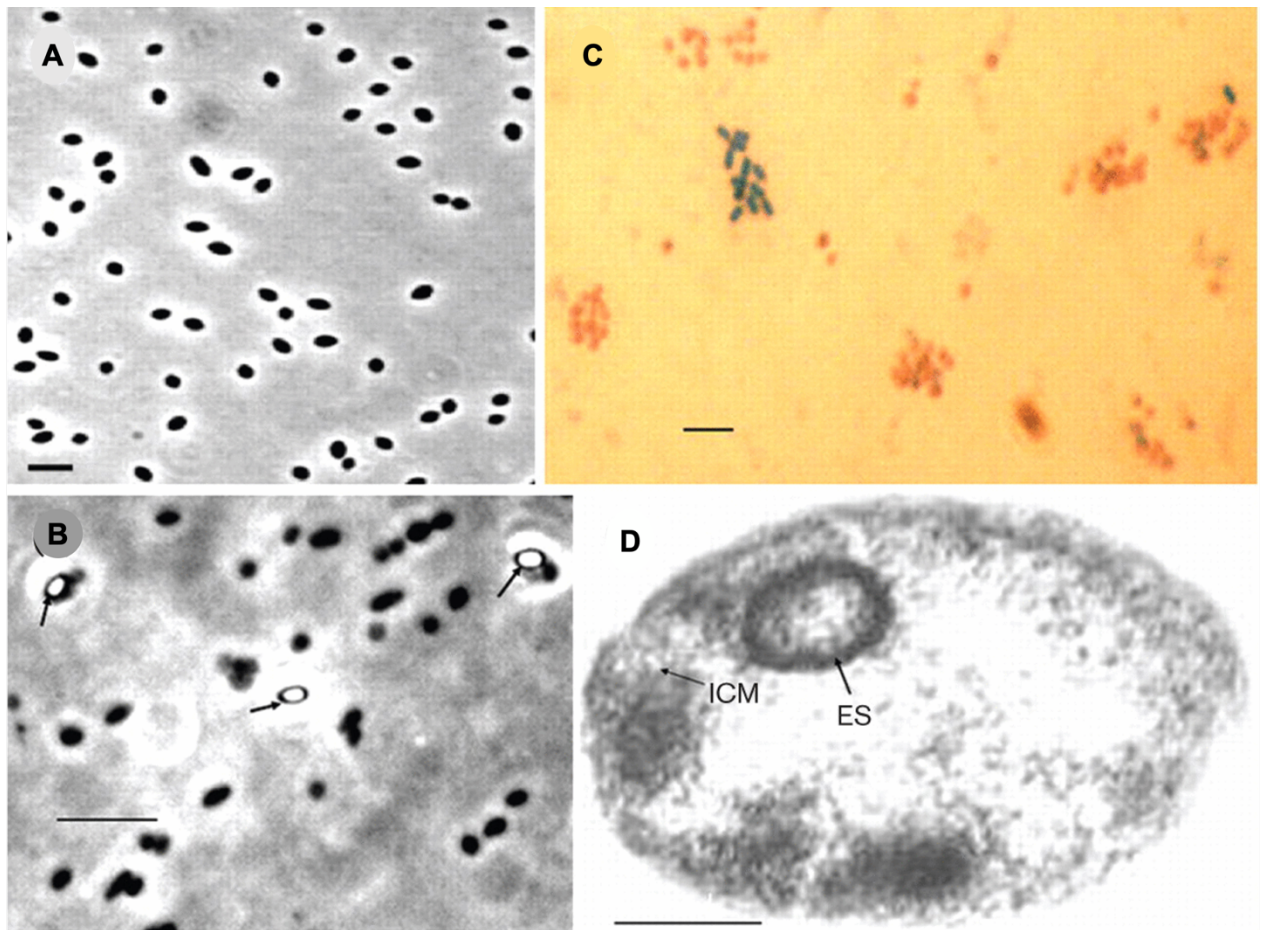


Figure 5. – Micrographs of *R. johrii* JA192 (T).

(a) Phase-contrast image of healthy vegetative *R. johrii* cells. (b) The phase-contrast image reveals phase-bright objects in sporulating *R. johrii* cells (arrows). (c) Malachite green-retained by sporulating *R. johrii* cells appears in green color. (d) The transmission electron micrograph reveals the sporulating *R. johrii* cell that harbors vesicular inner cellular membrane (ICM) structures and a thick-walled endospore (ES). Scale bar 2.5 μm in (a), 5 μm in (b), 5.5 μm in (c), and 0.39 μm (d). Adapted from Girija *et al.*, 2010 (35).

In another study, Ajithkumar *et al.* (34) also reported endospore formation outside of Firmicutes phylum. The authors showed for the first time that the species *Serratia marcescens*

subsp. sakuensis (strain no. 9; KRED^T), a member of Proteobacteria, can sporulate. *Serratia marcescens* is a pathogenic bacterium that infects humans and causes bacteremia, urinary tract infections, and nosocomial infections (36, 37). Drug-resistant of this bacterium is a causing factor of pre-native babies' mortality in neonatal intensive care units (38).

S. marcescens is a Gram-negative facultative anaerobic bacterium that can form red pigments on agar plates. The strain KRED^T was discovered in Japan in wastewater. The authors showed that this strain could sporulate after isolation, which is not the case for other strains of *S. marcescens* (34). Endospores formation by strain KRED^T was investigated with several approaches such as heat-resistance and TEM. The TEM analysis revealed an endospore structure with an outer membrane and a peptidoglycan layer but lacking spore coat and membrane (**Figure 6**). Though not all features of endospores were visualized, Ajithkumar *et al.* concluded that *S. marcescens subsp. sakuensis* (strain no. 9; KRED^T) is a sporulating bacterium.



Figure 6. – Transmission electron micrograph of *Serratia marcescens subsp. sakuensis* (strain no. 9; KRED^T).

Transmission electron micrograph section showing rod-shaped *S. marcescens* cells with (arrowheads) and without putative endospore structure. Scale bar 0.2 μ . Adapted from Ajithkumar *et al.*, 2003 (34).

1.1.5.5 Putative endospore formation in Mycobacteria

The phylum Actinobacteria includes over 200 species (39), many of which are highly pathogenic and categorized into three major clinical groups based on their pathogenicity: *Mycobacterium tuberculosis* (*Mtb*), *Mycobacterium leprae*, and nontuberculous mycobacteria (NTM) species (40, 41). *MTB* and *Mycobacterium leprae* are obligative pathogens and are not found as free-living members. In contrast, NTM can survive in soil and water; they are opportunistic pathogens that can cause pulmonary disease resembling tuberculosis, lymphadenitis, skin disease, or disseminated disease (42, 43). Recently, a global health concern was raised after the increase in the prevalence of NTM-derived pulmonary disease (44). Pathogenic mycobacteria are known to persist as latent pathogens in their hosts without causing any adverse symptoms (45). They can grow and multiply inside host cells, such as macrophages (46), which raises concerns about detection and treatment of these pathogenic bacteria. Therefore, understanding the latency mechanisms of these pathogenic mycobacteria can provide a basis for the prevention and treatment of mycobacterial diseases.

A paper by Ghosh *et al.* reported that *Mycobacterium marinum* (*M. marinum*) can sporulate (47). They showed that “endospore-like” phase-bright objects, lacking during exponential growth of *M. marinum* (47), were later detected in the same culture during the stationary phase (**Figure 7A**). *M. marinum* is a slow-growing NTM that causes tuberculosis-like disease in fish and frogs. It can also cause opportunistic infections in humans, leading to pathological conditions such as aquarium granuloma disease (48, 49). Large outbreaks of infection due to this mycobacterium have been described in association with swimming pools, and awareness of the disease has increased as more cases are being recognized and reported worldwide (50)

Ghosh *et al.* proposed that *M. marinum* can form latent endospores that can persist and confer resistance to treatments, which contrasts with textbook describing endospore formation to occur exclusively in the Firmicute classes, Bacilli, and Clostridia (15). The identification of *M. marinum* as a spore-forming mycobacterium poses global concerns. It opens new perspectives on the prophylaxis of mycobacterial infections as an important human pathogen, but also as a model for tuberculosis (51). Ghosh *et al.* identified multiple physicochemical properties that characterize “spore-like” phase bright particles in *M. marinum* cultures (47). They reported recovery of *M. marinum* cells after heat treatment on days 3 and 30, respectively, and the retention of malachite green by spore-like particles of *M. marinum*. They also showed that the spore-like particles are structurally similar to *B. subtilis* spores using scanning electron microscopy (SEM) and traditional transmission electron microscopy (TEM) (**Figure 7B**). While the authors were unable to detect a definite hit of key sporulation-specific transcription factors, they suggested that sporulation in *M. marinum* may have occurred in the stationary phase by activating several genes that are homologous to those involved in *B. subtilis* sporulation (29). These findings were refuted by Traag *et al.* (52), who failed to detect the presence of phase-bright objects by light microscopy over periods that extended up to 12 weeks under the growth conditions described by Ghosh and colleagues. The authors showed that *M. marinum* lacks essential sporulation genes and is unable to form spores *in vitro* and *in vivo*. They proposed that the spores detected by Ghosh *et al.* (47) resemble those produced by *B. subtilis* and thus were likely a contamination.

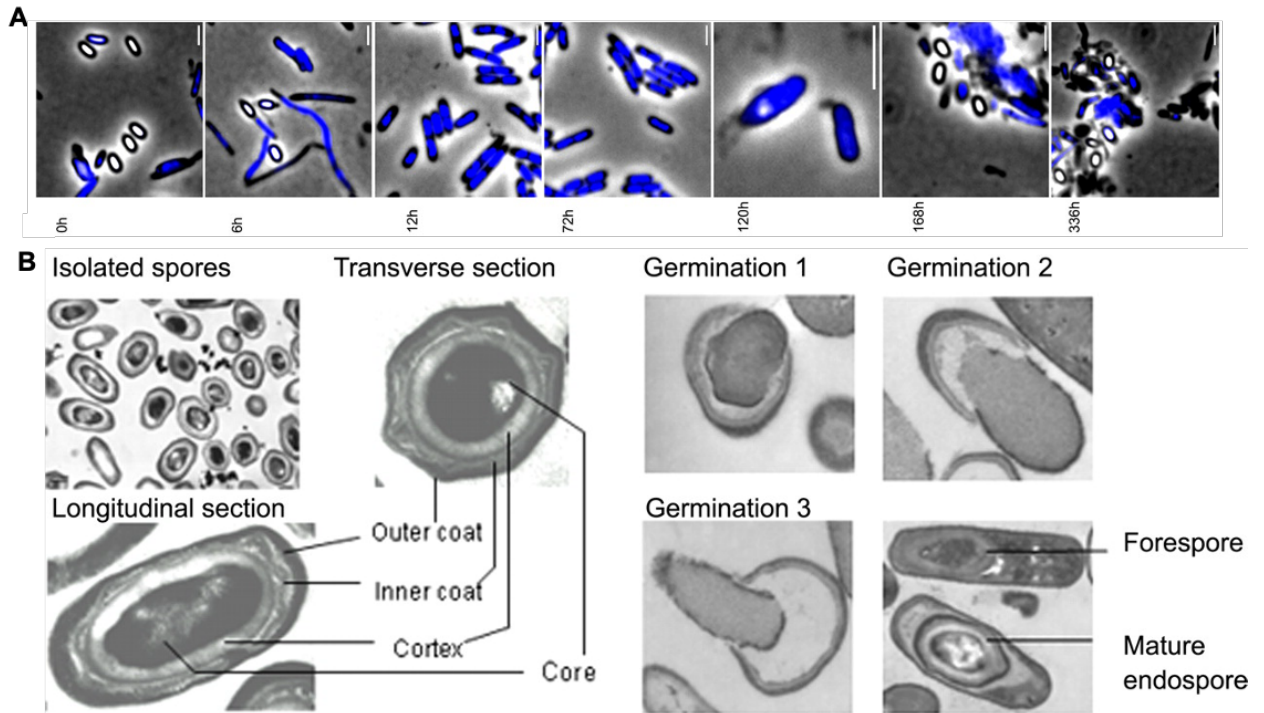


Figure 7. – Fluorescence microscopy and TEM images of *M. marinum*.

(A) Fluorescence images of *M. marinum* at different growth stages showing the disappearance of putative endospores at exponential growth (12 - 72 hours). Scale bar: 1 μ . (B) Thin-section TEM images show isolated spores (6,000 \times magnification); a mature spore of the transverse section (60,000 \times magnification); a mature spore of the longitudinal section (60,000 \times magnification); germination 1–3 (different stages of germinating spores at 6 h) (40,000 \times magnification); and a forespore and a mature endospore at day 5 (30,000 \times magnification. Adapted from Ghosh *et al.*, 2009 (47).

1.1.6 Storage granules

Storage granules are essential elements of metabolism in several organisms of bacteria, archaea, and eukaryotes. Bacteria store different types of macromolecules, such as polyphosphate, glycogen, and lipids, in the form of storage granules. Prokaryotic cells contain at least one type of storage granules, which can be used as an energy source under particular conditions. Most storage granules are lipophilic compounds that are stored as inclusion bodies in bacterial cytoplasm. However, some bacteria, such as lactobacilli and methanogenic bacteria, lack lipid granules.

1.1.7 Types and functions of storage granules

Storage granules in bacteria accumulate in different forms, such as triacylglycerols, wax esters, polyhydroxyalkanoates, and polyhydroxybutyrates. The storage of lipids mainly occurs at the core of storage granules protected by a layer of amphiphilic elements such as proteins.

1.1.7.1 Polyhydroxyalkanoates (PHAs) and polyhydroxybutyrates (PHBs)

PHAs were discovered in *Bacillus megaterium* around 90 years ago (53). Later, the presence of PHA was observed in several other bacterial members such as lactobacilli and Enterobacteriaceae. For example, in *Ralstoni eutropha*, PHAs accumulate as intracellular inclusion bodies and represent approximately 90% of bacterial dry weight (54) (**Figure 8A**). PHAs accumulate in bacterial cells in spherical intracellular inclusion bodies. They possess a diameter that ranges between 200 and 500 nm. In *R. eutropha* H16, PHBs are around 500nm in diameter (**Figure 8A**).

PHAs are polyesters made of various (R)-hydroxycarboxylic acids and are involved in several metabolic pathways (55). PHAs represent storage granules for carbon and energy source in bacteria. Besides, the accumulation of PHAs in bacterial cells may improve the cell's resistance to stress, such as freezing conditions. Bacteria accumulate PHA storage granules under conditions with excessive amounts of carbon. These polyesters are synthesized from either fatty acids or carbon sources.

PHB is a form of bacterial PHAs and is considered the most abundant polyester in bacteria and has been shown to accumulate in both eukaryotic and prokaryotic cells (56). These polyesters accumulate as a carbon source and constitute almost 80% of the cellular dry weight in several bacteria, such as in *Alcaligenes eutrophus*.

1.1.7.2 Triacylglycerols (TAGs)

TAGs accumulate as intracellular inclusion bodies and have been reported to exist in many bacteria, such as *Mycobacterium* sp. and *Rhodococcus* sp. (57, 58). TAGs consist of fatty acid triesters of glycerol, and their structure and composition vary among bacteria are affected by many factors, including carbon source and growth stage (59). TAGs play a significant role as reserve compounds and energy sources. They also represent a reservoir of evaporation-resistant lipids that could be oxidized to produce water under unfavorable dehydration conditions. TAGs are stored in spherical lipid bodies, with quantities and diameters (50 to 400 nm) depending on the particular species and cultivation media. For example, under high nitrogen and carbon conditions, cells of *R. opacus* contain few TAGs. When cultured in a medium containing low nitrogen-to-carbon ratio, TAGs inclusion bodies increase to reach their maximum yield in late stationary phase.

TAGs were characterized for the first time in *R. opacus* (PD630) (**Figure 8B**) (53), where their composition was shown to vary based on the growth conditions of bacteria. They mainly consisted of 87% TAGs, with various other components such as proteins and fatty acids. When cells were grown in specific conditions supplemented with acetic acid and gluconic acid, the composition of TAGs in *R. opacus* constituted 36.4% of hexadecenoic acid, 19.1% of octadecenoic acid, and around 12% of heptadecanoic acid.

1.1.7.3 Wax esters (WEs)

Wax esters were discovered decades ago, mainly in the genus *Acinetobacter* (60). WE biosynthesis was reported in many species in actinomycetes, such as in the pathogenic bacteria *Mycobacterium tuberculosis* (61). They were shown to play a role as storage elements, where they can occupy about 30% of cellular dry weight in some species of bacteria.

Wax esters may occur in different forms in diverse bacterial species and under different conditions. They are present in different shapes such as flat, rectangular, and disk-shaped inclusion bodies. For example, WEs form intracellular spherical granules of 100 - 200 nm diameter in *Acinetobacter calcoaceticus* ADP1 (**Figure 8C**) and rectangular structure in *A. calcoaceticus*

HO1-N (**Figure 8D**) (53). Besides, the presence of alkane hydrocarbon hexadecane was shown to induce *Acinetobacter* (M-1) to store WEs in the form of disk-like bodies lacking membrane structure (**Figure 8E**). Furthermore, WEs can exist as intracellular and extracellular bodies (62).

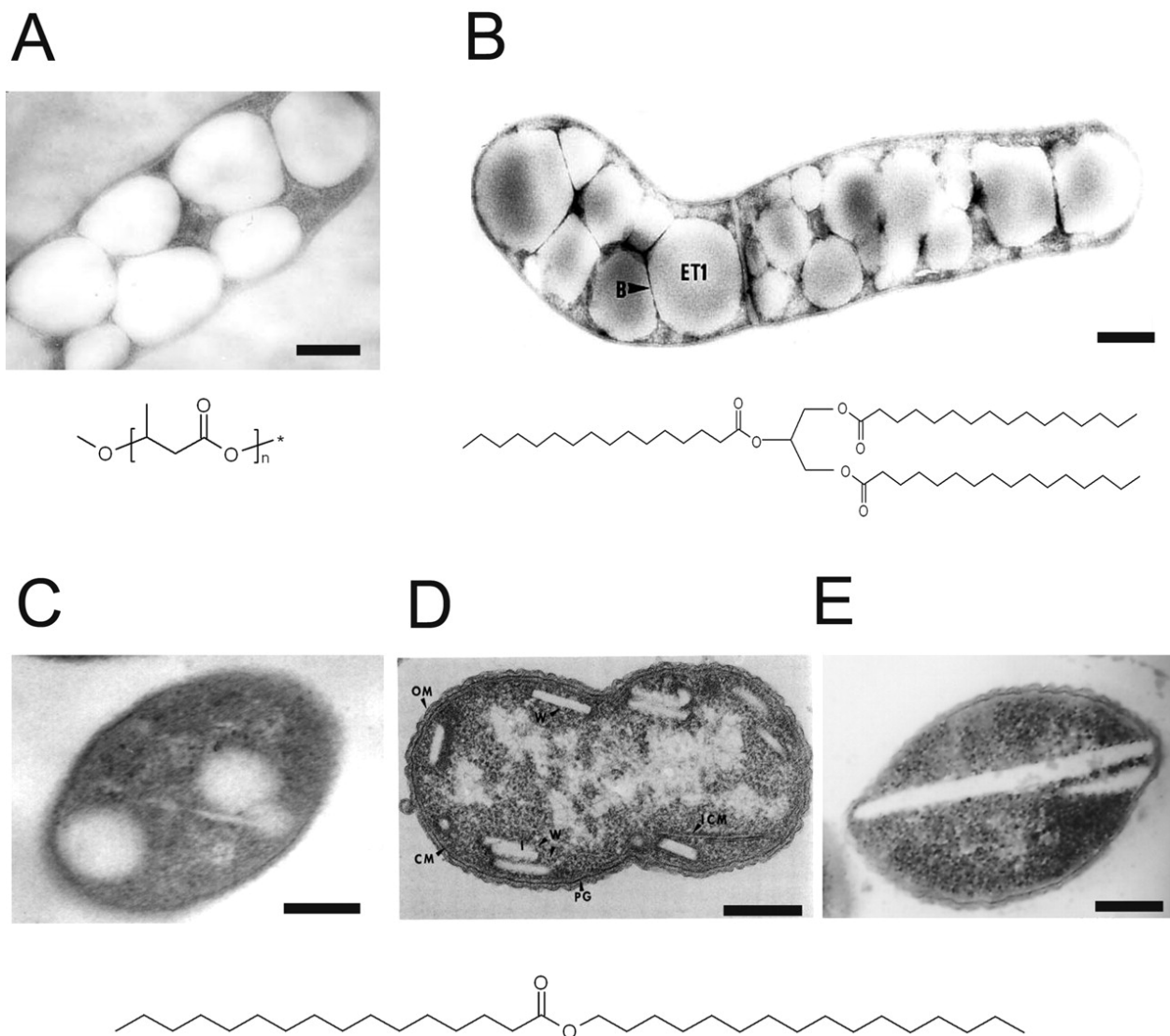


Figure 8. – Structure of intracellular lipid storage granules in prokaryotes.

(A) *R. eutropha* H16 cell with accumulating PHB inclusions. (B) *Rhodococcus opacus* PD630 cell from late stationary growth phase accumulating massive amounts of TAG inclusions. (C) *Acinetobacter calcoaceticus* ADP1 cell with three spherical WE inclusions. (D) *Acinetobacter* sp. strain HO1-N accumulating small rectangular WE inclusions; (E) *Acinetobacter* sp. strain M1 accumulating large disc-like WE inclusions. Abbreviations: B, boundary layer; CM, plasma

membrane; ET, electron-transparent TAG inclusion; ICM, intracellular plasma membrane; OM, outer membrane; PHA, PHA inclusion; PG, peptidoglycan; W, wax ester inclusion. Bars, 0.2 μm . Reprinted from Wältermann M *et al.*, 2005 (53).

1.2 Bacterial Cytoskeletal Proteins and DNA Segregation

1.2.1 Bacterial cytoskeleton

For a long time, bacteria were thought to lack a cytoskeleton and internal cellular organization. This view has drastically changed with the rapid advances in the field of bacterial cell biology. The revolution in structural biology grounded by super-resolution microscopy in live-cell imaging has yielded useful information about the bacterial homologs of cytoskeletal structures. Over the last 30 years, the dogma has entirely overturned by identifying bacterial cytoskeletal proteins resembling the three main types of eukaryotic cytoskeletal proteins that possess diverse structures and functions. Indeed, bacteria are now considered highly organized spatially and temporally (63, 64).

The discovery of the tubulin-like protein FtsZ cytoskeletal proteins in prokaryotic cells in the early 1990s was the breakthrough finding that laid the first stone in unearthing bacterial cytoskeleton (65). In 2001, Jones *et al.* showed that *B. subtilis* possesses actin-like protein MreB and Mbl that can form filamentous helical structures and play critical roles in cell shape maintenance (66). Despite low sequence similarity with eukaryotic cytoskeletal proteins, the bacterial cytoskeleton contains homologs of the main eukaryotic cytoskeletal proteins such as actin, tubulin, and intermediate filaments (IFs) (**Figure 9**).

It is now widely accepted that cytoskeleton acquisition was the most significant step in eukaryotic cell evolution (67, 68). Extensive investigations have been done to elucidate the evolutionary track of cytoskeletal proteins and their role in bacterial growth and life cycle. Bacterial cytoskeletal proteins are highly similar in structure to the eukaryotic cytoskeletal proteins, suggesting that the eukaryotic cytoskeleton can trace its evolutionary origins to bacterial ancestors

(69). Like eukaryotic cytoskeleton, bacterial cytoskeleton contains stable and dynamic filamentous structures that can assemble and disassemble in response to stimuli to regulate cellular functions and structures (70). Unlike eukaryotic cytoskeletal elements, bacterial cytoskeletal homologs polymerize into several superstructures other than filaments, such as rings, tubes, sheets, moving patches, and meshes (**Figure 9**) (71).

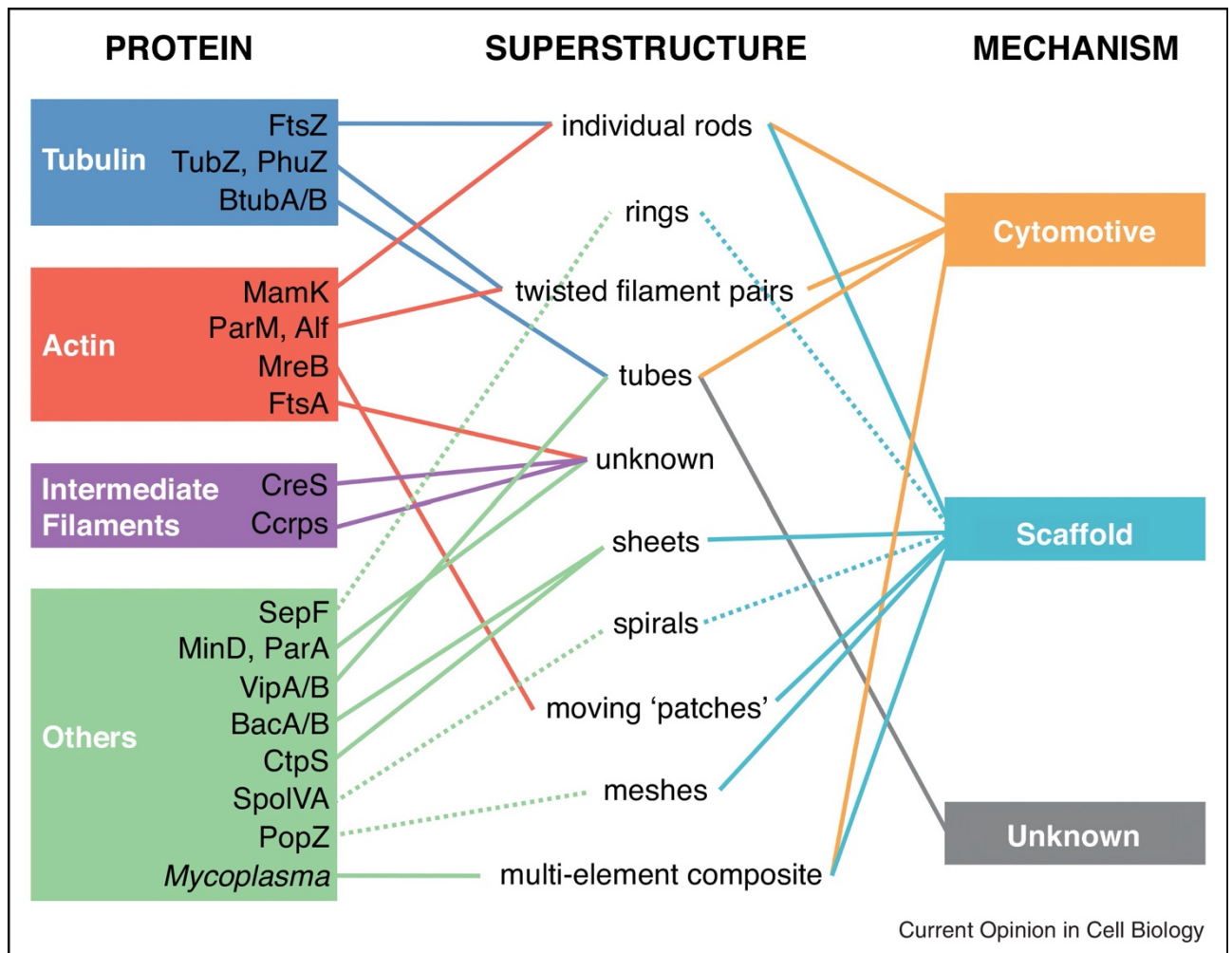


Figure 9. – Superstructures and functions of bacterial cytoskeleton proteins.

Bacterial cytoskeletal proteins are tailored to perform specialized functions within the cell through evolved superstructures. Connections with weaker evidence are represented as dashed lines. Reprinted from Pilhofer *M et al.*, 2014 (70).

1.2.2 Bacterial tubulin homologs

Tubulin has long been considered a hallmark protein unique to eukaryotes. Six tubulin superfamily members are conserved in all eukaryotes (72, 73), including α -, β -, and γ -tubulins. Of importance, α - and β -tubulins bind as heterodimers that assemble in protofilaments to form the microtubules. GTP hydrolysis by β -tubulin weakens the binding affinity of tubulin for adjacent molecules, thereby favoring depolymerization and resulting in their dynamic behavior (74, 75). This dynamic behavior is momentous because most microtubule-targeting drugs aim to suppress microtubule dynamics, as in the case of anticancer drugs that target microtubules to cease cell proliferation (76).

Bacterial and eukaryotic tubulins share functional properties that have been conserved through evolution. The first evidence for a bacterial homolog of tubulin came with the discovery of FtsZ, which is one of the best-characterized tubulin homologs in bacteria. It forms ring-shaped polymers (65, 77) and recruits, directly or indirectly, divisome components to provide a significant driving force for cell division (78). Due to its involvement in cytokinesis, FtsZ is considered the principal target of treatments regulating cell division in bacteria. Despite the low sequence similarity between tubulin and FtsZ, sharing only $\sim 10\%$ identity (70, 79), their crystal structures show near-identical protein folds (**Figure 10**) (80, 81).

While FtsZ is the most common tubulin homolog in prokaryotes. Almost all bacteria and archaea contain the tubulin homolog FtsZ due to its significant role in cell division. At least four other tubulin-like protein families have been identified with a restricted distribution in bacteria. For example, TubZ and RepX are *Bacillus* plasmid-encoded tubulin-like proteins that play essential roles in the stability of plasmids that encode them (82, 83). Similarly, monomeric TubZ has a very similar structure to α/β -tubulin (84) but forms right-handed helix filaments consisting of two protofilaments (**Figure 10**) (70, 85). On the other hand, BtubA and BtubB in *Prostheco bacter* (86) are much more similar in sequence to eukaryotic tubulins than FtsZ, TubZ, and RepX.

Only *Prostheco bacter* species have been shown to contain genes with higher sequence-homology to eukaryotic tubulin than FtsZ (87). These genes are the bacterial tubulin α homolog

(*btubA*) and bacterial tubulin β homolog (*btubB*), which have unknown physiological functions (88). The striking similarity of their structure with eukaryotic tubulin supports the hypothesis of their horizontal transfer from a eukaryotic host to *Prostheco bacter* (79, 88). Despite high sequence homology with eukaryotic tubulin, BtubA and BtubB possess different biochemical properties. Unlike eukaryotic tubulins, BtubA and BtubB have weak dimerization property and can fold easily without any chaperone (89). Nevertheless, both BtubA and BtubB protofilaments are GDP-bound and show a dynamic instability property like eukaryotic tubulin (90).

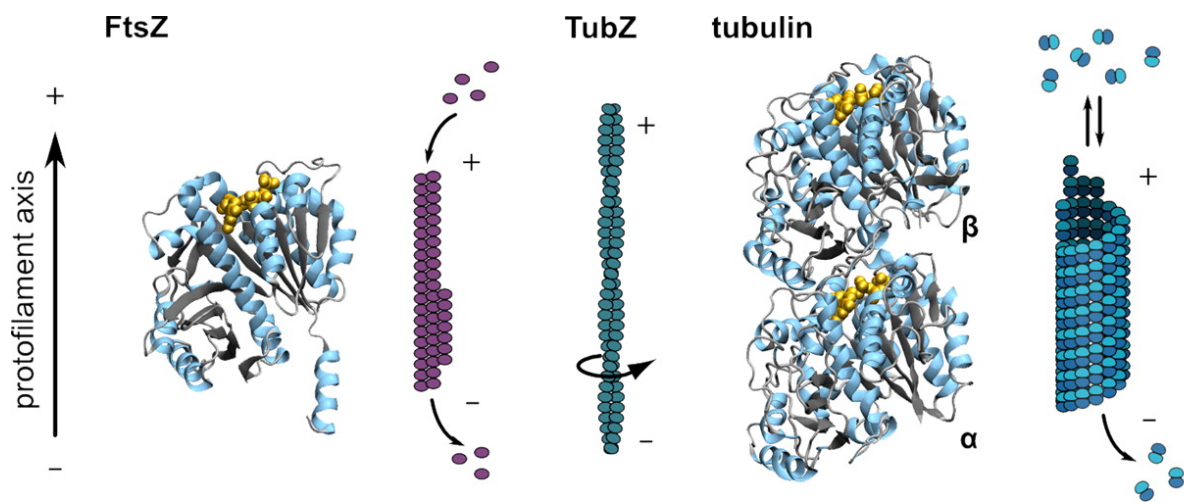


Figure 10. – Structural homology between prokaryotic and eukaryotic cytoskeletal intermediate filaments.

The prokaryotic cytoskeletal proteins FtsZ and TubZ show substantial structural conservation with eukaryotic tubulin. Adapted from Wickstead *B et al.*, 2011 (70).

1.2.3 Intermediate filament-like proteins in bacteria

Several types of IFs with similar sequence and structural characteristics exist in vertebrates and are involved in a broad range of functions. They were initially classified into five groups: (1) type I (acidic) keratins, (2) type II (basic) keratins, (3) vimentin and desmin, (4) α -internexin and

neurofilament proteins, and (5) lamins (91). Intermediate filaments (IFs) interact with multiple proteins and molecular factors that perform specific functions in different cell regions (92). While their proper assembly and function *in vivo* requires interaction with actin and tubulin (93), IFs can self-assemble *in vitro* without any association with other proteins (94). IFs acquired their name from their 10 nm diameter, which is intermediate between actin (~7nm) and tubulin (~25nm) diameters (91). In contrast to tubulin and actin that form long polarized filamentous structures, IF proteins form unpolarized structures of extended dimers(70).

IFs were first thought to be unique to animal cells (95) until the identification of IF homologs in bacteria (96, 97). CreS, or crescentin, is an IF protein found in the aquatic bacterium *Caulobacter crescentus* (98), where it forms helical filaments essential for the vibrioid or helical cell shapes of *Caulobacter*. In the absence of crescentin, *Caulobacter crescentus* lose their curved helical shape and adopt a rod morphology (98). While it has about 25% sequence identity and less than 50% similarity to eukaryotic IF proteins, crescentin is considered an IF protein-homolog in bacteria based on its predicted protein domain organization (98). Well-known for its fast assembly, the crescentin elastic filaments traverse the length of *C. crescentus* and share viscoelastic properties like that of eukaryotic IFs. Even though they form stiff dynamic filaments that maintain the curvature of *C. crescentus*, crescentin filaments differ from eukaryotic IFs in their poor mechanical resilience (99).

1.2.4 Actin-like proteins in bacteria

Bacterial actin homologs share an evolutionary conserved tertiary structure with the eukaryotic actins (**Figure 11**). They are considered actin homologs despite their low sequence similarities with eukaryotic actin, sharing only 13% primary sequence identity and less than 30% similarity (100). Five conserved motifs can be found in both eukaryotic and bacterial actin homologs. Three of these evolutionarily conserved motifs (phosphate 1, phosphate 2, and connect 1) share the typical actin structural fold, including the most conserved region of the actin ATPase domain (**Figure 11**) (100-102).

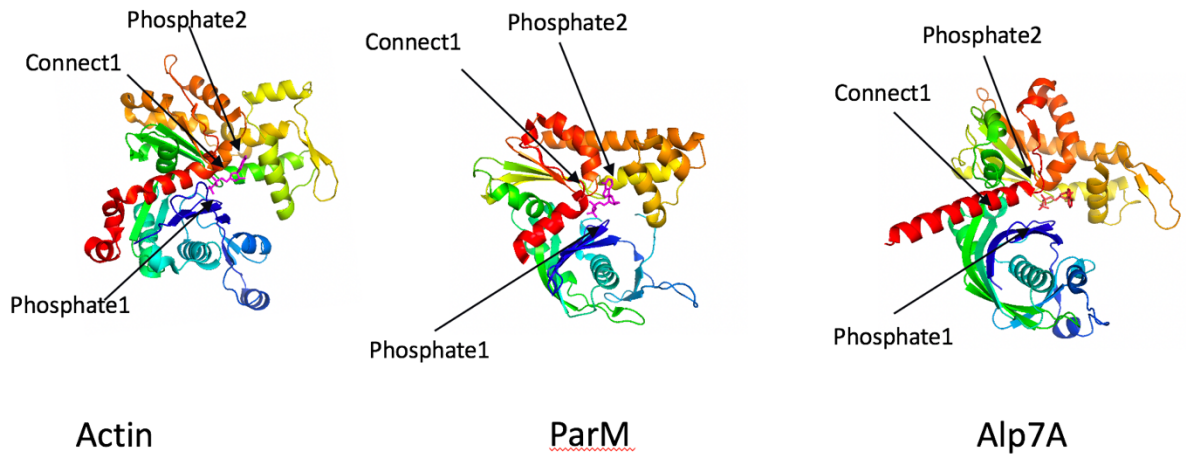


Figure 11. – Conserved tertiary structures of bacterial actin and actin.

The prokaryotic cytoskeletal proteins ParM and Alp7A exhibit considerable structural similarities with eukaryotic actin. The three proteins contain a connecting domain and two phosphate-binding domains.

Actin is one of the most abundant proteins in eukaryotic cells, and it exists either as a monomer (G-actin) or as a linear microfilament (F-actin) (103). ATP binding and hydrolysis regulates the transition between the two forms. This transition contributes to the rapid displacement of the filament due to extension at one end and shrinkage at the other, allowing the cell to remodel itself in response to external or internal stimuli (103). Eukaryotic and bacterial actins polymerize into dynamic filaments under the effect of regulatory proteins and nucleotide-induced conformational changes (81). The Dynamic actin filaments and are involved in various cellular activities ranging from cell shape determination to subcellular structure organization (**Figure 12**) (104).

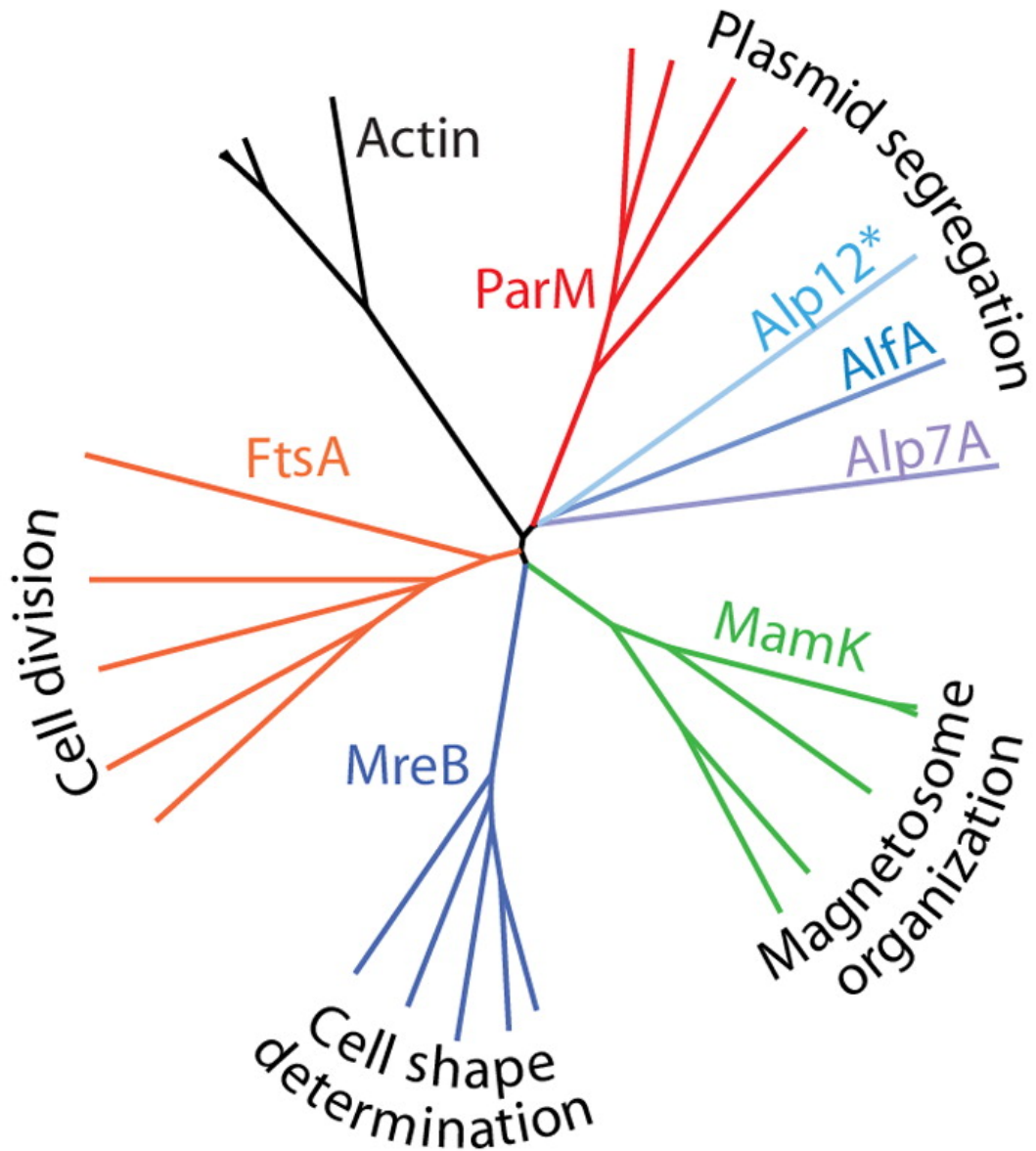


Figure 12. – Phylogenetic tree of bacterial actin.

Phylogenetic tree of actin-like proteins showing designated functions of characterized members.

Adapted from Ozyamak E *et al.*, 2013.

Bacterial actin-like proteins (Alps) are either encoded on chromosomal DNA or mobile genetic elements such as plasmids. The most known models of chromosomal encoded Alps are MreB, which is highly conserved Alps involved in cell shape determination. MreB assembles into

patches with properties different from eukaryotic actin filaments (105, 106). It plays a role in cell shape maintenance and defines the position of cell wall synthesis by forming a helical structure below the cell membrane(66). MamK is another type of bacterial Alp responsible for magnetosome organization in *Magnetospirillum* (107).

Alps encoded on mobile genetic elements are diverse and are involved in several cellular functions. They are grouped into thirty distinct families. For example, ParM and Alp7A represent two distantly related Alp families that play an essential role in plasmid segregation. Alp7A and ParM are involved in the segregation of the pLS20 plasmid of *Bacillus subtilis* and the R1 plasmid of *Escherichia coli*, respectively (100, 108).

1.2.5 Other members of the bacterial cytoskeleton

Several proteins that can polymerize into filaments were considered part of the bacterial cytoskeleton, despite being unrelated to the three primary eukaryotic cytoskeletal protein homologs (109). These proteins act as scaffold proteins that play regulatory and structural roles in maintaining bacterial cell organization.

Walker A cytoskeletal ATPases (WACAs) are filament-forming proteins encoded in most bacterial species and in archaea. WACAs are considered bacterial cytoskeletal proteins that lack eukaryotic homologs (81). ParA and MinD are WACA bacterial proteins involved in DNA segregation and division septum placement, respectively. ParA requires ATP to assemble into a filamentous structure, and its disassembly requires the accessory protein ParB that stimulates ATP hydrolysis. On the other hand, bactofilins are filament-forming cytoskeletal proteins, such as BacA and BacB, which localize to the stalk's pole and act as a molecular scaffold for stalk morphogenesis in *Caulobacter* (110).

1.2.6 Plasmid segregation in bacteria

The DNA of most bacteria exists as a single circular chromosomal DNA that interacts with several proteins and RNA molecules in the cytoplasm to form an irregularly shaped structure called

the nucleoid. Advances in the field of microbiology revealed that bacteria possess a complex genome arrangement. In addition to the single circular chromosome in bacteria, the bacterial genome may include multiple chromosomes and extra-chromosomal DNAs (111).

Some bacteria, especially antibiotic-resistant ones, may contain extra-chromosomal DNAs, called plasmids, which encode various genes involved in antibiotic resistance, detoxication, and bacterial virulence (112). Plasmids play a role in the spread of antibiotic resistance, which is considered a global health issue (113, 114). They range in size from less than 1 kilobase pairs (Kbps) to more than 1000 Kbps, and typically exist in a circular form. Plasmids are transmitted through horizontal gene transfer, thus affecting bacterial evolution by transmitting genetic material through bacteria from the same or different species (115). Some bacteria may contain multiple plasmids; the most common example is the pathogenic bacteria *B. burgdorferi* which causes Lyme disease and holds both linear and circular plasmids (116). Some bacteria can hold multiple plasmids, while others may lose plasmids with time or due to incompatibility (117). Plasmids contain a stretch of DNA that acts as an origin of replication, called replicon, allowing them to replicate independently within a cell. Small-sized plasmids exploit the host replicative enzymes to make copies of themselves, while larger plasmids may carry genes specific for their replication (118).

1.2.7 Plasmid segregation mechanisms

High copy number plasmids (50-800 plasmids per cell) segregate by cytokinesis, while low copy number plasmids (1-5 plasmids per cell) are usually transmitted by active segregation (119). The number of plasmids per cell is mainly regulated by the nature of its origin of replication. A good understanding of bacterial plasmid segregation may shed light on bacterial evolution. Besides, specific bacterial cytoskeletal proteins are considered a desirable target for medical treatments due to their involvement in plasmid segregation and maintenance of antibiotic resistance (100, 120). Such therapeutics generally help in reducing the distribution of antibiotic resistance genes.

1.2.7.1 Active segregation of plasmid

The most studied active segregation system in bacteria is the ParMRC system of the R1 plasmid in *Escherichia coli* (108). ParM, an actin homolog of 37.5 kDa, is located downstream of the gene encoding the adaptor protein ParR (13.3 kDa) and is surrounded by the centromere-like DNA region ParC (121). The segregation process starts with the attachment of the R1 plasmid from both ends by antiparallel protofilaments (**Figure 13**). Plasmid partition by ParM requires ATP hydrolysis, which is followed by the bi-directional growth of protofilaments to establish a stable filamentous structure. Finally, the ParM filaments disassemble when the plasmid reaches the end of the cell (122). Fluorescent microscopy of labeled ParMRC proteins showed that bound ParM monomers lead to the segregation of two R1 plasmids by adding monomers at the DNA-bound end of the protofilaments (123). ParM filaments are supposed to segregate plasmids in a sliding mechanism as suggested by their crystalline structure. Crystallization of the DNA-binding protein ParR revealed that the protein forms a tight dimer (124) and assembles into a helical array when binding to successive DNA repeats (125).

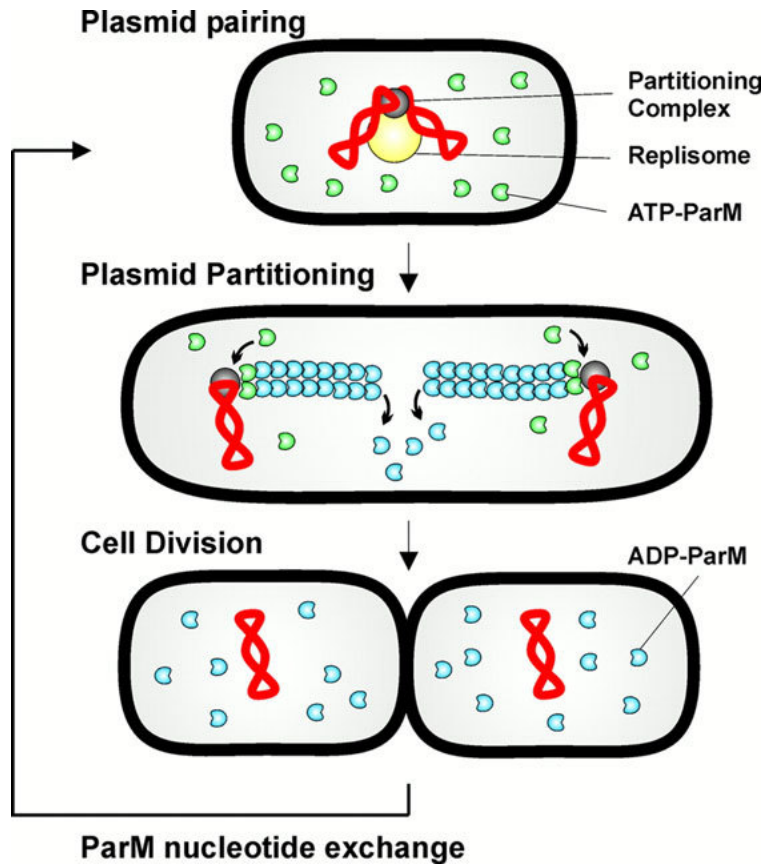


Figure 13. – A schematic representation of plasmid partitioning by ParM in *E. coli*.

Adapted from Moller-Jensen *et al.*, 2002 (121).

1.2.8 Alp7A

Since their discovery in 2001, studies have indicated that Alps in bacteria constitute 35 distinct families involved in various cellular functions (66, 100). Alp7A is one of the studied Alps, discovered by Derman *et al.* in 2009 (100). The bacterial *alp7A* gene is encoded by the plasmid pLS20 of the Firmicute bacterium *Bacillus subtilis* (*B. subtilis*) natto IFO3335 (100, 126, 127). The pLS20 plasmid encodes proteins involved in the transfer of the tetracycline resistance-coding plasmid pBC16 from wild type *B. subtilis* natto IFO3335 to other *Bacillus* species such as *B. cereus*, *B. thuringiensis*, and *B. subtilis* (128). The pLS20 plasmid is ~55 kbp long and is considered a conjugative plasmid in *B. subtilis*, where it plays an essential role in bacterial evolution by mediating horizontal gene transfer (129).

The *alp7A* gene is located downstream of *alp7R* gene in the *alp7ARC* operon. The *alp7A* gene encodes a 391 amino acid protein, whereas the *alp7R* encodes a small size DNA-binding protein of 134 amino acids with high charged residues. Alp7R binds specifically to the centromere-like region *alp7c*, which is considered a part of a tripartite operon (100, 130). Moreover, Alp7R was shown to control the function and cellular concentration of Alp7A protein (130). Like other plasmid segregation systems, the pLS20 origin of replication is located near the segregating operon (100).

1.2.9 Polymerization and function of Alp7A in bacteria

Investigations on Alp7A using fluorescent tags in *B. subtilis* and *E. coli* showed that Alp7A is localized in the cytoskeleton of bacterial cells (100, 130). In *Escherichia coli* (*E.coli*), Alp7A showed long filamentous structures that resemble actin filaments in eukaryotes without any auxiliary factors (100). Alp7A filaments were shown to span the cells when overexpressed in *E. coli* cells (**Figure 14**).

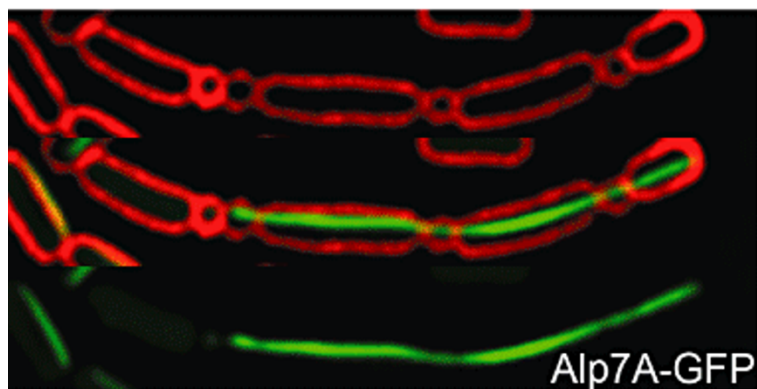


Figure 14. – Fluorescence microscopy image of Alp7A-GFP in *E. coli*.

Alp7A-GFP, green color, shows long filamentous structures that span the cells. *E. coli* cells are represented here in red color. Adapted from Derman Al *et al.*, 2009 (100).

In contrast to ParM, fluorescence light microscopy (fLM) on Alp7A polymers showed dynamic instability, suggesting different plasmid segregation mechanisms by these two bacterial actin homologs. The fLM analysis of *B. subtilis* cells expressing GFP-tagged Alp7A revealed filaments that possess treadmilling and dynamic instability properties. Treadmilling is the growth from one end of the filament, whereas dynamic instability is the filaments' growth and rapid shrinkage (131). These findings revealed a novel plasmid segregation mechanism by Alp7A in *B. subtilis*. Of importance, the stability of the plasmid (over 30 generations) relied on Alp7AR heterodimers (**Figure 15**) (100). Mutagenesis of Alp7A was performed to study the relationship between its filamentous structure properties and function. Based on the predictions of nucleotide-binding sites in Alp7A, several mutations were generated. Mutation E180A in the connect-1 site of Alp7A led to a static form of filaments (100), whereas mutation D212A in the phosphate-1 region of Alp7A prevented filament formation and only a diffuse signal could be observed under fLM.

Like actin and ParM, the function of Alp7A relies on its structure. Indeed, the lack of assembled filamentous structure was shown to affect the function of Alp7A. Besides, Alp7A was shown to be is afunctional in the absence of Alp7R protein and the *alp7c* sequence (130).

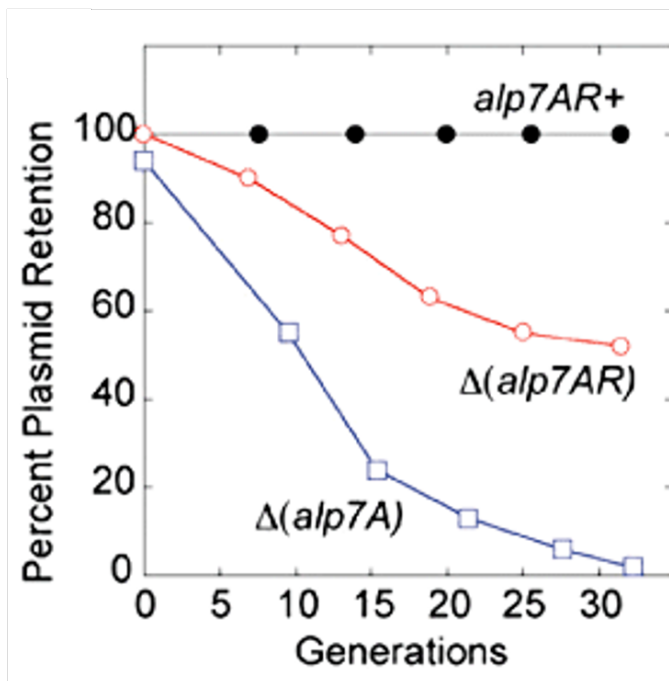


Figure 15. – Plasmid retention by Alp7AR in *B. subtilis*.

In the presence of Alp7AR, the plasmid is stable for more than 30 generations. In the absence of Alp7A or Alp7AR, the number of plasmids decreases over generations. Adapted from Derman Al *et al.*, 2009 (100).

1.3 Justification of methods used for the detection of bacterial ultrastructure

During this doctorate, we combined molecular biology, biochemistry, and structural biology techniques to characterize bacterial ultrastructure *in vivo* and *in vitro*.

1.3.1 Microscopy

Microscopy is the field that uses microscopes to visualize and investigate small objects that can't be seen by the naked eye. Advances in microscopy have revolutionized biology, particularly the field of microbiology. There are three main branches of microscopy: optical, electron, and scanning probe microscopy. Different techniques are used to detect, visualize, and characterize bacteria and bacterial substructures. Here, I will describe the techniques used in my investigations.

1.3.1.1 Light and Phase contrast microscopy

Light microscopy (LM) is a powerful method for imaging biological cells. Biological sample structure is revealed under LM due to modifications in the refractive index that scatters light. However, under certain circumstances, variations between the refractive index of biological structures and their surrounding matrices can be reduced, leading to a limitation in structure detection. With the invention of phase-contrast microscopy by Zernike in 1934, this limitation was solved (132).

Phase contrast microscopy is a technique that uses LM to show high-contrast images of samples such as cell cultures, microorganisms, and subcellular structures. By this technique, samples can be used in their native state (i.e., unlabeled, not fixed, and unstained). The phase contrast technique applies changes in phase comparable to amplitude, which reveals structural features as difference in contrast in the imaged specimen.

1.3.1.2 Cryo-electron tomography (cryo-ET)

Cryo-electron tomography (cryo-ET) is an advanced approach of electron microscopy (EM) used to explore cellular ultrastructure and macromolecules. Cryo-ET experiments are executed under cryogenic condition to preserve the liquefied samples and their structural integrity (133). The sample preparation for cryo-ET employs plunge freezing in liquid ethane or ethane-propane mixture without any chemical treatment (134). With cryo-ET, cells and molecules are preserved in their natural hydrated intact state free of artifacts that result from plastic embedding, chemical fixation, or dehydration used in traditional EM sample preparation (133). The revolution in EM technology helped improve the resolution to ~4nm, where the data are collected with robust full digital and direct electron detection cameras (135). With cryo-ET approach 2D projection images are recorded in tilt series (i.e., 0° to -60°, and 0° to +60°) to be 3-D reconstructed with subtomogram averaging (136).

1.3.1.3 Correlative light and electron microscopy (CLEM)

Identifying structures within a complex cellular milieu can be challenging. By correlative light-electron microscopy, localization of subcellular structures is more manageable and grants more accurate analysis. The samples can be imaged with LM under ambient temperature or frozen conditions, depending on the experimental aim and the nature of the biological sample. EM “finder” grids with featured letters and numbers are used to localize subcellular targets during each experiment. After sample loading on EM finder grids, imaging with LM under cryogenic or ambient temperatures allows the identification and localization of targets on the grid. Grids are then loaded onto TEM for high-resolution tomograms acquisition of the specified targets. Such experimental approach allows for the accurate identification of subcellular structures using LM, then imaging of the same structures at high resolution using EM. For example, one can label a protein of interest with a fluorescent tag, which can be easily identified by fLM, then correlate its ultrastructure with EM.

1.3.1.4 Scanning electron microscopy (SEM) and energy-dispersive x-ray analysis (EDX)

SEM provides detailed high-resolution images of the surface of a specimen. This technique was considered challenging to the microbiology field due to difficulties in sample preparation

protocols that require chemical treatment to increase the specimen's conductivity. Indeed, bacterial imaging requires a moisture medium that is considered challenging for this technique because it reduces the contrast of the image and limits the microscopy performance (137).

Energy Dispersive X-ray (EDX) is a powerful technique used in several fields such as biomedical and clinical research. EDX technique provides qualitative and quantitative information on a specimen's composition. This technique reveals the types and amounts of elements in the targeted specimen. Microorganisms are particularly suitable for such analytical approach due to their delicate nature.

1.3.1.5 Single particle electron microscopy (EM) of macromolecules

Single particle EM is a method to determine the structure of macromolecules. The macromolecules display different orientation when loaded onto an EM grid for imaging. With this method imaging of macromolecules can be attained under ambient temperature (negative stain) or under cryogenic temperature with no chemical artifacts (138). Single particle analysis is applied to analyze the collected TEM projection images of macromolecules by averaging hundreds to thousands of EM projections, same orientation, to ameliorate signal-to-noise ratio. This technique can attain near-atomic resolution that would help investigate the structure of a protein. The method uses 2D projection images of the sample to reconstruct a 3D density map (139). When a protein complex is purified and loaded onto an EM grid, the complex falls onto the grid in different orientations. Data is collected on thousands of particles, then classified by computational methods to reconstruct the different forms of the protein complex. Because of the demanding nature of this method, it is recommended to perform preliminary validation of the purified protein of interest before proceeding with the technique.

1.3.2 Phenotypic methods

Phenotypic methods rely on using treatment protocols to identify specific biochemical and biophysical characteristics of bacteria and their substructures.

1.3.2.1 Dipicolinic acid (DPA) detection

DPA is a unique and significant component of mature endospores (31). During the sporulation process, DPA is produced in the mother sporulating cell then delivered into the developing spore (31). Thus, detection of DPA would indicate the presence of mature endospores in bacterial cultures.

1.3.2.2 Heat resistance of mature endospores

Heat resistance is considered a hallmark feature of spores. The spore's coat has been shown to play a role in spore's heat resistance. During the dormant state, spores are dehydrated and do not show metabolic activity, enabling them to withstand extreme environmental conditions such as high heat(140). Under adequate nutritional conditions, spores are capable of germinating again. In contrast, vegetative cells will not be able to survive and proliferate after heat treatment.

1.3.2.3 Differential staining of bacterial spores

Differential staining is a method widely used by microbiologists to identify whole cells or cellular substructures such as endospores. A typical differential staining method is Gram staining to distinguish between Gram-negative and Gram-positive bacteria. Acid-fast staining is another well-known differential staining method to detect bacteria and bacterial subcellular structures with resistant property to decolorization by acids. The ability to resist decolorization with acid alcohol confers acid fastness to the bacterium or its substructures. For example, *Mycobacteria* contain high concentrations of mycolic acid in their cell wall (141), which prevents non-acid fast dyes, such as crystal violet, from penetrating easily into the bacterium. Once inside the wall, the cells will not de-stain or decolorize easily. The high concentrations of dye (e.g., crystal violet) used to stain these bacteria will be retained and appear pale purple that is hard to analyze. On the other hand, acid-fast dyes can easily penetrate these bacteria, which would facilitate the staining at lower concentrations, and hence, improve the visualization and detection of these bacteria.

2 Objectives and hypothesis

Bacteria play vital roles in the environment and in both health and disease of humans and other organisms. Infectious diseases caused by bacteria are among the top ten leading causes of death worldwide, particularly in lower- and middle-income countries (WHO fact sheet, 2021). Therefore, understanding bacterial mechanisms of infection and survival is essential to identify new targets in the ongoing fight against infectious disease and resistance to therapy. In this thesis we were interested in investigating two bacterial survival and resistance mechanisms: endospore formation and segregation of plasmids encoding antibiotic resistance genes.

2.1 Project 1: Characterization of phase-bright objects in members of Proteobacteria and Actinobacteria

Endospores represent a dormant state of bacteria that enables them to withstand extreme conditions and persist for years. Endospore formation is unique to members of the phylum Firmicutes; however, recent studies have reported endospore formation in three bacterial species that belong to other phyla: *R. johrii* and *S. marscescens* from the phylum Proteobacteria, and *M. marinum* from the phylum Actinobacteria (34, 35, 47). Such studies suggest a wider spread of endospore formation that could have contributed to the diversification and speciation of modern phyla (15). Indeed, sporulation involves tight cooperation of hundreds of genes distributed across the chromosome, hindering acquisition of this pathway through horizontal gene transfer (15, 142, 143). Therefore, if confirmed, presence of the ability to form endospores across distantly related bacterial phyla suggests an ancient nature of the process and can provide clues to the characteristics of the last bacterial common ancestor (15). Thus, confirmation and further characterization of endospore formation in these organisms can bring valuable insight into the physiology of these species and the role of endospore formation in diversification and speciation of modern phyla.

Mature endospores, storage granules, and dense accumulation of cellular debris may appear phase-bright when imaged with phase-contrast light microscopy (LM). Three studies detected

phase-bright objects using phase-contrast LM in *R. johrii*, *S. marcescens*, and *M. marinum* (34, 35, 47). In the three studies, TEM was used to provide high-resolution images of plastic-embedded sections of bacterial cells, which showed features of putative endospore structures. The authors concluded that the features observed with TEM were endospores. Misinterpretations of inclusion bodies could result from sample preparation artifacts in these studies. An alternative approach would be the use of cryogenic methods, such as cryo-ET, which can preserve cellular ultrastructure near native state. In addition to LM and EM imaging approaches, the authors implemented microbiology techniques to validate the presence of endospores in the three species. Since endospores can survive heat treatment, the authors of the three studies were able to detect viable cells after heat treatments at temperatures where vegetative bacterial cells could not survive. No experiments were applied to determine the composition of the observed phase-bright objects.

We hypothesized that the phase-bright objects visualized in *R. johrii*, *S. marcescens*, and *M. marinum* are not endospores and could potentially be storage granules or cellular debris. To test this hypothesis, we aimed to reproduce the experiments done in the three studies and investigate the structure and composition of the phase-bright objects using advanced microscopy and analytical approaches. Our main objectives are:

1. Determine the structure of the observed phase-bright objects using cutting-edge microscopy techniques such as correlative light electron microscopy (CLEM) and cryo-electron tomography (cryo-ET).
2. Characterize the composition of the phase-bright objects using analytical approaches such as Energy Dispersive X-Ray (EDX) and lipidomics.

2.2 Project 2: Characterization of Alp7A structure *in vivo* and *in vitro*

Studying bacterial Alps highlights bacterial actins' plasticity and their evolutionary role in developing novel cellular functions. Many Alps are considered primary factors for the independent segregation and stability of plasmids encoding antibiotic resistance genes. Hence, the study of Alps and their role in plasmid segregation would contribute to the therapeutic targeting of antibiotic resistance.

Recent studies have identified Alp7ARC as a novel plasmid segregation mechanism in *B. subtilis* (100, 130). This segregation machinery employs the bacterial actin homolog Alp7A to segregate the tetracycline resistance encoding-plasmid pLS20. The gene encoding the bacterial actin is found upstream of Alp7R, predicted to encode a DNA-binding protein. The stability of the plasmid in cells was shown to be dependent on the Alp7ARC, indicating an essential role in plasmid segregation.

Our preliminary investigation showed that Alp7A assembles into a novel tubular nanostructure. This is of particular interest because most bacterial Alps are known to form filaments inside the cells. We hypothesized that Alp7A segregates pLS20 in *B. subtilis* via a novel mechanism. We aimed to study Alp7A using cutting-edge microscopy techniques. Our objectives in this project were to:

1. Determine the native structure of Alp7A in *B. subtilis in vivo*. For this, we used mutant *B. subtilis* (Δ ponA) transformed with mini-pLS20 plasmid constructs coding for Alp7ARC machinery or GFP-tagged Alp7A. Imaging of Alp7A *in vivo* started by visualization of GFP-tagged Alp7A in *B. subtilis* under fLM. Multiple biochemical approaches were then used to validate the expression of Alp7A before applying CLEM and cryo-ET for a higher resolution imaging.
2. Characterize the structure and function of Alp7A *in vitro*. We specifically aimed to visualize the structure of Alp7A using cryo-EM in the presence or absence of ATP *in vitro*. We used different Alp7A constructs and applied several purification methods, including affinity chromatography, size exclusion chromatography and ammonium sulfate precipitation.

3 Materials and Methods

3.1 Project 1: Characterization of phase-bright objects in members of Proteobacteria and Actinobacteria

3.1.1 Bacterial growth conditions

R. johrii and *S. marcescens* cells were purchased from Leibniz-Institut DSMZ bacterial strain collection. *R. johrii* JA192 cells (DSM 18678) were grown as previously described by Girija *et al.* (35). Briefly, cells were grown aerobically at room temperature in *R. sphaeroides* medium consisting of 4 mM KH₂PO₄, 1 mM MgCl₂·6H₂O, 7 mM NaCl, 22 mM NH₄Cl, 0.04 mM CaCl₂·2H₂O, 17 mM sorbitol, 28 mM sodium pyruvate, 1.5 mM yeast extract, 1L distilled water, 1 ml Trace element solution SL7, and 20 ng Vitamin B₁₂ solution. *S. marcescens* cells (DSMZ 30121) were grown in Luria-Bertani (LB) broth medium at 32 °C with shaking at 200 rpm as previously described by Ajithkumar *et al.* (34). For *M. marinum* bacteria, strain ATCC 927, were grown under two different conditions. They were grown on plates containing either: 1.5X Luria-Bertani (LB) broth composed of 3g tryptone, 1.5g yeast extract, 3g NaCl, and 200mL H₂O, pH 7.5; or 7H10 agar plates supplemented with 0.5% glycerol and 10% oleic acid-albumin-dextrose complex (OADC) at 30 °C. *B. subtilis* strain 168 bacteria were used as a positive control for endospore formation and were grown in LB at 37°C with continuous shaking at 200 rpm.

3.1.2 Phase contrast microscopy

Mature endospores appear phase-bright when imaged with phase-contrast microscopy. To detect potential endospores, *R. johrii*, *S. marcescens* and *M. marinum* cells displaying phase bright objects were collected, washed with 1x phosphate buffer saline (PBS pH 7.4) composed of 137 mM NaCl, 27mM KCl, 10 mM Na₂HPO₄, 1.8 mM KH₂PO₄, and spotted onto a microscope slide. Cells were visualized using an upright Zeiss Axio Imager M2 Optical Microscope (Carl Zeiss, Oberkochen, Germany) 506 monochrome camera, oil objective lens 100x / 1.46 NA.

3.1.3 Cryo-electron tomography (cryo-ET)

To characterize the bacterial cells and their ultrastructure in a near-native state we used cryo-ET (133, 144). *R. johrii*, *S. marcescens*, *M. marinum* and *B. subtilis* cells were loaded onto a glow-discharged quantifoil-Cu Finder R 2/2 electron microscopy (EM) grids, supplied with 20-nm colloidal gold as fiducial markers (Sigma-Aldrich). EM grids were plunge-frozen in a liquid ethane-propane mixture kept at liquid nitrogen temperatures using an automated vitrification device (Vitrobot, ThermoFisher Scientific, Waltham, USA). Subsequently, grids were loaded onto autogrids for cryo-ET data collection. Tilt-series were collected on an 300kV Titan Krios (ThermoFisher Scientific) equipped with a Falcon 2 camera at the FEMR facility at McGill University. Typically, tilt series were collected at 18-22.5 Kx magnification, with 1 to 3 degrees oscillations and a final dose of 30-150 e^-/A^2 . Three-dimensional reconstructions were calculated with IMOD using the weighted back-projection method (145).

3.1.4 Correlative light and electron microscopy (CLEM)

The nature of the phase-bright objects observed in *R. johrii* and *M. marinum* was investigated using CLEM, which correlates the LM data with cryo-ET. Cells were lightly fixed using 2.5 % paraformaldehyde in 30mM phosphate buffer to facilitate correlation and minimize the cells' movement on the EM grid. After 15 minutes of incubation, cells were washed twice with 150 mM phosphate buffer and resuspended in 150 mM phosphate buffer. Fixed bacterial cells were loaded onto Cu Finder R 2/2 EM grids (EMS, Hatfield, USA) coated with 1 mg/ml poly-L-lysine, then imaged at room temperature using an upright Zeiss Axio Imager M2 Optical Microscope (Carl Zeiss, Oberkochen, Germany) equipped with 506 monochrome camera, 100x oil objective lens, Phase 3, NA 1.46. Once grid maps were obtained with LM, 20-nm colloidal gold (Sigma-Aldrich) was added to the cells, and the grids were cryogenically preserved as described above. The EM grids were loaded onto autogrids for cryo-ET data collection. For the CLEM experiment, the same cells that appeared phase-bright under LM were identified in the EM, and tilt series were collected on those cells.

3.1.5 Scanning electron microscopy (SEM) and energy-dispersive x-ray analysis (EDX)

R. johrii cells were fixed by 12.5% paraformaldehyde in 150mM sodium phosphate buffer (73.6 mM K₂HPO₄, 26.4 mM KH₂PO₄) pH 7.5, then washed three times with 150mM sodium phosphate buffer (146). Glow-discharged copper quantifoil R2/2 grids were coated with poly-L-lysine hydrobromide solution (1mg/ml) and dried for 30 mins at 60 °C. Fixed cells were loaded onto the grids and immediately imaged in 1x PBS to prevent any sample dryness. Images were collected with an oil objective lens 100x/ 1.46 NA on Carl Zeiss microscope. The grids were subsequently air-dried and examined using JEOL JSM-7400F (JEOL Ltd., Tokyo, Japan) operated at 5 kV without any coating. EDS with a silicon-drift detector (Octane, EDAX Inc., Mahwah, NJ, USA) at 10 kV was used for elemental analysis of regions of interest.

3.1.6 Dipicolinic acid (DPA) detection

The presence of DPA was measured at time-points when phase-bright objects were detected: day 7 for *R. johrii*, day 65 for *S. marcescens*, days 3, 7, and 14 of *M. marinum*, and day 7 for *B. subtilis* (positive control). For the DPA detection, all cultures were treated similarly after a spore-purification protocol and measurements were performed using a standard colorimetric assay (147). Since autoclaving releases DPA, 5 ml of the suspensions of *R. johrii*, *S. marcescens*, *M. marinum* and *B. subtilis* containing ~ 10 mg (dry weight) were autoclaved for 15 minutes at 15 lb/in². The suspension was cooled to ambient temperature, acidified with 0.1 ml of 1.0 N acetic acid, and incubated for 1 hour to cluster the insoluble material. To remove cellular debris, the suspension was centrifuged at 1500 x g for 10 minutes. To every 4 ml of supernatant, 1 ml of 1 % of Fe (NH₄)₂(SO₄)₂•6H₂O and 1 % of ascorbic acid in 0.5M acetate buffer (pH 5.5) was added. DPA induces color change that can be detected at 440 nm. All the samples were measured for changes in optical density at 440 nm within 2 hours of the experiment. A similarly treated suspension was used as a blank in which 1 ml of water was substituted for the color reagent. A standard curve was achieved using the commercially available DPA (Sigma-Aldrich) (147).

3.1.7 Heat resistance of mature endospores

After induction of the phase-bright objects in *R. johrii*, *S. marcescens*, and *B. subtilis* (positive control), cells were washed with sterile, deionized water, spun at 10,000 x g for 10 min, and resuspended in chilled water. As published previously, the suspensions of *R. johrii* and *B. subtilis* were wet heated at 80 °C, and *S. marcescens* was heated at 65 °C for 15, 30 min, and 1 hr to kill any vegetative cells (34, 35). And *M. marinum* cells were harvested after 3, 7, 14, and 30 days of growth, respectively. The cells were divided into four aliquots, 3 of which were exposed to heat shock at 65 °C for 15, 30, and 60 min, respectively, while the fourth aliquot was not exposed to heat shock. Since spores are resistant, heat treatment would be survived by mature endospores only. After heat treatment, samples were centrifuged for 10 min at 10,000 x g. The pellets were washed five times to remove contaminating cellular debris and plated on agar plates. Plates were then incubated at 30 °C for *R. johrii*, 32 °C for *S. marcescens*, and 37 °C for *B. subtilis* to check cell recovery of heat-resistant spores. On the other hand, *M. marinum* pellet was plated at 30 °C on 1.5x LB and 7H10 agar plates supplemented with 0.5% glycerol and 10% OADC (148). The agar plates were incubated for 7 days (for *R. johrii*, *S. marcescens* and *M. marinum*), and overnight (for *B. subtilis*), a sufficient time for all species to undergo germination and resume vegetative growth.

3.1.8 Differential staining of bacterial spores

R. johrii and *B. subtilis* cells were heat-stained with 5% malachite green, washed with water, and counterstained with 2.5% safranin, and crystal violet respectively (149). The *M. marinum* cells were grown as mentioned above at 30 °C for 3 and 14 days, then subjected to acid-fast staining using Ziehl-Neelsen (149). *B. subtilis* was used as a positive control in this experiment. Cells were heat-fixed on microscopic slides, heat-stained with malachite green (5% wt/vol in water), washed with water, and counterstained with crystal-violet (2.5% wt/vol in ethanol) (150). The samples were subsequently washed with water, and cells were visualized using an upright Zeiss Axio Imager microscope equipped with an Axio 506 monochrome camera and an oil objective lens 100x/1.46 NA.

3.1.9 Whole cell lipidomic analysis of *R. johrii*

Lipidomic analysis relies on the use of mass spectrometry for the identification and quantification of subcellular lipids. This technique can analyze complex lipids; however, it is sensitive to the quality of lipid extracts. For complex lipids, methyl-*tert*-butyl ether (MTBE) is the optimal solvent used, instead of chloroform, for better extraction quality. Usage of this organic compound in whole cell lipidomic analysis insures fast, simple, and pure lipid extraction (151).

R. johrii cells displaying phase-bright properties were obtained as described above. As a negative control, *R. johrii* grown in LB for 2 days and lacking phase-bright objects were used. The whole-cell lipidomic analysis with MTBE-based membrane lipid extraction protocol (151) was used with modifications. Briefly, samples in 1.5 mL Eppendorf vials were first mixed with 300 μ L ice-cold methanol and 10 μ L internal standards. The mixture was then sonicated in an ice-water bath for 15 min for protein precipitation. One mL MTBE was added to the mixture, followed by vortex mixing for 20 min at room temperature for thorough lipid extraction. Next, 200 μ L LC-MS grade water was added to induce phase separation, and the samples were further mixed for 30 s. After settling for 10 min, the upper layer containing the lipids was transferred to new Eppendorf vials. The solvent was evaporated to dry the lipid samples using a vacuum concentrator at 4 °C. 100 μ L isopropanol/acetonitrile (1:1, v/v) was added to reconstitute the dried residue. The reconstituted solution was vortexed for 30 s and centrifuged at 14000 rpm at 4 °C for 15 min. The resulting supernatants were transferred to glass inserts for liquid chromatography-tandem mass spectrometry (LC-MS/MS) analysis. Only lipids above the noise level (1000 average intensity) were considered in the analysis.

3.1.10 Detection of genes required for endospore production

We compiled a list of genes associated with sporulation using the Clusters of Ortholog Genes (COGs) database (5, 42). We then screened the genomes of *S. marcescens* subsp. *sakuensis* KREDT (35), and *Rhodobacter johrii* JA192 (34) for corresponding KEGG (152), and TIGRFAM (153) (hidden Markov models (HMMs) of these genes using HMMER 3.2.1) (154). Genes without representative HMMs were identified using local alignment against sequences from *B. subtilis* 168

and *Clostridium perfringens* SM101 using a minimum percent identity of 30% and an E value of 1E-25. *B. subtilis* 168 (monoderm sporulator), *Acetonea longum* DSM 6540 (diderm sporulator), and *Escherichia coli* DSM 30083 (diderm non-sporulator) were included as sporulating and non-sporulating controls.

3.2 Project 2: Characterization of Alp7A structure *in vivo* and *in vitro*

We studied the structure of Alp7A *in vivo* and *in vitro* in *B. subtilis* and *E. coli* using a combination of structural, molecular, and biochemical approaches.

3.2.1 Plasmid constructs for investigating Alp7A *in vivo*

The wild type *B. subtilis* has a diameter of ~1.5 µm, which is inadequate for cryo-ET that requires samples with thickness <0.5 µm. Hence, a mutant *B. subtilis* (Δ *ponA*) generated by Dr. Pogliano's lab was used in this study (27). The mutation in the *ponA* gene, encoding a class A penicillin-binding protein (PBP1), showed no effect on cell morphology and division of the slender mutant of *B. subtilis* (27). To determine the *in vivo* structure of Alp7A, three strains of *B. subtilis* were generated by transforming the slender mutant using three mini-pLS20 plasmid constructs: (1) *B. subtilis* strain 3266 (Δ *alp7AR*), containing a mini-pLS20 plasmid with the origin of replication and lacking *Alp7AR* operon; (2) *B. subtilis* strain 3267 (Alp7A-GFP), containing a mini-pLS20 plasmid encoding Alp7A tagged with GFP at its C-terminus to visualize and localize the intracellular filaments under fLM, cryo-ET, and CLEM; and (3) *B. subtilis* strain 3268 (*alp7ARC*), containing a mini-pLS20 with the *alp7ARC* operon, which was used as a positive control to investigate the native structure of Alp7A under cryo-EM (100).

The mini-pLS20 plasmid was constructed by Dr. Derman (UCSD). Briefly, they applied PCR amplification of *B. subtilis* natto strain IFO3335 (BGSC 27E1) genomic DNA (127), with the following primers:

5'-CTGTAATGCATTCATTAGCCTCCAATCTTATAGTGAAACTCCGCAAACCTTC-3' and 5'-GTACTGCTAGCGTTGCTCAGGGCGTCTGTGTTG-3.'

The product was ligated to plasmid pHW1520 between NsiI and NheI restriction sites, after cutting the amplicon with the corresponding restriction enzymes as described by Derman *et al.* (100).

3.2.2 Cell culture preparation

B. subtilis slender mutant strains were taken from a frozen glycerol stock and grown at 30 °C on agar plates (2g LB, 1.5g agar, and 100 ml dH₂O) supplemented with 10 µg/ml tetracycline (100, 155). A single colony of each strain was dispersed in LB culture supplemented with 10 µg/ml tetracycline and incubated overnight at 30 °C with shaking at 200 rpm. The following day, each culture was diluted (1/100) to an OD₆₀₀ between 0.5 and 0.7, then induced with 0.5% xylose (100).

3.2.3 SDS-PAGE and Immunoblotting of Alp7A-GFP

Sodium dodecyl sulfate-polyacrylamide gel electrophoresis (SDS-PAGE) was performed to detect Alp7A protein at its expected molecular weight of ~45 kDa. After 3 to 4 hours of *B. subtilis* cells induction with 0.5% xylose, cells were lysed in Laemmli buffer at 95 °C for 5 minutes. The lysates were run on SDS-PAGE gel and stained with 0.1% Coomassie Brilliant Blue R-250 (156).

For western blot analysis, the SDS-PAGE gel was equilibrated for 10 minutes in Towbin transfer buffer (25 mM Tris, 192 mM glycine pH 8.3, 20% MeOH) and transferred to a wet polyvinylidene difluoride (PVDF) membrane. After transfer, the membrane was blocked for 1hr at room temperature using 5% fat-free dry milk in Tris Buffer Saline (TBS)- Tween 20 solution (TBST; 0.05M Tris-HCl, pH 7.5; 0.15M NaCl, 0.1% Tween 20). Subsequently, the PVDF membrane was incubated with the primary antibody (anti-GFP, Sigma, 1:1000 in TBS) for 1 hour with shaking (157). The PVDF membrane was then washed three times with TBST (8 min each) and incubated with HRP-conjugated Goat anti-mouse IgG (Biorad) for 1 hour at room temperature. The PVDF membrane was washed three times with TBST and one time with TBS (50mM Tris, PH 7.6; 0.2% NaN₃, 150mM NaCl), then revelation was performed in the dark with HRP substrate (12mg 4-chloro-1-naphthol diluted in 4 ml of methanol, 16 ml of TBS, and 100 µl H₂O₂).

3.2.4 Fluorescence microscopy of Alp7A-GFP

After induction with 0.5% xylose, *B. subtilis* cells (strain 3267) were harvested by centrifugation for 5 mins at 13200 rpm (Beckman Coulter 20R microfuge). After discarding supernatant, the pellet was resuspended in ~15% of the remaining supernatant volume, and a 3 μ l drop of the resuspended pellet was added to a poly-L-lysine-coated microscope slide. FM4-64 dye (Molecular Probes, Invitrogen) was used to stain bacterial membranes in red color and was added to a final concentration of 2 μ g/ml. The FM4-64 dye was either added to the suspension or added directly to the microscope slide (130). The cells on the slide were covered with a coverslip then visualized using an upright Zeiss Axio Imager M2 Optical Microscope (Carl Zeiss, Oberkochen, Germany), Axiocam 506 monochrome, oil objective lens 100x /1.46 NA.

3.2.5 Cryo-ET of Alp7A-GFP and Alp7ARC in *B. subtilis*

Cryo-ET was used to characterize the structure of Alp7A in its native-state at high resolution. Visualization was performed on *B. subtilis* strain 3267 either treated or not with lysozyme at 200 μ g/ml for five minutes. No lysozyme treatment was performed on strain 3268. *B. subtilis* cells were loaded onto a glow-discharged gold grids (Au R 2/2, Quantifoil, (EMS, Hatfield, USA), supplied with 20-nm colloidal gold as fiducial markers (Sigma-Aldrich). EM grids were plunge-frozen in a liquid ethane-propane mixture at liquid nitrogen temperature. Grids were imaged and cryo-ET data collected using a 300 kV Titan Krios (ThermoFisher Scientific) equipped with a Falcon 2 camera at the Facility for Electron Microscopy Research (FEMR) at McGill University. Tomograms were collected at 18 Kx magnification. Images were processed and 3D reconstructed using IMOD software.

3.2.6 CLEM of Alp7A-GFP

CLEM was used to facilitate the localization and validate the identity of the observed filaments. *B. subtilis* strain 3267 cells were grown and induced with 0.5% xylose as mentioned above. Cells were fixed by 2.5% paraformaldehyde in phosphate buffer saline (PBS) (137 mM NaCl, 2.7 mM KCl, 10 mM Na₂HPO₄, and 1.8 mM KH₂PO₄, PH 7.4). Afterward, cells were washed three times with PBS and re-suspended in fresh PBS solution. Fixed cells were loaded onto

gold finder grids (Au NH₂ R 2/2, Quantifoil (EMS, Hatfield, USA)) coated with 1 mg/ml poly-L-lysine.

After loading the sample on the grids, 20-nm colloidal gold (Sigma-Aldrich) was added as fiducial markers. Then, cells were plunged frozen in ethane/propane mixture and imaged by fLM, using a Linkam cryo-stage (CMS196), which maintains samples vitrified in liquid nitrogen (-196 °C). The cells on the Au R 2/2 Quantifoil EM grids were visualized using an upright Zeiss Axio Imager M2 Optical Microscope Axiocam 506 monochrome, air objective lens 100x /1.46 NA (Carl Zeiss, Oberkochen, Germany). Photomicrographs were obtained with EGFP channel excitation at 448 nm and emission wavelengths between 500 and 600 nm. Cryo-ET data was collected at 14 Kx magnification, with 1 to 3 oscillation degrees and a final dose of 30-110 e⁻/Å². Three-dimensional reconstruction was performed using IMOD software.

3.2.7 Conventional resin section of Alp7A-GFP for TEM

The preparation of *B. subtilis* for the conventional resin sectioning was challenging due to its thick cell envelop and being liable to technical artifacts. After cell growth and induction of Alp7A-GFP, 2 to 3 ml of cells were harvested by centrifugation to obtain a pellet. A 1 ml of 4% paraformaldehyde (PFA, pH 7.3) (BDH; Toronto, ON, Canada) and 0.1% glutaraldehyde (Electron Microscopy Sciences; Washington, PA) was added to the pellet, then stored at 4 °C for 20 minutes. After centrifuging at 13200 rpm, the supernatant was discarded, and the pellet was rinsed with 0.1 M phosphate buffer (PB, pH 7.2) for 5 min then centrifuged; this step was repeated 4 times. Subsequently, the cells were fixed by adding 1% osmium for 30 mins. Fixation solution was discarded after centrifugation for 20 seconds at 13200 rpm. Next, dehydration was done by adding alcohol at different concentrations (30%, 50%, 70%, 80%, 95%, and 100%) for two rounds every 15 mins and centrifugation applied between each step. Samples were incubated overnight in a 1:1 mixture of 100% ethanol (ETOH) and 100% LR white resin (London Resin Company; Berkshire, UK). The incubated sample were then centrifuged, and mixture 2 of 2:6 of 100% ethanol (ETOH) and 100% LR white resin was added to the pellet for 1 hour at 4 °C. After centrifugation, the pellet was incubated in 1 ml of 100% LR white resin for 1 hour. This step was repeated 3 times. After harvesting the pellet, polymerization started by encapsulating the samples with 100% LR white resin at 60°C for 2 to 3 days (158, 159). Afterward, samples were cut using a diamond knife into

sections with thickness ranging between 70 nm and 72 nm. Sections were loaded on formvar-carbon-coated 200-mesh copper grids. The sections were stained with 0.75% uranyl-formate for 2 min, washed with distilled water, incubated in plumb (lead) for 1 min, and imaged by FEI Tecnai T12 Transmission Electron Microscope (TEM) equipped with a LaB6 filament and an acceleration voltage of 120 kV (Eindhoven, The Netherlands).

3.2.8 Chemically competent *E. coli* cells preparation

LB agar plates were streaked with *E. coli* strain at 37 °C. The next day, one colony was picked and suspended in 100 ml LB Broth, until reaching an OD600 of 0.4, followed by centrifugation at 3000 g for 10 min. The supernatant was discarded, and the pellet was resuspended in 0.1M CaCl₂ and incubated for 30 minutes on ice. After centrifugation at 3000 g for 10 min at 4 °C, supernatant was discarded, and pellet resuspend in 0.1M CaCl₂ + 15% glycerol. Aliquots of competent cells were stored at -80°C (160).

3.2.9 Plasmid transformation into *E. coli* with heat shock method

A 50 µl of competent cells was thawed on ice, then gently mixed 3 µl of plasmid and incubated for 5 minutes. Heat shock was performed by placing the mixture at 42 °C for 1 minute, then placed back in ice for 5 minutes. Next, 2 ml of LB was added to the mixture and incubated at 37 °C for 1 hour. After centrifugation at 5000 rpm for 5 minutes, the pellet was resuspended in 200 µl of LB, and streaked on agar plates with the appropriate antibiotics (161).

3.2.10 Plasmid Expression and purification of Alp7A-His using *E. coli* Arctic express (DE3) bacterial cells

Alp7A-His tagged at C-terminus was cloned into the pET-22b(+) plasmid vector (Novagen) using the BamHI and XhoI restriction sites. The pET-22b(+) vector including Alp7A-His was then transformed into Arctic Express (DE3, Agilent #230192) competent cells for expression and purification. Briefly, agar plates were streaked with *E. coli* DE3 cells from frozen glycerol stocks and incubated overnight at 37 °C on LB agar plates supplemented with gentamycin 20ug/ml and

ampicillin 100ug/ml. One colony was inoculated the next day and incubated overnight at 37 °C with ampicillin 100ug/ml. The next morning, the cell mixture was diluted 1/100 and incubated at 37 °C with shaking until it reached an OD600 of 0.5. The temperature was decreased to 14 °C and cells were induced with 0.2 mM Isopropyl β -d-1-thiogalactopyranoside (IPTG) for 24 hours. Cell pellets were stored at -80 °C at this stage.

The pellet was resuspended in depolymerization buffer (100 mM KCl, 25 mM Tris-HCl [pH 7.5], 1 mM dithiothreitol [DTT], 1 mM EDTA) before lysis with sonication and clarification by centrifugation at 13000 rpm for 30 min. Supernatant was transferred into separate beakers containing 0M, 0.5M, 1.5M, and 2.5M ammonium sulfate, respectively. The mixtures were stirred overnight at 4 °C. The next morning, 1 ml was taken from each beaker and centrifuged to check for the presence of pellets. No pellet appeared at ammonium sulfate concentrations less than 1.5M. Pellets were frozen at -20 °C for 3 days, then thawed and resuspended with polymerization buffer (100 mM KCl, 25 mM Tris-HCl (pH 7.5), 1 mM DTT, 1 mM MgCl₂). The resuspended mixture was precleared using dialysis cassettes with a maximum capacity of 3 ml. ATP was added to the cleared solution to a final concentration of 5 mM, and the polymer was pelleted by centrifugation at 70,000 rpm for 25 min.

SDS-PAGE and western blot using a monoclonal anti-histidine antibody (ThermoFisher Scientific #MAI-21315) were applied to analyze the eluate after protein purification. Further results validation was done by collecting pellets and imaging using negative stain EM by applying 4 μ l of the polymer to glow-discharged carbon-coated copper grids (EMS-FCF200-Cu) and incubation for 30 seconds. Grids were washed 3 times with PBS buffer, then stained with 0.5% uranyl acetate. Grids stained with uranyl acetate were examined in an FEI Tecnai 12 microscope (Eindhoven, The Netherlands). Technai T12 microscope was operated at an acceleration voltage of 80 kV and a magnification of 150 Kx. Images were recorded using an XR280 CMOS camera.

3.2.11 Alp7A purification from *E. coli* DE3 bacterial cells

Plasmid pET-22b(+) with untagged Alp7A was transformed into *E. coli* BL21 (DE3) competent cells using the BamHI and XhoI restriction sites. Cells were grown in LB with ampicillin

100ug/ml, then induced with 0.02 mM IPTG at 19 °C overnight. The ammonium sulfate precipitation method was first used to purify the untagged Alp7A. BL21 cells expressing Alp7A were incubated in lysis buffer (25 mM Tris-HCl (pH7.6), 100 mM KCl, 1 mM EDTA, 1 mM DTT, 1 mM PMSF), then sonicated 20 times for 30 seconds each, with 30 seconds rest between each sonication on ice. The mixture was centrifuged for 1 hour at 170,000 g at 4 °C. Ammonium sulfate was added slowly to the supernatant to reach a 50% concentration (29.1 g per 100 ml), followed by agitation for 1 hour at 4 °C. The mixture was then centrifuged for 30 min at 170,000 g at 4 °C. The supernatant containing Alp7A was then transferred to a clean ultracentrifuge tube and brought to room temperature using an ambient water bath. A 5 mM ATP/6 mM MgCl₂ solution was then added to induce polymerization. After incubation for 15 minutes, the polymer was pelleted by centrifugation for 20 min at 170,000g at 25 °C, then resuspended in 1/10 volume of cold depolymerization buffer (25mM Tris (pH 7.6), 200 mM KCl, 5mM EDTA, 1mM DTT). The eluate was evaluated by SDS-PAGE, followed by TEM.

Ammonium sulfate products were purified by size exclusion chromatography using a superdex 200 10/300 G1 column (GE Healthcare Biosciences, Uppsala, Sweden). Columns were pre-equilibrated with 25 mM Tris-HCl (pH = 7.6). Size exclusion chromatography fractions were evaluated for purity by SDS-PAGE. For precise identification of Alp7A, we used Mass spectrometry analysis, a robust and recognized method with the principle of separating charged molecules in the gas phase after ionization according to their mass/charge ratio. Mass spectrometry analysis was done at the Institute de recherches cliniques de Montréal (IRCM).

Eluate fractions were imaged by TEM FEI Tecnai T12 microscope (Eindhoven, The Netherlands). Technai T12 microscope was operated at an acceleration voltage of 80 kV and a magnification range between 3000x to 110000x. Images were recorded using an FEI Eagle 4 k × 4 k CCD camera. Images were recorded using an FEI Eagle 4 k × 4 k CCD camera.

3.2.12 Alp7A-GFP-His expression and purification from *E. coli* C43 (DE3) cells

The *alp7A-gfp* gene was obtained from *B. subtilis* strain 3267 using standard PCR protocol (Qiagen miniprep kit). We introduced a 6-His tag at the C-terminus of Alp7A-GFP to facilitate purification. The PCR product was subcloned into a pET22(b+) plasmid vector (Novagen) between NdeI and XhoI restriction sites. Sequences were PCR-amplified using the following primers:

5'-GGAATTCCATATGAATATTTCTCGTATGAACGTGGACTTGGAAACAGTATG-3'
5'-CCGCTCGAGTTTGTAGGGCTCATCCATGCCATGTGTAATCCC-3'

The pET22(b+) vector containing Alp7A-GFP-His was validated by sequencing the recombinant vector at the Genome Quebec Innovation Center (McGill University, Montreal, Canada).

Alp7A-GFP-His expression was induced in *E. coli* C43 (DE3) cells by 0.02 mM IPTG at 19°C overnight. The cells were pelleted the next day by centrifugation at 5000g for 20 minutes and lysed in buffer A (50 mM Tris-HCl pH 8, 100 mM KCl, 2mM DTT, 1 mM PMSF) supplemented with 1 mg/ml lysozyme and cOmplete™ Protease Inhibitor Cocktail (Roche, Mississauga, Canada). The mixture was then sonicated 10 times, 2 minutes each, separated by 2 minutes rest. Next, lysates were cleared by centrifugation at 5000 g for 1 hour. The supernatant was discarded, and a solution containing 8M urea and 1% triton 100x was added to the protein-enriched pellet and incubated with shaking for 1 hour. Subsequently, the supernatant was loaded on a 10 ml Ni²⁺-affinity column (GE Healthcare Biosciences, Uppsala, Sweden). The column was washed with 25 mM Tris-HCl, 100 mM KCl, 10 mM imidazole (pH 7.6), and the protein was eluted with 25 mM Tris-HCl, 100 mM KCl, 500 mM imidazole (pH 7.6). Peak fractions containing Alp7A were collected, concentrated on an Amicon Ultra column, loaded on a size exclusion chromatography using a superdex 200 10/300 G1 column (GE Healthcare Biosciences, Uppsala, Sweden), and finally eluted with buffer (25 mM Tris pH 7.6, 100 mM KCl, 1 mM MgCl₂, 1mM DTT).

SDS-PAGE was performed on eluate fractions, followed by TEM, where micrographs were captured before and after incubation with ATP 5mM, MgCl₂ 10mM, and immunolabeling. Micrographs were taken with an FEI Tecnai T12 TEM (Eindhoven, The Netherlands). Tecnai T12 microscope was operated at an acceleration voltage of 80 kV and a magnification of 3000x to 150000x. Images were recorded using an XR280 CMOS camera.

3.2.13 Immunogold labeling of Alp7A-GFP-His

Immunogold labeling was performed to identify Alp7A protein after purification on TEM. This technique uses antibodies to detect the intracellular localization of specific antigens by electron microscopy. Ultrathin sections of cells or tissues are labeled with gold-labeled antibodies

that bind specifically to the desired antigen. Gold particles of different diameters enable two or more proteins to be studied simultaneously. The Alp7A-GFP-His C-terminus was labeled with Ni-NTA-Nanogold for immunolabelling.

Briefly, Alp7A-GFP-His C-terminus purified protein was diluted to a final concentration of 10 µg/ml. A gel filtration buffer, without imidazole, supplemented with 10 mM magnesium and 5 mM ATP was freshly prepared. After two hours of incubation, 5 to 10 µg/ml of proteins loaded on glow discharged Cu R2/2 grids and washed 3 times with the gel filtration buffer without imidazole. Next, grids were incubated with Ni-NTA-Nanogold for 30 minutes, then Washed with the gel filtration buffer twice, and 10mM imidazole was added in the final wash to remove non-specific binding. Before data collection by TEM, grids were stained with 0.75 % uranyl-formate.

4 Results

4.1 Project 1: Characterization of phase-bright objects in members of Proteobacteria and Actinobacteria

4.1.1 Detection of phase-bright objects in the three bacterial species

Phase-contrast LM was used to detect phase-bright objects in *R. johrii*, *S. marcescens*, *M. marinum*, and *B. subtilis* (**Figure 16**). Vegetative cells of *R. johrii* appeared dark after two days of incubation on LB, whereas the presence of phase-bright objects (red arrows) was observed after seven days (**Figure 16A**) (162). The phase-bright objects in *R. johrii* appeared in dark healthy cells similar to those without phase-bright objects (black arrows). While *S. marcescens* cells were imaged after 7, 65, and 90 days, phase-bright objects were only observed after 65 days as previously reported (**Figure 16 B**) (162). Phase-bright objects in *S. marcescens* spanned the whole cell (red arrows). In addition, ghost cells (white arrows) and dark healthy cells (black arrows) also appeared in the images. The phase-bright objects were present in dark cells of *S. marcescens* that looked darker than nearby vegetative cells. After three days on 1.5X LB, *M. marinum* bacteria showed phase-bright objects (red arrows) (**Figure 16C**), whereas bacteria grown on 7H10 agar plates did not show any phase bright objects (**Figure 16D**). Finally, seven-day cultures of *B. subtilis*, strain 168, showed healthy cells (black arrows) and cells with phase-bright objects that spanned the whole cell (red arrows) (**Figure 16E**).

Altogether, as previously reported, our phase-contrast microscopy results showed phase-bright objects in *R. johrii*, *S. marcescens*, *M. marinum*, and *B. subtilis* following prolonged incubation under low nutrient conditions.

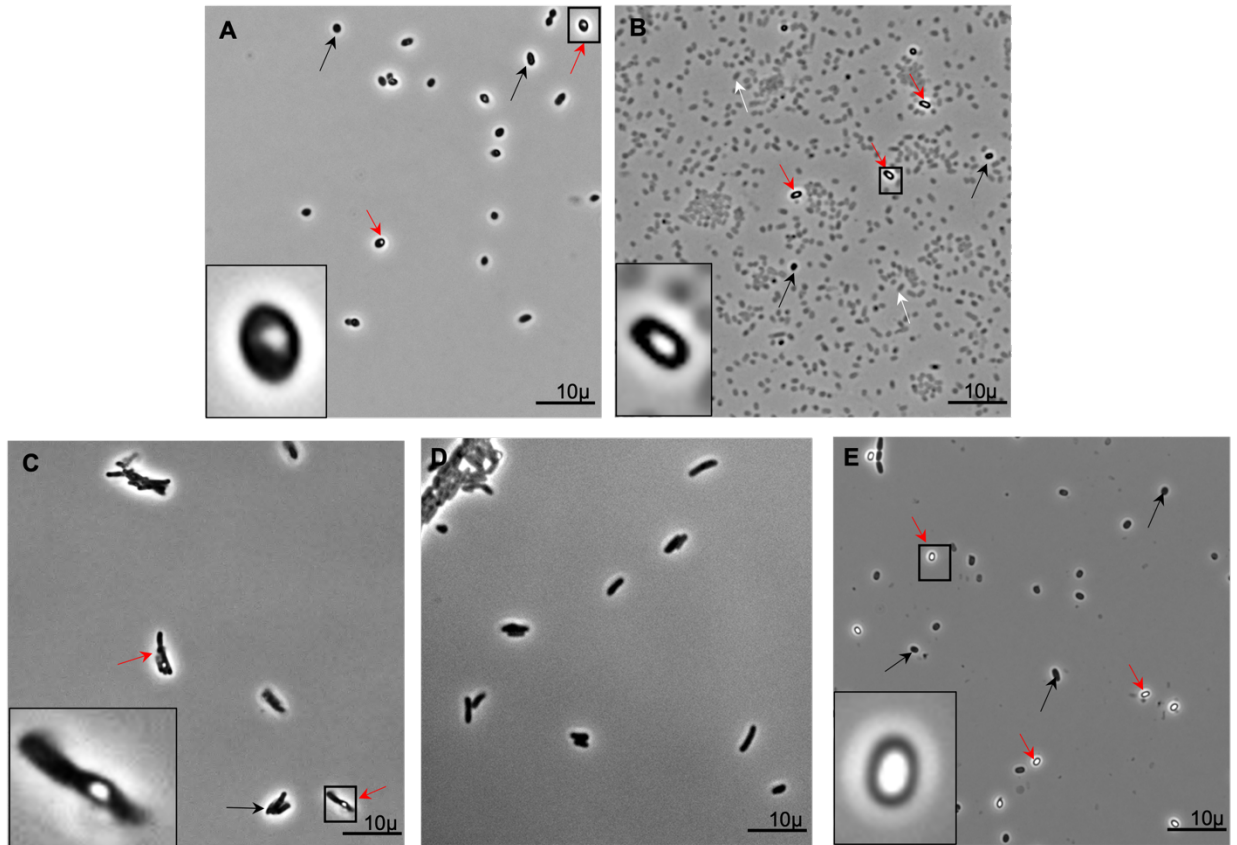


Figure 16. – Phase-contrast LM of *R. johrii*, *S. marcescens*, *M. marinum*, and *B. subtilis* cells induced for endospore formation.

(A) A seven-day culture of *R. johrii* cells showing phase-bright objects (red arrows) and healthy intact cells (black arrows). (B) *S. marcescens* cells showing three kinds of cell morphologies after 65 days: phase-bright objects (red arrows), healthy intact cells (black arrows), and dead “ghost” cells (white arrows) (162). (C) Phase-contrast LM image of *M. marinum* shows the presence of phase bright object structure within the cells (red arrows) and healthy typical cellular morphologies (black arrows). (D) LM image of *M. marinum* grown in 7H10 agar plates showed no phase-bright objects. (E) After seven days of culture, *B. subtilis* shows two kinds of cell morphologies, bright phase objects (red arrow) and healthy intact cells (black arrow). Scale bar 10 μm. Magnified inserts represent inboxed regions in each panel.

4.1.2 Cryo-electron tomography (cryo-ET) showed lack of spore-like structures in the three bacterial cultures with phase-bright objects

Cryo-ET was performed to characterize the phase-bright objects in extended cultures of *R. johrii* (7-day old culture) and *S. marcescens* (65-days old culture) (**Figure 17**).

Tomograms of *R. johrii* cells with phase-bright objects revealed large granular structures within the cell (**Figure 17A**). The structures were highly sensitive to the electron beam, as represented by the sample damage. There was no evidence of engulfing membranes, immature or mature spores in all samples (n=40). The granules' spherical nature in *R. johrii* resembled previously characterized storage granules (SG) in bacterial cells (163). Beam sensitivity was detected regardless of the total dose of electrons used (25 to 150 e-/A²), suggesting that the granules were rich in lipids.

Tomograms of *S. marcescens* were also collected on 65-day old cultures (**Figure 17B**). They showed the presence of two kinds of cellular morphologies: cells packed with cellular debris and cells void of any cellular material. An extensive examination of the samples (n=80) did not reveal any cells with intracellular membranes or reminiscent morphologies of engulfing membranes associated with sporulation stages. None of the cell morphologies displayed any features related to a cortex or proteinaceous spore coat characteristic of mature endospores. Together, these results confirmed that the phase-bright objects in *S. marcescens* are likely the result of cellular debris and dehydration.

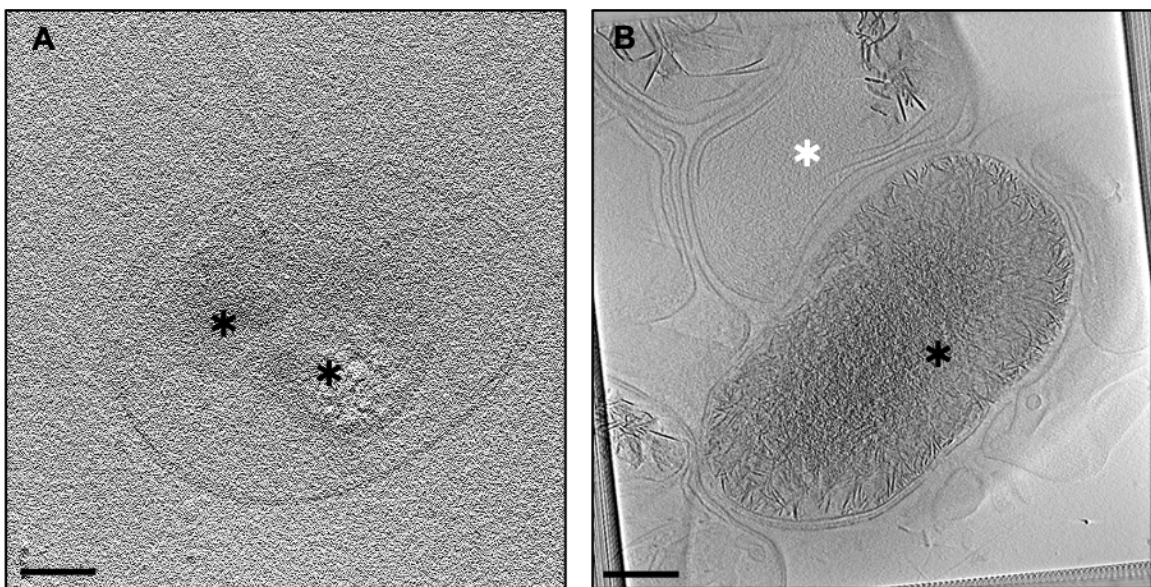


Figure 17. – Cryo-ET of *R. johrii* and *S. marcescens* reveals a lack of endospores.

(A) Tomographic slice through a 7-day old *R. johrii* cell showing a granular structure (black stars). (B) Tomographic slice through a 65-day old *S. marcescens* cell showing dead cells with (black star) and without (white star) cellular debris (162). Scale bar 200 nm.

Similarly, we could not detect any endospore features in the tomograms of *M. marinum*, which revealed two cell morphologies (**Figure 18**): healthy intact cells lacking internal structures, and healthy intact cells with granular structures. None of the two cell morphologies showed any endospore-related structures (**Figure 18A**).

In comparison, tomographic slices of sporulating *B. subtilis* showed different stages of engulfment with clear inner and outer spore membranes (IsM and OsM, respectively) (**Figure 18B**) (162).

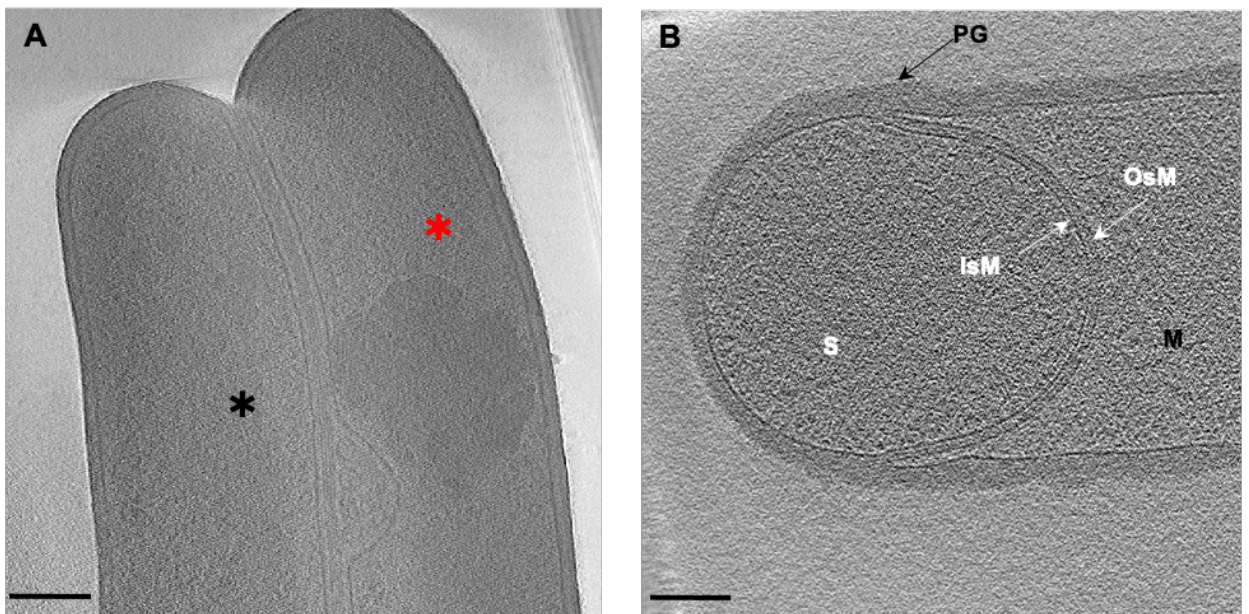


Figure 18. – Cryo-electron tomography of *M. marinum* and *B. subtilis* showing morphologies of phase bright objects.

(A) Tomographic slice through *M. marinum* showing healthy normal cells with granular structures (red star) and healthy normal cells lacking granular structure (black star). (B)

Tomographic slice through *B. subtilis* showing mother cell and future spore (endospore). S, spore; M, mother cell; IsM, inner spore membrane; OsM, outer spore membrane. Scale bar 200 nm.

Further examination of *M. marinum* cells revealed putative polyphosphate granules (PolyP), resembling those described by Schaefer *et al.* (164), contained in small circular dense bodies. These PolyP granules usually accumulate in cells as an energy source under extreme conditions (164). Several other cellular features embodied in storage granules were also detected, such as membrane invagination, septum, and putative lipid inclusions (**Figure 19**).

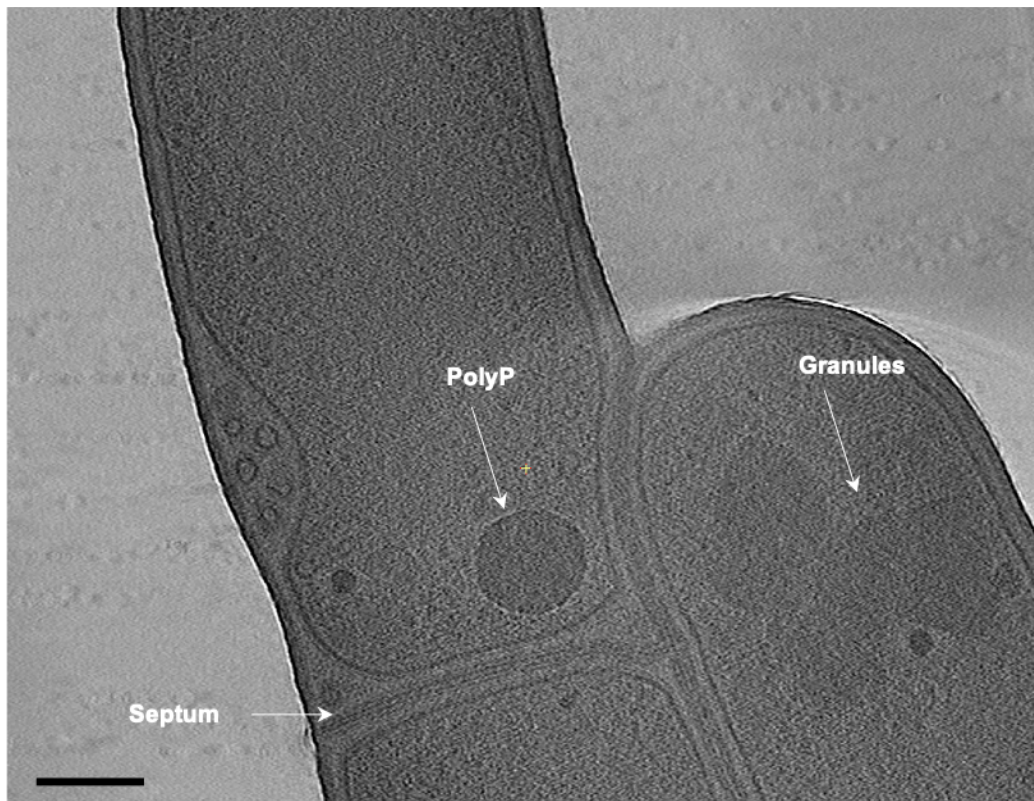


Figure 19. – Cryo-tomogram of *M. marinum*.

A tomographic slice through *M. marinum* showing healthy cells with different cellular structures. Septum, putative granules, and polyphosphate storage granules (PolyP). Scale bar 200 nm.

4.1.3 Phase-bright objects in *R. johrii* and *M. marinum* resemble the structure of storage granules under CLEM

To further confirm the nature of the phase-bright objects observed in *R. johrii* and *M. marinum*, we performed correlative light-electron microscopy (CLEM). CLEM enables the imaging of the same cell at low and high resolutions with reduced chance of changes in the sample during the process of data collection. Cells possessing phase-bright objects were identified with phase-contrast microscopy and examined at higher resolution with cryo-ET. CLEM images of *R. johrii* showed that cells lacking phase-bright objects lacked any kind of substructures (**Figure 20A**), whereas cells with phase-bright objects contained 1-3 granular structures that were 200 to 250 nm in diameter (**Figure 20B**).

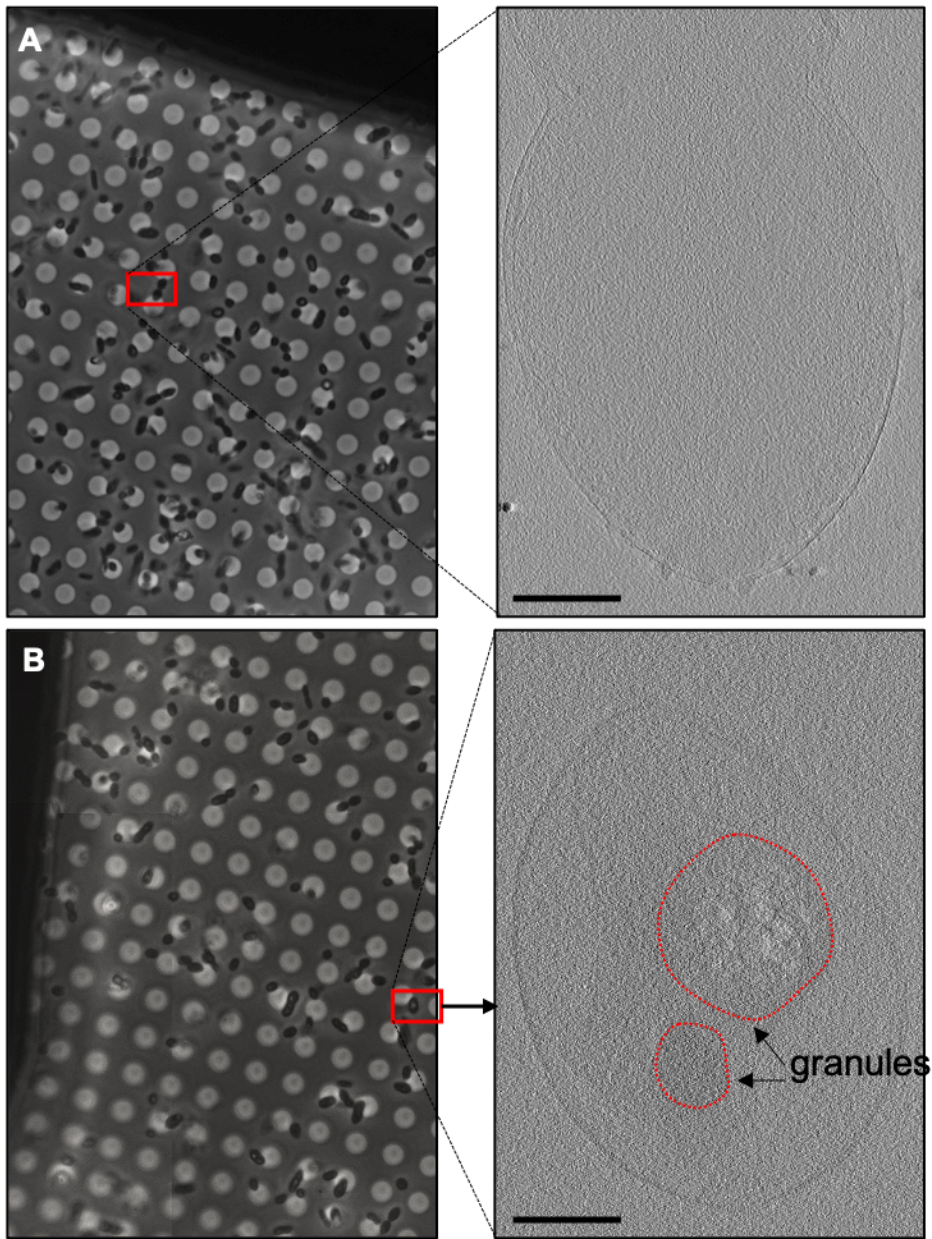


Figure 20. – Correlative light and electron microscopy (CLEM) images of *R. johrii*.

(A) Left: LM atlas of *R. johrii* cells (boxed) lacking phase-bright objects. Right: a tomographic slice of the same cell showing lack of sub-cellular structures. (B) Left: *R. johrii* cell (boxed) displaying a phase-bright object (162). Right: a tomographic slice of the same cell showing two granular structures. Scale bar 200nm.

Similarly, the phase-bright objects observed under LM in *M. marinum* cells correlated with granular structures shown under cryo-ET (**Figure 21**).

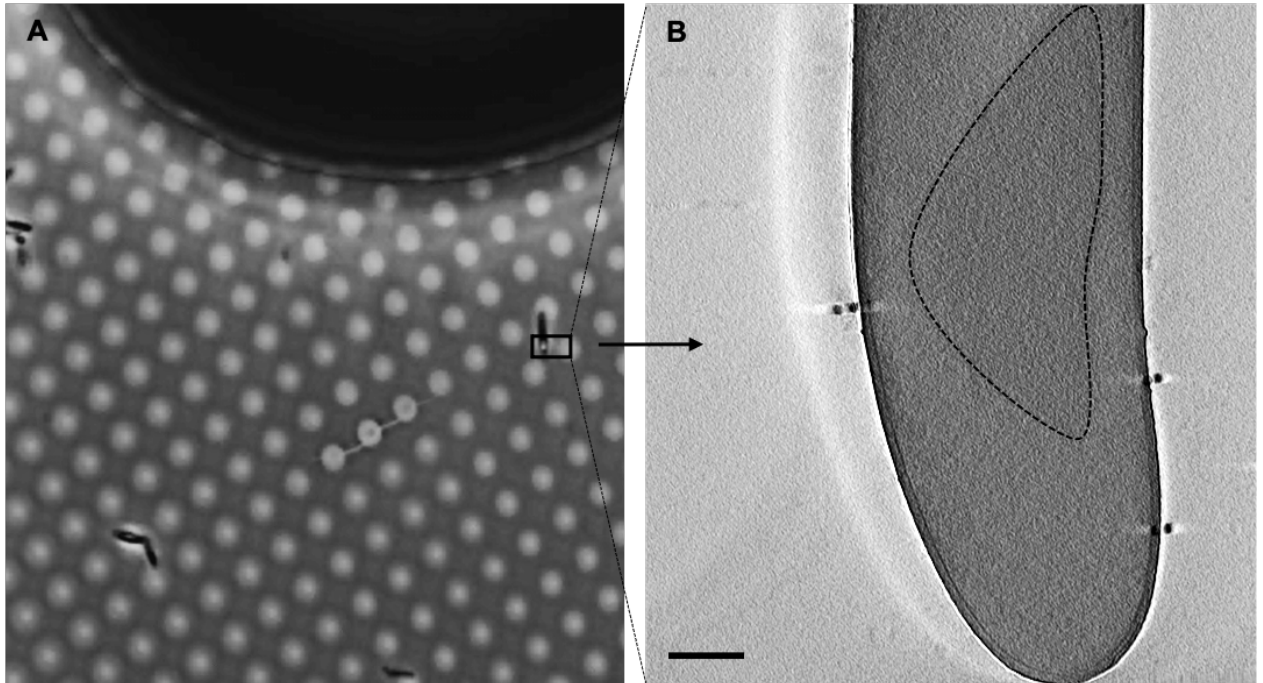


Figure 21. – Correlative cryo-light and electron microscopy of *M. marinum*.

(A) Light microscopy (LM) atlas and (B) tomographic slice of the same *M. marinum* showing phase bright object. Scale bar 200nm.

Taken together, both CLEM and cryo-ET results suggest that the phase bright objects seen in *R. johrii* and *M. marinum* are likely granular structures that do not show any features associated with endospore formation.

4.1.4 Scanning electron microscopy (SEM) and energy-dispersive x-ray analysis (EDX)

To determine the composition of the storage granules, we performed CLEM experiments (LM and SEM) in combination with EDX compositional analysis on *R. johrii* cells. Scanning electron microscopy (SEM) showed bulge structure in cells containing phase-bright objects, while other *R. johrii* cells showed no bulges (**Figure 22A, B, C**). EDX spectra were collected on a storage granule and the cytoplasm area lacking storage granules (Figure 22E). Elemental analysis of the storage granule (blue line) revealed 80.2 % carbon (C), 13.3% oxygen (O), and 6.5% copper (Cu) (due to the copper of the EM grid). On the other hand, cytoplasmic analysis (red spectrum) revealed lower counts for carbon (61.7%) and oxygen (10.8%), similar levels of copper at 6.6%, and elevated counts for nitrogen (N, 20.9%) (**Figure 22E**). These data suggested that the granules observed in *R. johrii* were likely composed of lipids, enriched in carbon and oxygen atoms.

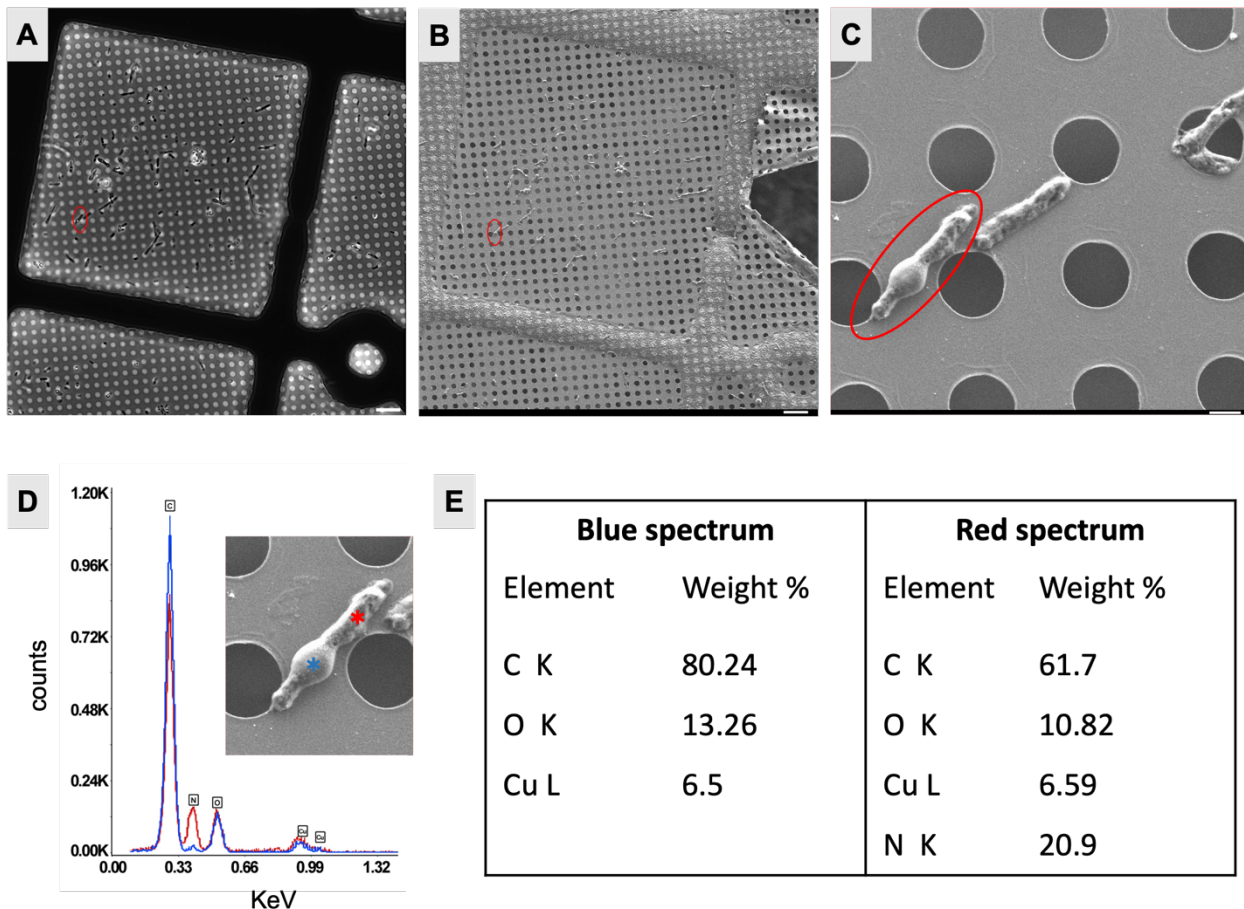


Figure 22. – Correlative light and scanning electron microscopy in *Rhodobacter johrii*.

(A) Phase contrast light microscopy (LM) image showing the presence of storage granules (phase-bright objects) inside a *R. johrii* cell (red circle). (B) An SEM image of the same *R. johrii* cell in panel A (red circle). (C) A higher resolution SEM image of *R. johrii* correlated to the phase contrast LM image showing difference in morphology between cells with storage granules (red circle), compared to those without storage granules. (D) EDX analysis of a storage granule. The elemental compositions within the storage granule and a random location on the same bacterium is shown in blue and red asterisks, respectively. Major peaks are assigned. Data show elevated levels of carbon in the granule area, compared to the other parts in the cell. (E) Semiquantitative analysis of the granule structure in *R. johrii* (162). Scale bar 10 μm in (A, B), 1 μm in C.

4.1.5 Proteobacteria and Actinobacteria do not possess phenotypic features of endospores

Independent of microscopy methods, endospores have traditionally been identified in samples through their biochemical and biophysical characteristics, particularly high DPA concentrations, heat resistance, and differential staining.

Endospores contain packed DNA and high amounts of DPA (31). We measured DPA in samples of *R. johrii*, *S. marcescens*, *M. marinum*, and *B. subtilis* cultures following endospore induction and purification protocols. (**Table 1**). While DPA concentration in *B. subtilis* was measured at 6.74 $\mu\text{g/ml}$ after 7 days, the average DPA concentrations in *R. johrii* (7 days), *S. marcescens* cells (7 and 65 days), and *M. marinum* (3, 7, and 14 days) were below the detection limit.

Table 1 - Analytical detection of endospores in bacteria by DPA concentration measurement.

Bacterial strains	DPA concentration ($\mu\text{g/ml}$)
<i>B. subtilis</i> (7 days old)	6.74
<i>S. marcescens</i> (7 days old)	Under standard curve
<i>S. marcescens</i> (65 days old)	Under standard curve

<i>R. johrii</i> (7 days old)	Under standard curve
<i>M. marinum</i> (3, 7, 14 days old)	Under standard curve

The heat resistance properties of endospores can be detected by the ability of cells to recover following exposure to high temperatures. Each bacterial strain was subjected to a specific temperature treatment to test its ability to withstand extreme heat conditions. We applied a heat treatment of 80 °C to *R. johrii* on days 7 and 30, respectively. Heating at 60 °C was applied to *S. marcescens* at days 7 and 74, respectively. Furthermore, heat resistance test was performed at 65 °C for 15, 30, or 60 minutes on 3-, 7-, 14-, and 30-day old *M. marinum* (**Table 2**). No recovery was observed on agar plates five days after heat treatment of *S. marcescens*, *R. johrii*, and *M. marinum*. In contrast, *B. subtilis* recovered after heat treatment. In contrast, *B. subtilis* cultures treated at 80 °C for 15, 30, and 60 min yielded viable growth on solid media after a short 24-h recovery period. Thus, we were unable to replicate the results of Girija *et al.*, who detected viable cells following heat treatment of *R. johrii* at 80 °C for 20 min (35), and Ajithkumar *et al.*, who treated *S. marcescens* at 60 °C for 15 min (34).

Table 2 - Bacterial recovery after heat shock.

Strain	Age	Temperature	Recovery
<i>B. subtilis</i>	7 days	80 °C	+
<i>S. marcescens</i>	7 days	60 °C	-
	65 days	60 °C	-
<i>R. johrii</i>	7 days	80 °C	-
	30 days	80 °C	-
<i>M. marinum</i>	3 days	65 °C	-
	7 days	65 °C	-
	14 days	65 °C	-
	30 days	65 °C	-

We further investigated spore formation capacity in *B. subtilis*, *R. johrii*, and *M. marinum* by differential staining methods using malachite green, which is considered a primary stain for

bacterial endospore visualization (**Figure 23**). Malachite green enters cells after heat treatment, and, contrary to vegetative cells, it is retained by endospores after rinsing. Thus, adding a secondary stain such as crystal-violet, safranin, and acid-fast would stain vegetative cells purple to red, whereas spores would look green due to malachite green. We used crystal violet as a counterstain for *B. subtilis*, safranin for *R. johrii*, and acid-fast for *M. marinum* due to the nature of its unique outer membrane, characterized by the presence of mycolic acid (**Figure 23**). *B. subtilis* showed retention of malachite green in endospores (**Figure 23A, B**). On the other hand, while LM images revealed phase-bright objects in *R. johrii* and *M. marinum* samples (**Figure 23 C, E**), there was no recuperation of malachite green by cells in the same samples (**Figure 23 D, F**).

Together, these results indicate that *R. johrii* and *S. marcescens* cells did not possess the phenotypic features associated with endospore formation.

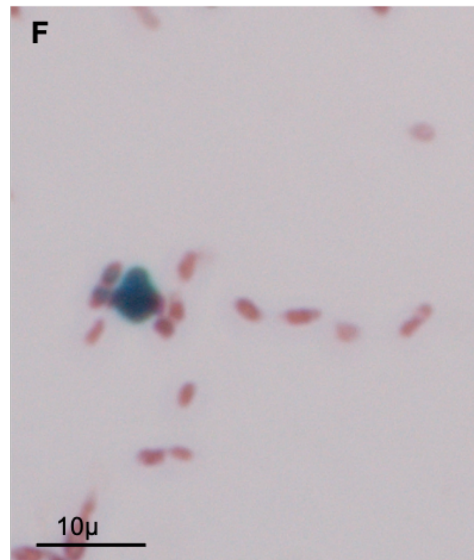
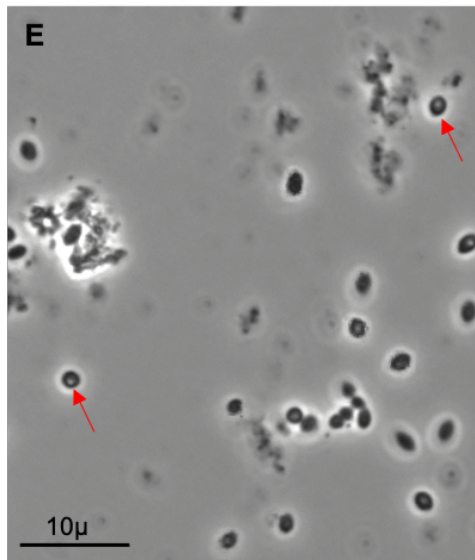
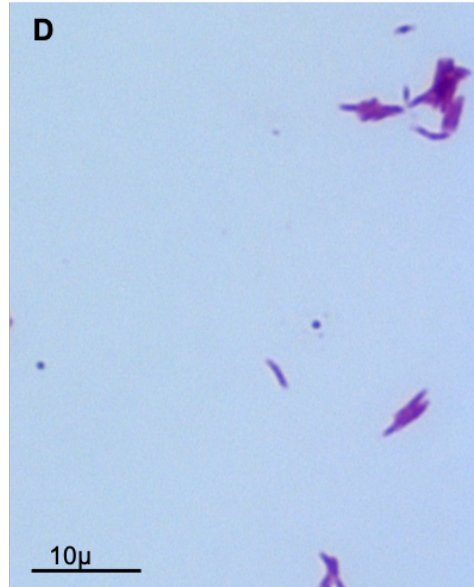
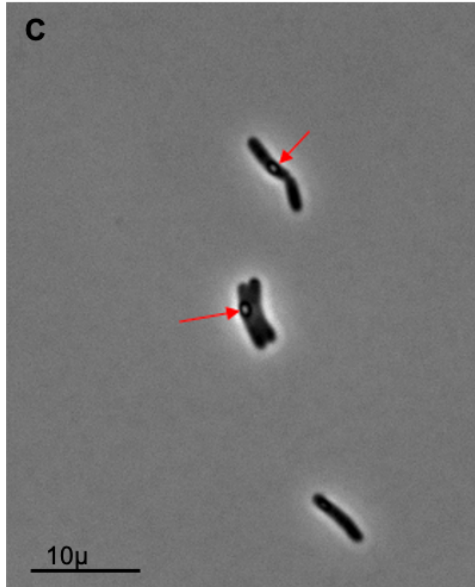
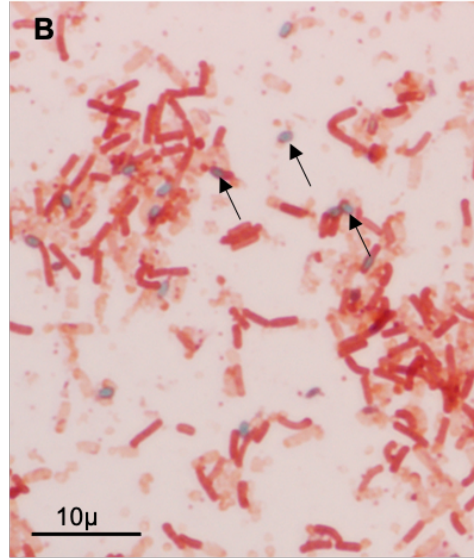
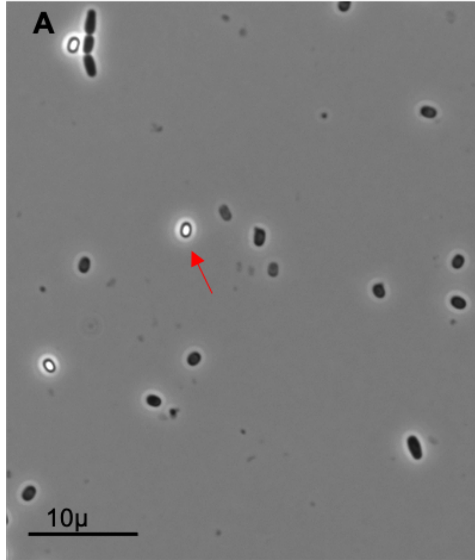


Figure 23. – Differential staining of *B. subtilis*, *M. marinum*, and *R. jhrii*.

(A) Phase-contrast LM image of *B. subtilis* shows spores as phase-bright objects (red arrows). (B) Retention of malachite green by spores in *B. subtilis* (black arrows). (C) Phase-contrast LM image shows the presence of phase-bright objects in *M. marinum* (red arrows). (D) Differential staining with malachite green in an *M. marinum* sample containing phase-bright objects. (E) Phase-contrast LM image shows the presence of phase-bright objects in *R. jhrii* (red arrows). (F) Differential staining with malachite green in a *R. jhrii* sample containing phase-bright objects.

4.1.6 The *R. jhrii* cells contain lipid storage granules

Based on our CLEM and EDX results, we hypothesized that the granules observed in *R. jhrii* are enriched in lipids with high and carbon and oxygen content. To characterize the nature of the granular composition, we performed whole-cell lipidomics analysis on 7-day old *R. jhrii* culture expressing phase-bright objects (granules). As a negative control we used *R. jhrii* cells grown for 2 days and lacking phase-bright objects. By comparing the two samples, we identified triacylglycerols (TAGs) as the main lipids found in *R. jhrii* cells expressing the phase-bright objects (**Table 3**) (162). TAGs were the predominant lipids detected in these bacteria with a fold-change ranging between 12 and 98 folds. TAGs are considered a major source of energy (59), and have been shown to accumulate in actinobacteria and mycobacteria either as peripheral deposits associated with the cell envelope or as inclusion bodies in the cytoplasm (165). Other lipids with more than 2-fold increase in granulated bacteria included phosphatidylethanolamines (PEs), phosphatidylcholines (PCs), and diacylglycerols (DAGs). These lipids are commonly found in bacterial membranes, suggesting that these cells remodel their membrane composition as an adaptive response to environmental conditions.

Taken together, the lipidomics analysis suggests that the observed phase-bright objects in *R. jhrii* are most likely storage granules enriched with TAGs, allowing cells to enter stationary phase and survive for longer periods under unfavourable conditions.

Table 3 - Whole cell lipidomic analysis on *R. johrii* with (+) and without (-) storage granules (162).

Lipid	Lipid class	R.j (-) average intensity	R.j (+) average intensity	Fold change R.j (+) / R.j (-)	P-value
PE 33:1; PE 16:0-17:1	PE	65	9595	147.84	4.71E-09
TAG 58:1; TAG 16:0-24:0-18:1	TAG	22	2083	93.81	1.81E-08
TAG 52:3; TAG 16:0-18:1-18:2	TAG	177	11873	67.19	1.24E-08
TAG 54:5; TAG 18:1-18:2-18:2	TAG	35	2096	60.41	1.37E-06
TAG 52:2; TAG 18:0-16:1-18:1	TAG	352	20313	57.72	1.93E-07
TAG 54:4; TAG 18:1-18:1-18:2	TAG	85	4640	54.46	2.37E-08
TAG 52:1; TAG 16:0-18:0-18:1	TAG	308	15138	49.15	1.22E-10
TAG 56:2; TAG 16:0-18:1-22:1	TAG	36	1741	48.89	5.37E-09
TAG 50:1; TAG 16:0-16:0-18:1	TAG	405	18801	46.43	7.39E-09
TAG 54:2; TAG 18:0-18:1-18:1	TAG	139	6230	44.82	2.37E-09
TAG 58:2; TAG 16:0-18:1-24:1	TAG	32	1341	42.04	9.59E-09
TAG 52:2; TAG 16:0-18:1-18:1	TAG	504	20710	41.06	5.93E-09
TAG 56:1; TAG 16:0-22:0-18:1	TAG	79	3138	39.72	8.65E-10
TAG 54:1; TAG 18:0-18:0-18:1	TAG	119	4675	39.35	1.15E-08
TAG 54:3; TAG 18:0-18:1-18:2	TAG	383	6570	17.15	3.93E-08
TAG 50:2; TAG 16:0-16:1-18:1	TAG	509	6263	12.30	1.90E-08
PE 32:0; PE 16:0-16:0	PE	208	2396	11.55	1.73E-06
PC 39:3e	EtherPC	231	2489	10.77	1.06E-08
PE 32:1; PE 16:0-16:1	PE	487	3744	7.68	3.84E-07
TAG 48:1; TAG 14:0-16:0-18:1	TAG	349	1726	4.94	2.00E-05
PE 35:2; PE 17:1-18:1	PE	1696	5240	3.09	6.92E-06
PC 36:4	PC	581	1760	3.03	4.93E-06
TAG 48:1; TAG 16:0-16:0-16:1	TAG	471	1188	2.52	4.51E-03
PC 32:1	PC	943	2058	2.18	4.46E-07
PC 34:1; PC 16:0-18:1	PC	9846	21158	2.15	6.50E-08
DAG 36:2; DAG 18:1-18:1	DAG	1482	3084	2.08	5.34E-08
PC 34:2; PC 16:1-18:1	PC	27148	54852	2.02	1.57E-06

4.1.7 *R. johrii* lacks essential genes of sporulation

Sporulation relies on a complex gene regulatory network involved in the stepwise process of endospore formation. Hundreds of sporulation-related genes have been detected in various spore-formers. Many of these genes perform redundant functions (e.g., histidine kinases) or are part of general pathways related to the sporulation process, such as iron uptake and DNA repair proteins. While a common set of essential sporulation genes is yet to be identified, we assessed the genomes of *R. johrii* and *S. marcescens* for possessing genes that are conserved among all spore-forming bacilli and clostridia and have been experimentally shown to play essential roles in endospore formation (Table 4) (13, 33). Our analysis showed that out of 86 sporulation genes, only two (*etfA* and *spoVN*) have significant hits in *R. johrii*, and only one gene (*spoVR / ycgB*) in *S. marcescens*. Of interest, the non-sporulating bacterium *Escherichia coli*, used as a negative control in this analysis, possesses potential orthologs of four sporulating genes, more than the two strains under investigation. Both *R. johrii* and *S. marcescens* completely lack essential proteins such as the SpoIIDMP peptidoglycan remodeling complex required for spore cortex formation, the SpoIIQ-SpoIIIAA-AH channel complex involved in communication between the mother cell and the prespore and facilitating regulation of endospore maturation, as well as major components of the protein coat (e.g., SpoIVA) (29, 31). Besides, both strains lack the master regulator of sporulation encoded by all endospore formers, Spo0A. Further, all five sporulation sigma factors, SigE, SigF, SigG, SigH, and SigK, were absent in the two strains. Finally, *R. johrii* and *S. marcescens* lack DpaB, required for DPA production, which plays a major role in resistance and dormancy of the spore through core dehydration (31). However, a homolog of *etfA*, a gene involved in DPA synthesis in some Clostridia, was identified in *R. johrii* and *E. coli* but not in *S. marcescens* (Table 4). In summary, this analysis corroborates the lack of *R. johrii* and *S. marcescens* genomes to major structural and regulatory sporulation genes. These results are in concordance with those of Ajithkumar *et al.*, which were also unable to detect genes related to endospore formation in *S. marcescens* (34).

4.2 Project 2: Characterization of Alp7A structure *in vivo* and *in vitro*

4.2.1 SDS-PAGE validated the of Alp7A in *B. subtilis* strains

In this study, we used a slender mutant of *B. subtilis* with an average width of ~800 nm to visualize Alp7A under EM due to the size limitation associated with the thickness of wild-type *B. subtilis*. Alp7A was introduced into the slender mutant of *B. subtilis* using mini-pLS20 constructs encoding GFP-tagged (strain 3267) or untagged (strain 3268) Alp7A under the control of xylose-inducible promoter. Besides, a mini-pLS20 plasmid lacking the *alp7ARC* operon ($\Delta alp7AR$) was introduced into *B. subtilis* (strain 3266), which was used as a negative control.

SDS-PAGE stained with Coomassie Brilliant Blue R-250 was performed on protein extracts to verify the expression of Alp7A in the three strains. The SDS-PAGE gel showed a light band of Alp7A-GFP at ~72 kDa in strain 3267, in this strain GFP molecular weight is 27 kDa and Alp7A 45 kDa, so the band of protein of interest (Alp7A-GFP) is expected at a molecular weight of 72 kDa. Similarly, a light band corresponding to untagged Alp7A was observed at ~45 kDa in strain 3268 (**Figure 24**). No band corresponding to Alp7A was observed in strain 3266 containing $\Delta alp7AR$ mini-pLS20 plasmid (**Figure 24**). None of the strains showed intense bands of Alp7A, indicating low yield of the protein.

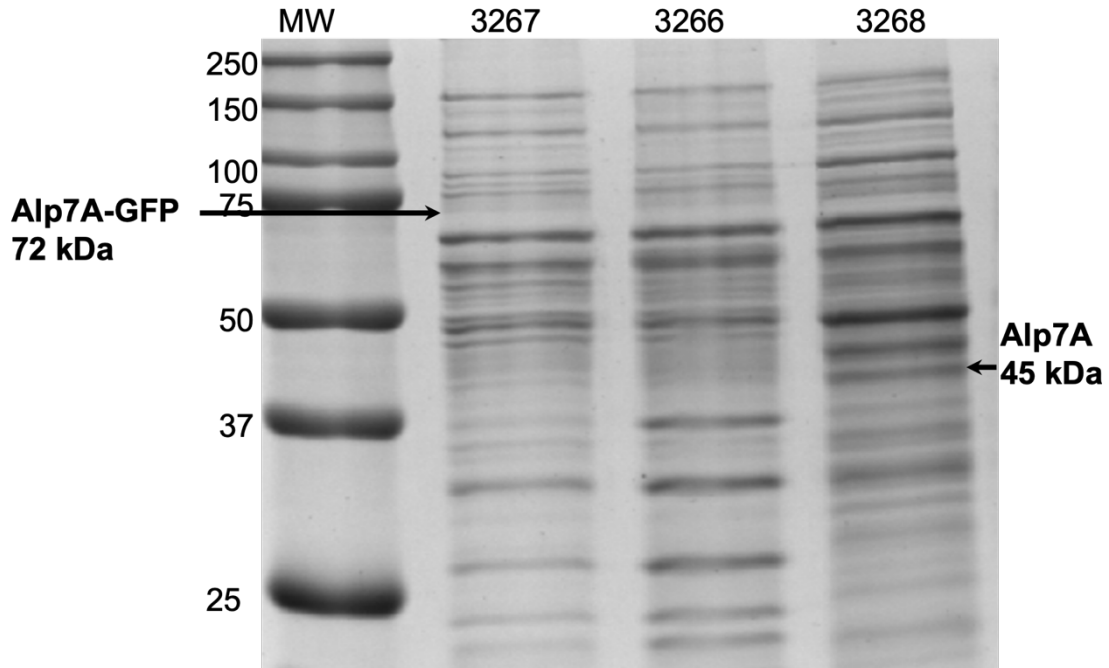


Figure 24. – SDS-PAGE of Alp7A in *B. subtilis* cells.

SDS-PAGE analysis showing the expression of Alp7A in the three strains of *B. subtilis*: strain 3267 (Alp7A-GFP), strain 3266 ($\Delta alp7AR$), and strain 3268 (Alp7ARC). MW, molecular weight ladder.

B. subtilis strain 3267 was further analyzed by fLM to visualize the structure of Alp7A in its natural environment. After confirming the expression of ALp7A-GFP in strain 3267 by western blot (**Figure 25A**), imaging of cells was performed by fLM at room temperature. Bright field imaging (**Figure 25B**) showed filamentous structures of Alp7A (green filaments) in *B. subtilis* cells. Filamentous structure of Alp7A-GFP was also observed after GFP excitation at room temperature (**Figure 25C**). Similar results were observed after staining of cells with Fm4-64 (stains the plasma membrane), confirming the presence of Alp7A-GFP filaments inside *B. subtilis* cells (**Figure 25D**).

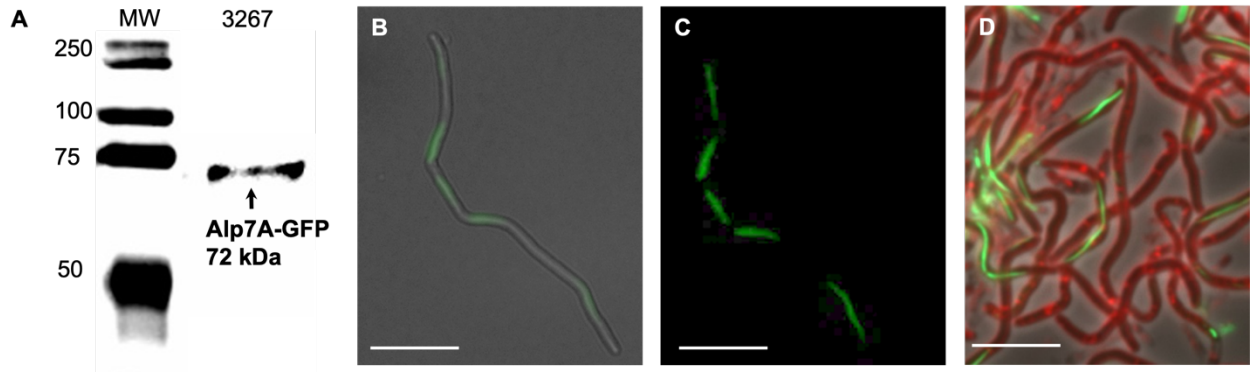


Figure 25. – Expression of Alp7A-GFP in *B. subtilis* strain 3267.

A) Western blot analysis of *B. subtilis* strain 3267 expressing Alp7A-GFP showing a band at ~45 kDa. B) *B. subtilis* cells in bright field under fLM, showing the presence of Alp7A-GFP filaments in green color. C) fLM showing Alp7A-GFP filaments. D) fLM image showing Alp7A-GFP filaments (green) inside *B. subtilis* cells (red, stained with Fm4-64 dye). Scale bar 10µm.

4.2.2 Cryo-ET of *B. subtilis* showed potential filamentous structure of Alp7A

Cryo-ET was performed to analyze the protein at high resolution (18 Kx) in its near native state inside the cells. Bacterial cells were treated with lysozyme 200 µg/ml for five minutes to loosen their cellular membrane and obtain better resolution of cryo-ET density maps. Tomogram of *B. subtilis* strain 3267 showed clear filamentous structures inside the cells treated with lysozyme (**Figure 26A**). Similarly, very fade filamentous structures were observed in control cells not treated with lysozyme and expressing either Alp7A-GFP (**Figure 26B**) or untagged Alp7A (**Figure 26B**).

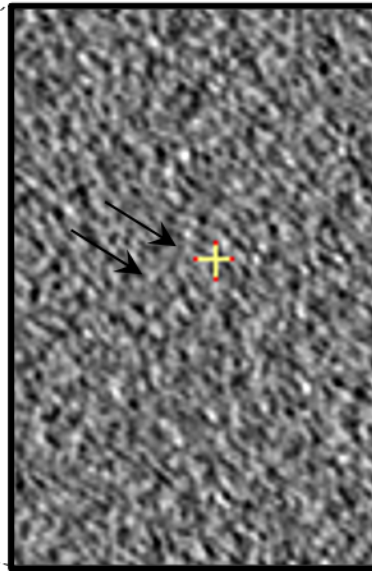
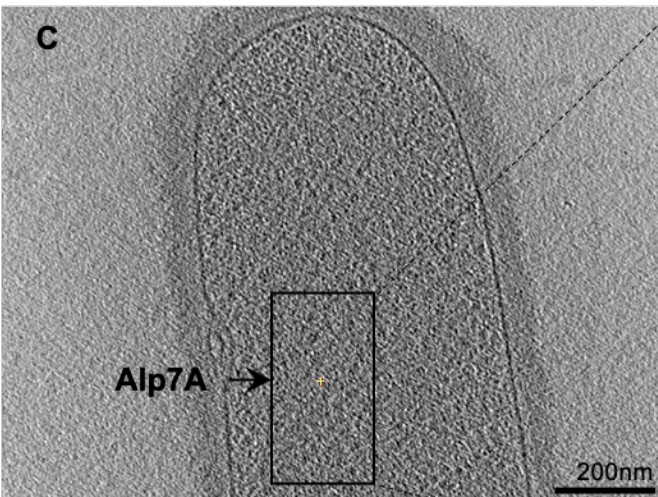
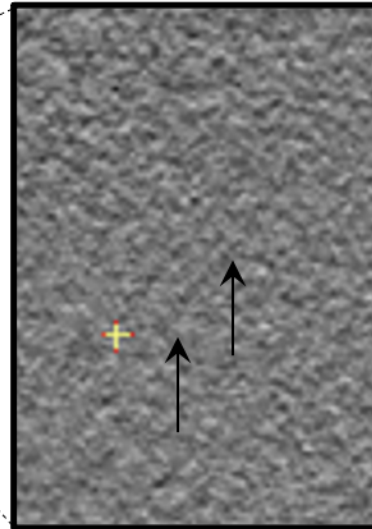
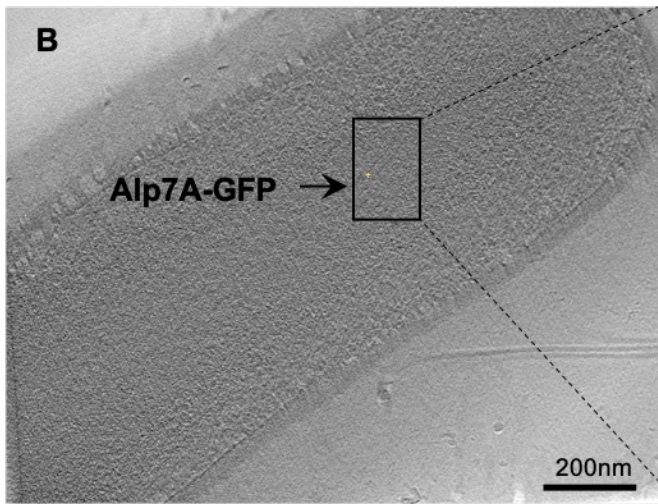
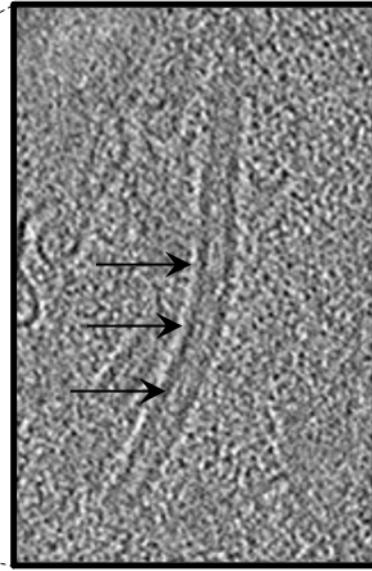
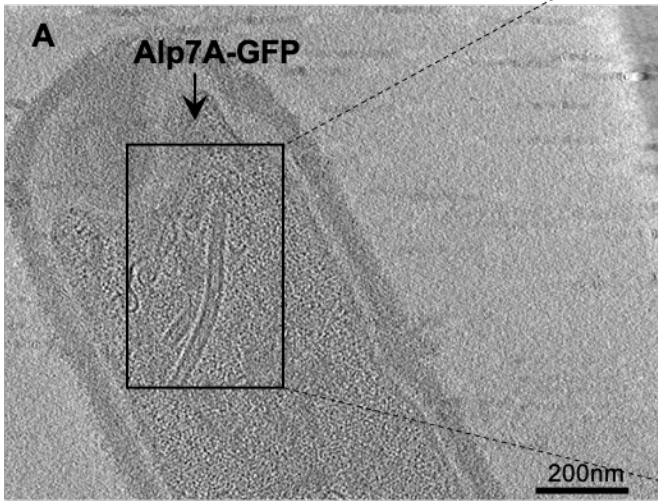


Figure 26. – Cryo-ET of Alp7A and Alp7A-GFP in *B. subtilis*.

Tomographic slice of *B. subtilis* strain 3267 showing Alp7A filaments (black arrows) in cells treated (A) or untreated (B) with lysozyme. C) Tomographic slice showing potential Alp7A filaments (arrows and cross) in *B. subtilis* strain 3268. Scale bar 200nm.

4.2.3 CLEM and LR white resin sections validated the filamentous structure of Alp7A-GFP in *B. subtilis* strain 3267

We performed CLEM on *B. subtilis* strain 3267 to validate that the filamentous structures observed by fLM and cryo-ET in *B. subtilis* cells correspond to Alp7A filaments. Alp7A-GFP was imaged under cryogenic conditions, after optimizing the upright Zeiss Axio Imager M2 Optical Microscope to fit the Linkam cryo-stage (CMS196). *B. subtilis* strain 3267 cells were loaded on Au R 2/2 Quantifoil EM grids and imaged with cryo-fLM to localize Alp7A-GFP inside the cells (**Figure 27A**). Images were first analyzed to pick targets that were then imaged by cryo-ET. After correlating the target cells with the tomograms collection, we applied reconstruction of tomograms using IMOD. The cryo-ET images showed filamentous structures in *B. subtilis* cells, confirming that these structures are, indeed, related to the fluorescent Alp7A-GFP targets identified by cryo-fLM (**Figure 27B**). No similar structures could be observed in the negative controls, *B. subtilis* strain 3266 lacking Alp7A protein and non-induced 3267 cells (data not shown).

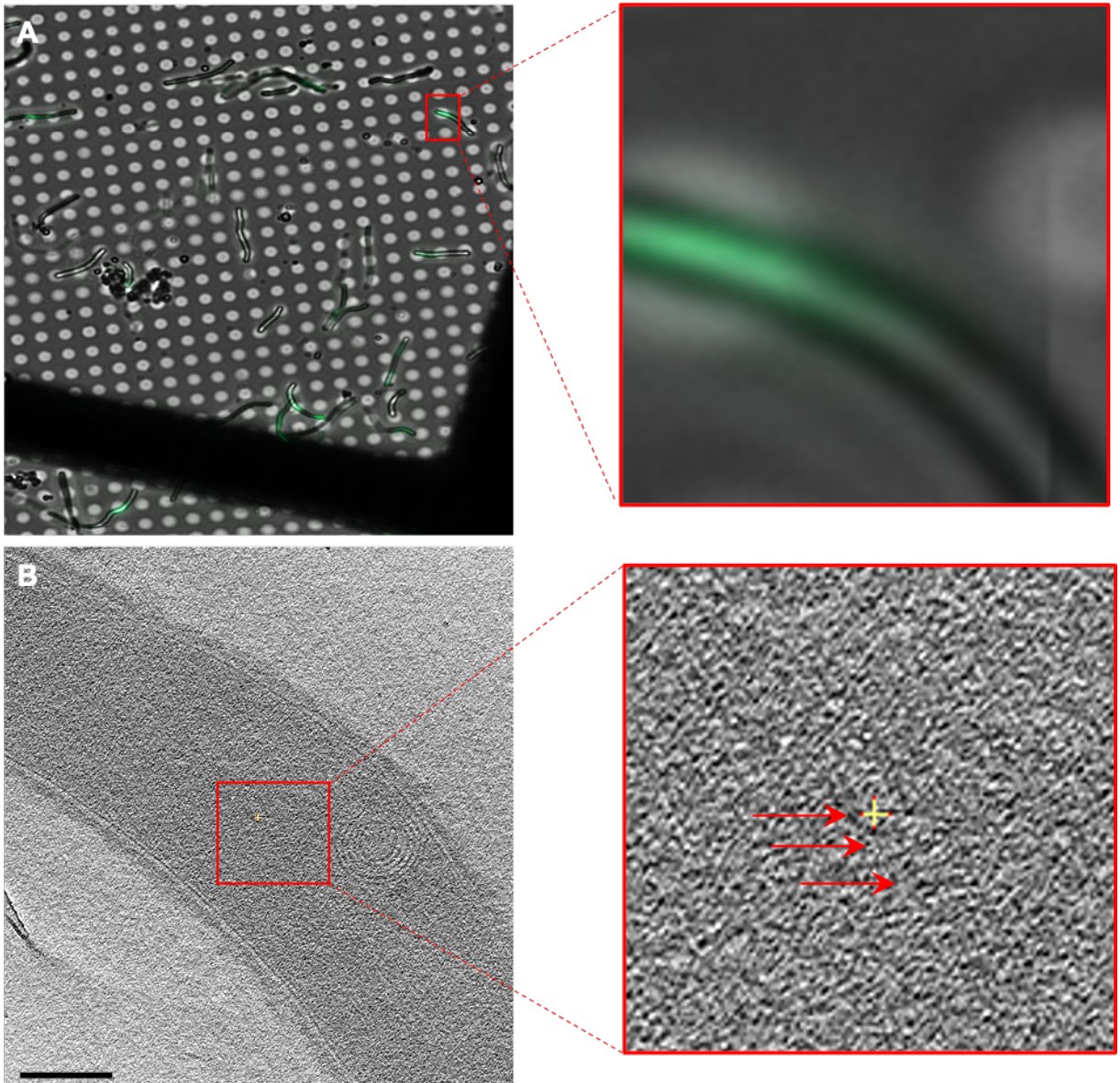


Figure 27. – Correlative light-electron microscopy (CLEM) of *B. subtilis* strain 3267.

A) Light microscopy (LM) atlas under cryogenic temperature, showing Alp7A-GFP in green color.
(B) Tomographic slice of the same *B. subtilis* cell. Scale bar 200nm.

We performed conventional resin embedding and imaging of bacterial slices to further support our observations and exclude the effect of bacterial cell thickness on cryo-ET imaging. Cellular sections of *B. subtilis* strain 3267, encoding Alp7A-GFP protein, showed filament-like structures in the bacterial cytoplasm under EM (**Figure 28**).

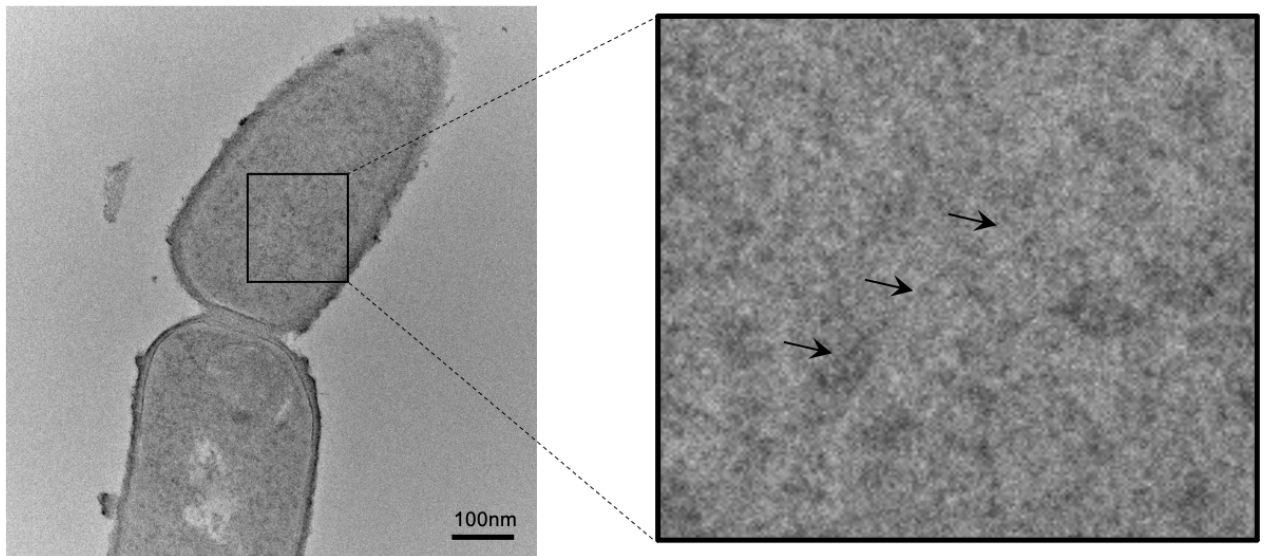


Figure 28. – LR white resin sectioning of *B. subtilis* strain 3267 expressing Alp7A-GFP.

EM projection of *B. subtilis* cell negatively stained with uranyl formate, showing filamentous structure of Alp7A-GFP inside the cell. Scale bar 100 nm.

Altogether, the results obtained by fLM, CLEM and resin embedding indicate that Alp7A forms filament structures that could play a role in the segregation and stability of the pSL20 plasmid.

4.2.4 Purification and visualization of Alp7A from *E. coli* Arctic Express (DE3) cells

We aimed to perform EM on purified Alp7A protein to characterize its structure and its mechanism of assembly and disassembly. We used a His-tagged form of Alp7A (Alp7A-His) to facilitate the purification of Alp7A protein using anti-His antibody. Alp7A-His was induced in *E. coli* Arctic Express (DE3) cells, then purified by ammonium sulfate precipitation, and imaged by EM. SDS-PAGE analysis of the purification eluate showed several bands in *E. coli* cellular pellet, but not in the supernatant that revealed an aggregation of proteins in pellet (**Figure 29A**). A major band was observed between 50 and 75 kDa in the cellular pellet eluate, which may correspond to GroEL (58 kDa), a highly expressed protein that aids in protein folding and is considered a major

contamination source in *E. coli* (**Figure 29A**). Yet, a light thin band was observed at ~45 kDa, possibly corresponding to Alp7A-His. Another band at a lower molecular weight (~27 kDa) was also observed, which could be a fragment of Alp7A-His or an unknown protein in *E. coli* (**Figure 29A**). To validate our observation, western blot was performed using anti-His antibody, which clearly showed the two bands at ~45 kDa and ~27 kDa (**Figure 29B**).

EM imaging of the purified extracts did not show any filamentous structure related to Alp7A. However, it showed mostly ring structures (top and side view), suggesting potential contamination of the Alp7A eluates (**Figure 29C**). We speculated that the observed ring-like structures are related to the highly expressed chaperone GroEL protein observed by SDS-PAGE (166).

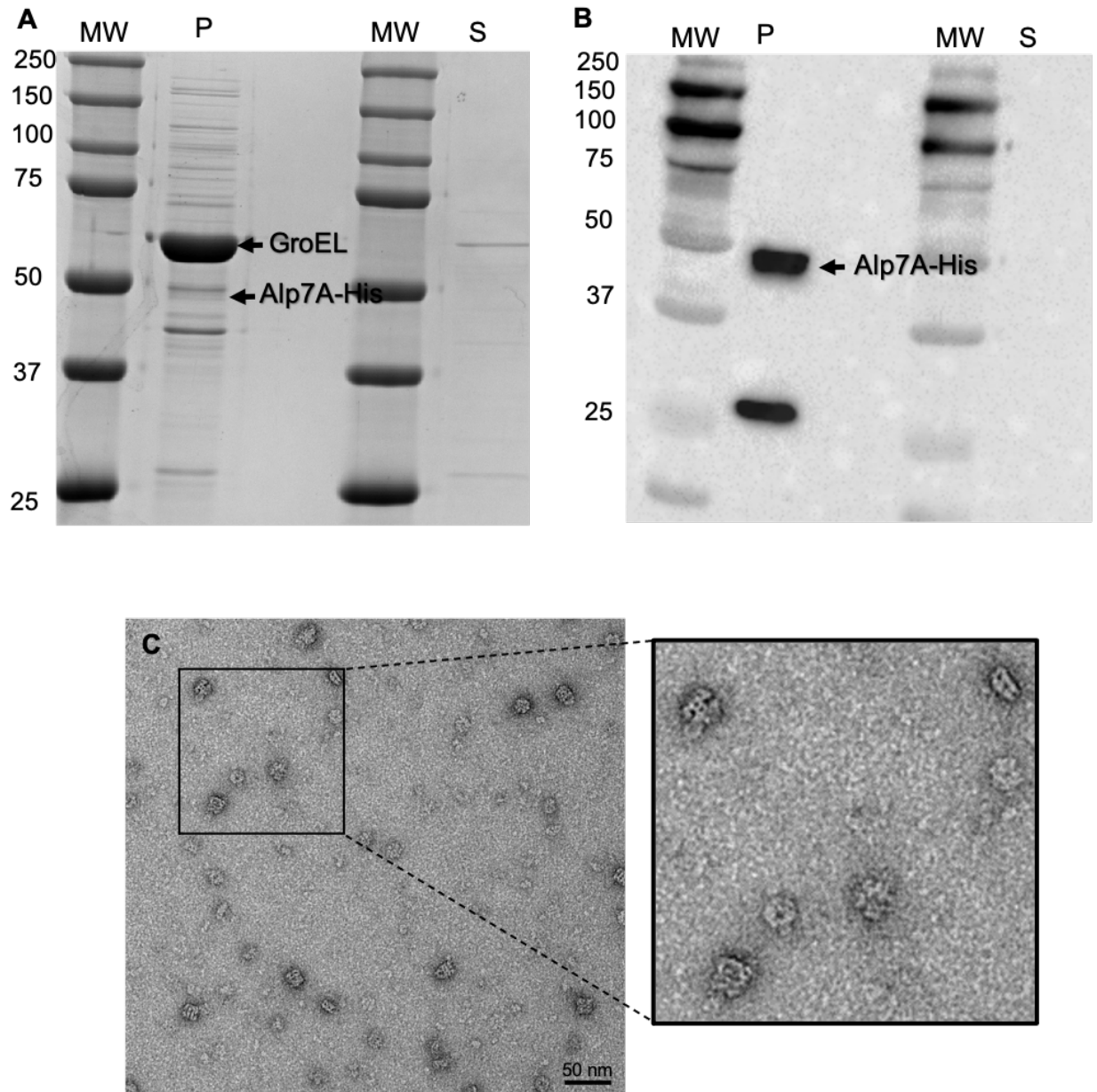


Figure 29. – Purification and Electron microscopy (EM) of Alp7A-His from *E. coli* Arctic express (DE3) cells.

- A) SDS-PAGE of Alp7A-His purified by ammonium sulfate from *E. coli* Arctic Express (DE3) cells. B) Western blot of purified Alp7A-His in ammonium sulfate eluate at 45kDa and lower molecular weight band at 27kDa that might be due to a degradation or contamination. C) Electron micrograph of the purified protein

showing ring-like structures. MW, Molecular weight; P, pellet; S, supernatant. Scale bar 50nm.

4.2.5 Purification and EM imaging of Alp7A-GFP-His from *E. coli* (DE3) cells

We could not specifically identify the structure of the purified Alp7A protein with the previous method by EM. Hence, we attempted to purify a GFP-His tagged form of Alp7A that can help identify the protein under fLM. Therefore, we expressed a Alp7A-GFP-His tagged in *E. coli*, which could be purified by affinity chromatography using anti-His antibody. We further concentrated the chromatography products by size exclusion chromatography to obtain eluates with higher purity. Aggregation of Alp7A protein was a major challenge during these purification trials. This was solved by the addition of 8M urea and 1% triton 100x, which aid in solubilizing the protein by breaking its weak bonds and disrupting its tertiary structure (167).

Affinity chromatography chromatograms showed a significant peak at ~121 ml (**Figure 30A**), which was loaded on an SDS-PAGE gel to identify the purified proteins. In correlation with the major peak revealed by the chromatogram, SDS-PAGE gel analysis revealed the presence of Alp7A-GFP-His (~72 kDa) in fractions A5 to A10, with a significant increase in protein yield in fractions A8, A9, and A10 (**Figure 30B**). In a second purification step, the fractions A8, A9, and A10 were combined and concentrated on an Amicon Ultra column, then loaded on a superdex 200 10/300 G1 column for size exclusion purification (**Figure 30C**). Size exclusion chromatography mainly allows protein purification based on their molecular size using polymeric beads in a column. The highest amount of protein was observed in fractions B9 to B12, with the highest peak present in fraction B10. SDS-PAGE gel analysis showed a band corresponding to Alp7A-GFP-His in all fractions, in addition to several other bands, indicating potential contamination or degradation of the protein (**Figure 30D**).

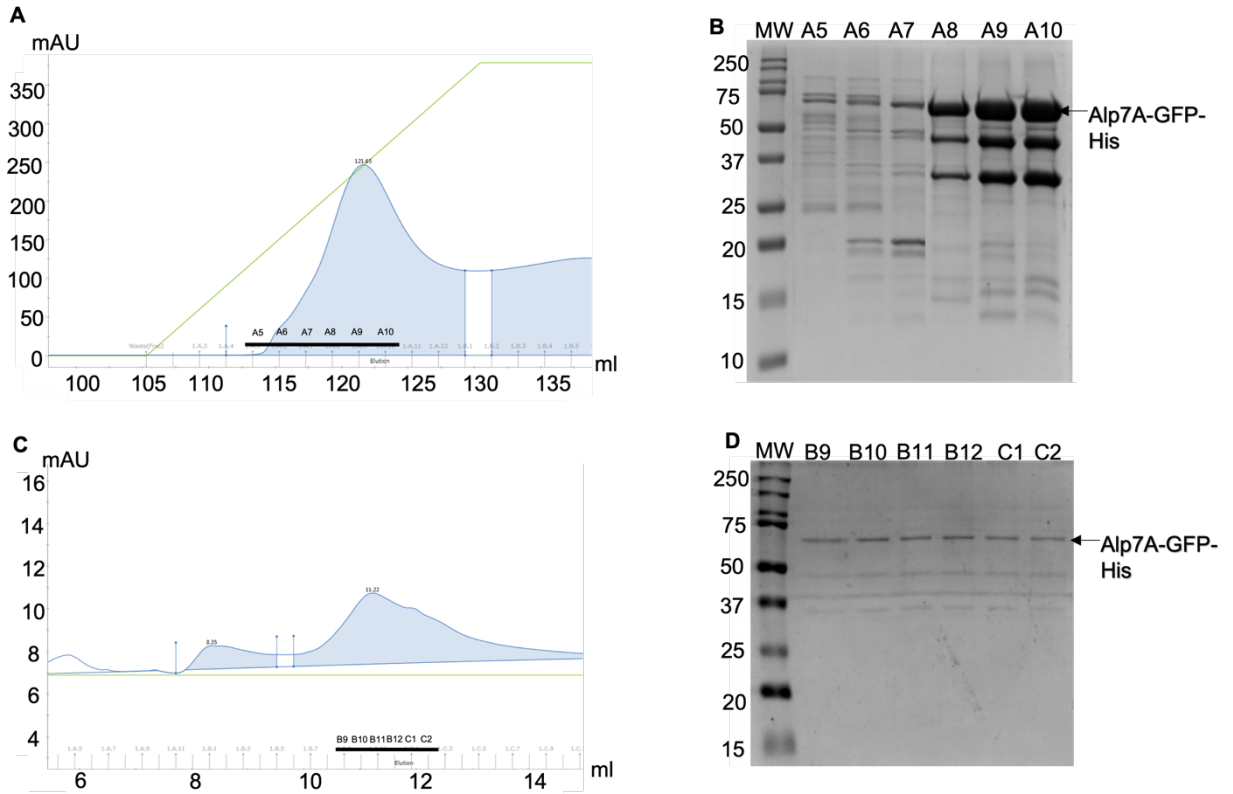


Figure 30. – Purification of Alp7A-GFP-His from *E. coli* (DE3) cells.

(A) Chromatogram of affinity chromatography showing a major peak at ~120 ml, including fractions A8 to A10. The green line represents the imidazole gradient. (C) SDS-PAGE of affinity chromatography fractions A5 – A10. (C) Chromatogram of size exclusion chromatography resulting in multiple peaks where Alp7A was eluted at ~11ml fractions from B9 to C2. (D) SDS-PAGE gel analysis verifying the eluted protein after size exclusion chromatography. MW, Molecular weight; mAU, milli-absorbance unit.

The presence of Alp7A-GFP-His in fraction B10 of size exclusion chromatography was validated by SDS-PAGE gel analysis (**Figure 31A**) and Western Blotting (**Figure 31B**). Western blot showed the presence of a band corresponding to Alp7A-GFP-His at ~72 kDa, and other two bands that at ~45 kDa and ~27 kDa, which could be a result of protein degradation. EM projections of the eluted protein in the absence of ATP showed a ring-like structure that could be a tetramer of Alp7A-GFP-His monomers (**Figure 31C**). After the addition of ATP, aggregation of protein occurred (**Figure 31D**), resulting in filament-like structures. Immune-gold labeling was used to

validate the relation of these aggregations to Alp7A protein. Results showed that the observed structures were unlabeled, suggesting contamination by misfolded proteins.

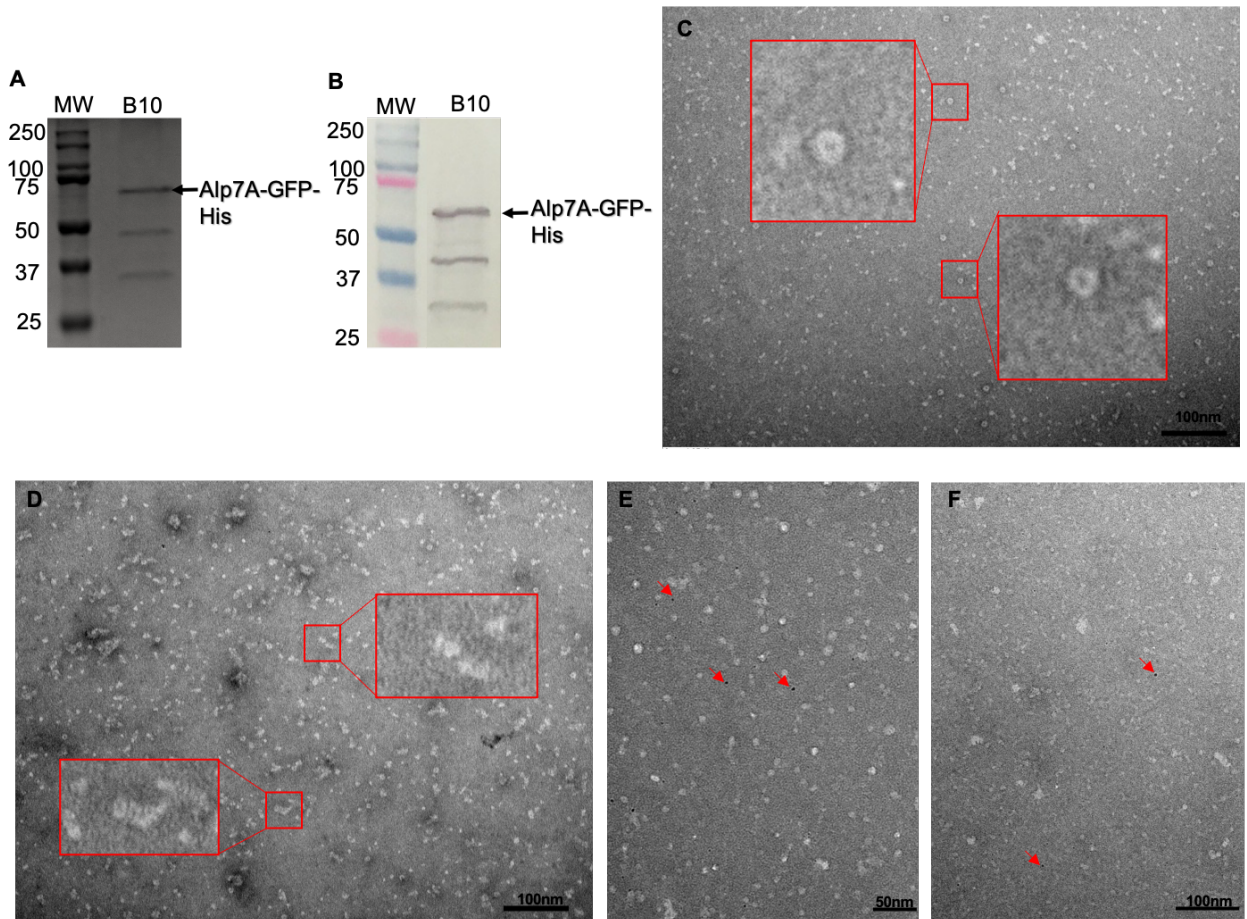


Figure 31. – EM visualization of Alp7A-GFP-His after purification from *E. coli*.

A) SDS-PAGE gels of fraction B10 after gel filtration. B) Western blot of fraction B10 after gel filtration. C) EM projection image of Alp7A-GFP-His negatively stained in the absence of ATP, showing ring-like structures. D) EM projection image of Alp7A-GFP-His negatively stained in the presence of ATP, showing protein aggregations. E - F) EM projection images of Alp7A-GFP-His after immuno-gold labeling at different magnifications. Red arrows point to gold beads at random positions. Scale bars 50 nm and 100 nm.

4.2.6 Purification of Alp7A from *E. coli* by ammonium sulfate precipitation and size exclusion chromatography

We assumed that the His tag is probably affecting Alp7A structure and function, preventing its proper visualization by EM *in vitro*. Hence, we hypothesized that purifying the native untagged form of the protein would result in a properly folded protein, which would hopefully assemble into filaments that can be visualized by EM *in vitro*. To purify the native form of Alp7A, we expressed untagged form of Alp7A in *E. coli*, then performed ammonium sulfate precipitation, followed by gel filtration and EM. According to the standard curve of the experiment, Alp7A remained soluble and eluted at ~55 ml with molecular weight of ~45 kDa (**Figure 32A**). However, contamination of the product can be easily observed by the presence of multiple peaks detected in the size exclusion chromatogram and by the multiple bands in the SDS-PAGE gel. The latter showed 3 bands in the fractions related to the peak of Alp7A: one main band at ~45 kDa, and two bands above and below this molecular weight (**Figure 32B**). EM images of elution fraction C3, containing the highest level and most pure eluate of Alp7A protein, showed filament-like structures and ring-like structures after incubation with ATP (**Figure 32C**). The three bands around 45 kDa in fraction C3 were analyzed by mass spectrometry, which identified the elongation factor of *E. coli* as the most abundant protein with a coverage up to 98% (386/394 aa). The second most abundant protein in this fraction was Alp7A, reaching a coverage of 78% (204/391 aa) (**Figure 32D**). These results suggest the presence of potential Alp7A filaments in the eluate, contaminated with EFTU1 of *E. coli*.

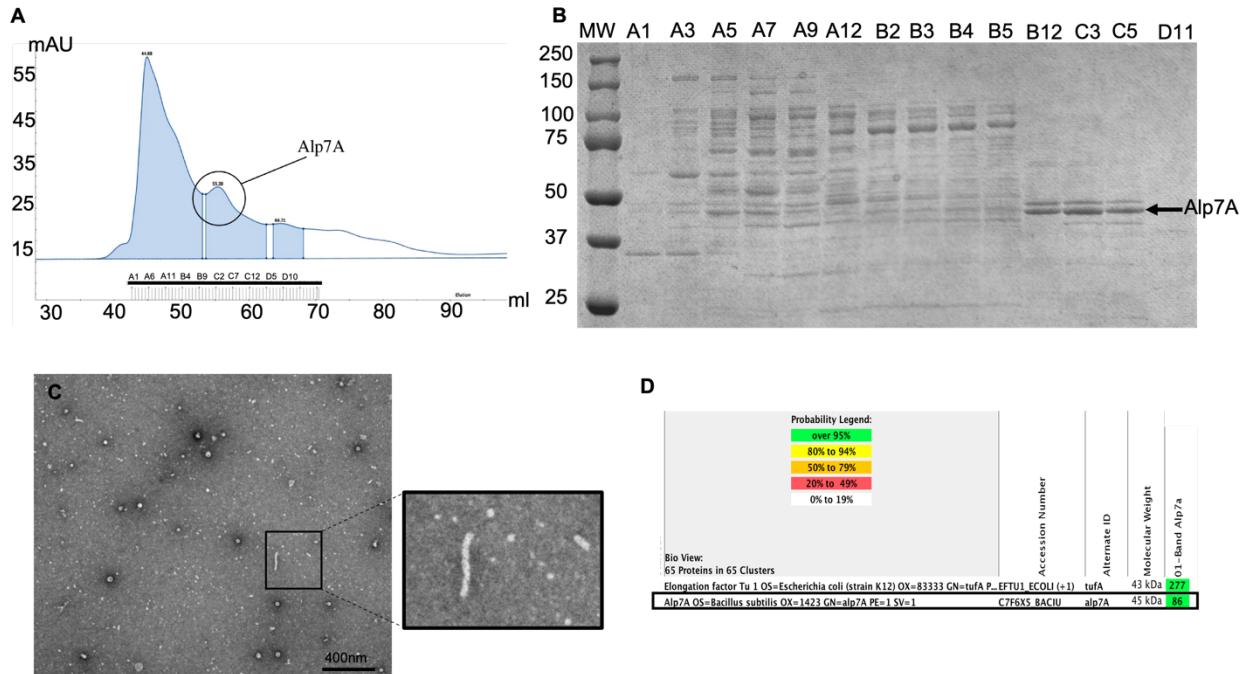


Figure 32. – Alp7A purification from *E. coli* (BL21).

A) Chromatogram of size exclusion chromatography after ammonium sulfate purification of Alp7A. B) SDS-PAGE analysis of the purification fractions. C) Electron micrograph of negatively stained untagged Alp7A after size exclusion chromatography, showing filament-like structures of Alp7A. D) Mass spectrometry results after gel filtration indicating Alp7A and EFTU1 as the most abundant proteins. Scale bar 400nm.

5 Discussion

5.1 Project 1: Characterization of phase-bright objects in members of Proteobacteria and Actinobacteria

Endospore formation is considered a hallmark of the Firmicutes phylum, mainly in the Bacilli and Clostridia classes (12, 13, 24). However, rare endospore production has been recently reported outside of Firmicutes, particularly in members of the phyla Proteobacteria and Actinobacteria (34, 35). These findings may affect our understanding of the evolutionary events surrounding outer membrane biogenesis and complex membrane remodeling events such as endospore formation. In addition, discoveries of wider distribution of endospore formation among pathogenic bacteria raise concerns about the detection and treatment of infections associated with *S. marcescens* and *M. marinum*. Therefore, using cutting-edge microscopy techniques, alongside biochemical and microbiological approaches, we aimed to characterize the nature of phase-bright objects and determine the endospore formation capacity in *R. johrii*, *S. marcescens*, and *M. marinum*. Using CLEM, cryo-ET, and traditional spore detection methods, including differential staining, heat resistance, and DPA measurement, we showed that the phase bright objects are non-spore structures in the three species. Our observations showed that the phase-bright objects in *R. johrii* and *M. marinum* are likely storage granules.

5.1.1 *M. marinum* are unable to sporulate and survive high temperatures

The results observed by Ghosh *et al.* showed phase-bright objects occupying 30% to 60% of the mother cells' cytoplasm. In contrast, our phase-contrast images showed phase-bright objects occupying only a small proportion of the mother cell in *M. marinum*. Interestingly, the phase-bright objects we observed in *B. subtilis* were very similar to those observed by Ghosh *et al.* in *M. marinum* (47). This observation indicates potential contamination of Ghosh *et al.*'s *M. marinum* cultures by *B. subtilis* (47). In this regard, the authors did not include positive or negative controls in their experiments, and their TEM analysis revealed high similarity with the structure of *B. subtilis* spores (52).

Our cryo-ET images showed pale and diffuse objects in *M. marinum* that do not resemble endospores. The observed objects did not possess any endospore-related features such as cortex, core, and proteinaceous coat. These observations were further validated using CLEM, confirming that the phase-bright objects observed under LM do not show endospore features under EM. Our observations rather propose that the phase-bright objects in *M. marinum* are putative storage granules of intracellular lipid inclusions, appearing as pale phase-bright objects under contrast microscopy (168, 169). Intracellular lipid inclusions arise under limited growth conditions, such as carbon-poor media, and are unique to Mycobacteria's stationary phase. The formation of storage granules in mycobacterium in minimal media was reported by several studies (164, 170). Another type of storage granules that we observed in *M. marinum* by cryo-ET was polyphosphate (PolyP) granules. The presence of different types of storage granules is considered a reason for the long persistence of mycobacterium under restricted conditions. Taken together, these observations indicate that several types of storage granules accumulate in *M. marinum* to help the bacteria endure stress under minimal growth conditions.

Following up on the experiments performed by Ghosh *et al.* (47), we performed the same biochemical spore detection methods using similar conditions. The authors reported that 40% of the *M. marinum* cells could survive heat treatment at 65 °C. Despite using the same strains and batches as those used by Ghosh *et al.*, our results showed that the cultures of *M. marinum* were unable to survive and grow after heat treatment. This is in line with the results obtained by Traag *et al.* (52), showing complete cell mortality in 30-days-old *M. marinum* cultures after incubation at 65 °C. These observations were further supported by the absence of DPA in our *M. marinum* cultures.

In summary, our findings demonstrate that it is implausible that *M. marinum* can undergo sporulation. Indeed, neither our study nor that of Traag *et al.* could reproduce the results of Gosh *et al.* showing the ability of *M. marinum* to sporulate and survive high temperatures *in vitro*.

5.1.2 Putative storage granules in *R. johrii* and *S. marcescens*

Tomographic slices analysis showed that the phase-bright objects resemble storage granules in *R. johrii*, while they are similar to cellular debris in *S. marcescens*, while they. Further validation

of these observations was performed using CLEM, which offers the possibility of confirming that the phase-bright objects observed under the EM correspond to the LM. These differences could be explained by variation in techniques used to characterize the endospores. Indeed, the results in the two articles were based on transmission electron microscopy TEM in detecting phase bright objects. TEM may provide reduced resolution and lead to misinterpretations of inclusion bodies. For example, osmium tetroxide may not penetrate compact structures such as spores during traditional cellular preparation, while fixative agents may destroy subcellular components and internal membranes essential for endospore characterization.

Our investigations into spore detection proceeded utilizing biochemical procedures similar to those used in the articles in question. Girija *et al.* discovered viable *R. johrii* strain JA192(T) cells after heat treatment at 80 °C (35), but other *R. johrii* strains could not withstand this temperature. On the other hand, Ajithkumar *et al.* reported growth of *Serratia marcescens* subsp. *Sakuensis*, after heat treatment for seven days and 3-month-old cells at 75 °C for 15 mins in nutrient growth broth (34). Despite using the same strains and batches as those used in both studies, our results showed that both species under study could not survive and grow after heat treatment, as previously reported. Our results were further supported by the absence of DPA in our cultures of *R. johrii* and *S. marcescens*. Previous observations by Girija *et al.* and Ajithkumar *et al.* (34, 35), could occur due to contamination with spore-forming bacteria in the batches used in both studies.

Taken together, CLEM, cryo-ET, and traditional spore detection methods (differential staining, heat resistance, and DPA measurement) disproved the presence of endospores in of *R. johrii* and *S. marcescens*. Our results indicated that the phase bright objects in *R. johrii* are putative storage granules, while those observed in *S. marcescens* are likely cell debris that result from cell death.

5.1.3 TAGs as a survival arsenal in *R. johrii* cells

Lipidomic analysis showed up to a 98-fold increase of TAGs in *R. johrii* cells with phase-bright objects, compared with control cells without phase-bright objects. TAGs are nonpolar triacylglycerols that occur as insoluble inclusions that serve as a major energy source in actinomycetes bacteria (59, 171). TAGs have been shown to accumulate in mycobacteria as either

peripheral deposits associated with the cell envelope or as inclusion bodies in the cytoplasm (165). In addition, *in vitro* studies on mycobacteria showed accumulation of TAGs and wax esters before starting a dormancy state when subjected to stress, such as low oxygen, high CO₂, low nutrient, and acidic pH (165, 172, 173). This suggests that *R. johrii* may store TAGs as an energy source that enables them to help them withstand stress conditions, represented here by low nutrient conditions.

5.1.4 Lack of sporulation genes in *R. johrii*, and *S. marcescens*

Sporulation requires specific expression and regulation of hundreds of genes (143, 174, 175) at different stages of sporulation. *B. subtilis* of Firmicutes phylum is considered the best-studied model of sporulating bacteria. It possesses over 500 genes involved in sporulation (174). Not all genes involved in sporulation are deemed essential for this process. Several homologs of these genes have been detected in different phyla, such as proteobacteria (176, 177), where they play a regulatory role not related to sporulation, such as cell division and development. Hence, identifying genes involved in sporulation could not be considered concrete evidence to support sporulating capacity in bacteria (13). Galperin *et al.* (13) reported a total of 60 conserved genes among all spore-forming bacilli and clostridia, of which we showed that *R. johrii* lacks more than 50% of these conserved sporulating genes. These observations further support the lack of sporulation capacity in *R. johrii* and *S. marcescens*. Similarly, Ajithkumar *et al.* were unable to detect genes related to endospore formation in *S. marcescens* (34), despite claiming that this species is a sporulating bacterium.

5.1.5 Conclusion

In contrast to the findings by Giriya *et al.* (35), Ajithkumar *et al.*(34), and Ghosh *et al.* (47), we showed using a combination of molecular biology and cutting-edge microscopy techniques that *R. johrii*, *S. marcescens*, and *M. marinum* are not endospore formers. The detected endospore-like structures in the three former studies could be a result of contamination with spore-forming bacteria in their cultures or to misinterpretation of artifacts produced by the used techniques. Our deeper characterization of the phase-bright objects at a higher resolution using TEM revealed that they correspond to lipid storage granules in *M. marinum*, TAGs in *R. johrii*, and cellular debris in *S. marcescens*. These results provide new insights for a better understanding the persistence of certain bacterial species under stress conditions. Yet, further investigations are required to characterize the

biochemical nature of these storage granules and their role in the survival of in *M. marinum* and *R. johrii* under unfavorable conditions.

Altogether, our study supports the concept that endospore formation is an evolutionary process limited to the phylum Firmicutes and highlights potential mechanisms of persistence of bacterial cells in *M. marinum* and *R. johrii* through storage granules.

5.2 Project 2: Characterization of Alp7A structure *in vivo* and *in vitro*

Bacterial pathogenicity and antibiotic resistance affect thousands of lives every year and generate an essential burden on our health care system. Disrupting plasmid segregation has tremendous potential for developing novel strategies to limit the distribution of antimicrobial resistance genes. This project investigated a newly characterized DNA segregation machinery, *alp7ARC*, responsible for the segregation of the pLS20 plasmid encoding the tetracycline resistance genes in *B. subtilis*.

Recent studies have indicated an essential role for Alp7ARC in the stability of the low copy number plasmid pLS20 in *B. subtilis*. *In vitro* investigations by Petek *et al.* (178) showed that Alp7A utilizes ATP to form two-stranded filaments that appear as ribbon-like bundles, which rapidly disassemble after ATP depletion (155, 178). The process of assembly and disassembly of the Alp7A filaments was shown to require a critical concentration of ATP. Alp7R, is known as DNA-binding protein of the Alp7ARC machinery, was shown to decrease the critical concentration associated with ATP hydrolysis for filaments formation (178). These findings highlighted the dynamic nature of Alp7A and suggested a role for Alp7R in the nucleation and stabilization of Alp7A filaments.

5.2.1 Alp7A forms filamentous structure in *B. subtilis*

We observed a filamentous structure of Alp7A under fLM in a slender mutant (Δ ponA) of *B. subtilis*. This was in line with the structure of Alp7A revealed by Derman and colleagues in wild-type *B. subtilis* cells using fLM (100).

It was challenging to localize Alp7A inside *B. subtilis* cells and visualize its ultrastructure (filament or tubular structure) by fLM due to the limited resolution of the technique to ~250 nm. While cryo-ET has the potential to study Alp7A at a higher resolution in its near-native state, the thickness of the slender *B. subtilis* (~800 nm) posed a major challenge to perform this technique. Hence, in some experiments we treated *B. subtilis* cells with lysozyme to loosen their membrane during tomograms collection and obtain clearer images of the cells' cytoplasm. Besides, the 300kV Titan Krios microscope available at FEMR was not optimized to image bacterial cells with such a thickness and required the installation of a Gatan imaging filter to visualize proteins *in vivo* inside bacterial cells. Other challenges that we faced during cryo-ET experiments included cell bubbling, missing wedges, dead cells, and focus shift.

A potential solution to consider at this point would be using a cryo-focused ion beam (cryo-FIB), a cutting-edge technology that provides access to structures deep inside cells via cryo-sectioning (179, 180). This approach overcomes the limitation of sample thickness associated with cryo-ET and enables structural investigation of macromolecules in their native state *in situ*. Unfortunately, the technique was not accessible at our institution, or in Canada, and required collaboration with labs abroad after considering samples stability and transportation issues.

5.2.2 Challenges during Alp7A purification for *in vitro* studies

Our initial purification trials showed that Alp7A is a very sensitive protein, and it remains active only two weeks after purification and storage at -80 °C. Therefore, it was highly recommended to start single-particle analysis from fresh protein samples.

We first tried to purify Alp7A-GFP directly from its native environment, *B. subtilis* cells strain 3267. However, the low yield of the protein resulted in the imaging of flagella instead of Alp7A filaments under EM (data not shown). Hence, we opted to use unique expression systems

that would produce higher amounts of the protein under controllable conditions. The initial purification experiments were performed using the *E. coli* Arctic express cells (DE3) expressing His-tagged Alp7A (Alp7A-His). However, the highly expressed groEL in these bacteria led to the contamination of Alp7A eluates, which mainly showed ring-like structures related to groEL under EM. Besides, it was challenging to obtain pure Alp7A-His monomers; instead, we could only get aggregations of the protein (inclusion bodies).

To overcome this problem, we induced Alp7A in another strain of *E. coli*, B121. Still, we faced another contamination challenge with the elongation factor EFTU1 in this bacterium. Mass spectrometry showed contamination with the highly abundant protein EFTU1 with an Isoelectric point (PI) of 5.30 and MW ~44 kDa, which is very similar to Alp7A with PI of 5.32 MW of ~45 kDa. Despite taking all precautions to reduce contamination, including cleaning and changing the purification columns, we could not obtain pure Alp7A due to the arduous separation of proteins with such physio-chemical similarities.

In our attempt to obtain the highest possible pure yield of Alp7A, we tried multiple other approaches, including purification from *E. coli* of untagged Alp7A protein, His-tagged Alp7A protein, and GFP-His-tagged Alp7A protein. Our purification trials suggested that the purification of untagged Alp7A protein using ammonium sulfate produced the purest Alp7A protein among all other purification trials. Despite following the same protocol of ammonium sulfate purification performed by Petek *et al.* (178), we could only obtain low yields of Alp7A contaminated with other *E. coli* proteins. We were able to verify the identity of the purified Alp7A protein by western blot and mass spectrometry. However, our immunogold labelling could not correlate the observed patches of filamentous structures under EM with Alp7A. It is worth mentioning that Petek *et al.* didn't perform any validation of their purified proteins to confirm its identity (178).

5.2.3 Conclusion and suggestions

Altogether, studying the structure of Alp7A was very challenging due to its aggregation, poor nucleotide affinity, and its possible regulation by Alp7R. A primary objective of our study was to use single-particle analysis and generate a pseudo-atomic model of Alp7A protein. Our study recommends using fresh samples to investigate the structure and dynamics of Alp7A in its

native state at a nanomolecular resolution. Unfortunately, we could not obtain a protein with sufficient purity to perform single particle analysis due to time limitations and several experimental challenges, including aggregation of Alp7A and contamination with highly expressed proteins. Alp7A cannot polymerize and would rather aggregate quickly under conditions that do not meet its critical ATP concentration. Expressing the protein outside its natural system might result in lower protein yield for several reasons, including improper codon usage and protein folding. Likewise, expressing single gene constructs may lead to protein aggregation and lower protein levels compared with strains expressing the complete operon. Furthermore, protein tags that aid in protein identification and purification may interfere with proteins functionality and folding.

At this stage, I would suggest purifying Alp7A after overexpressing it in its native host in *B. subtilis*. This can be better achieved by developing immunoaffinity columns using the specific anti-Alp7A antibodies that we developed in Tocheva lab. Another approach would be using other expression systems with proper codon optimization after considering any effect on protein conformation, function, and stability. Such approach requires validation of plasmid stability and Alp7A's filamentous structure and dynamics before purification. Further, consider using protein tags that would retain protein stability and proper folding, such as GST-tag, instead of using His-tagged Alp7A. While we could not achieve our main goals in this project, we gained extensive experimental expertise and knowledge that would provide basic concepts for investigating Alp7A in the future.

Articles and Contributions

Project I:

This project resulted in two manuscripts: one published and one in preparation.

The first published article entitled “No Endospore Formation Confirmed in Members of the Phylum Proteobacteria” was published in March 2021 in the journal *Applied and Environmental Microbiology*. I and Polina Beskrovnaya contributed equally to this work. This project was initiated with Isabelle Morneau who she did the phenotypic experiments on *S. marcescens* and preparation of cells for cryo-ET at Universite de Montreal. In this work, I optimized the CLEM experiments and was responsible for sample preparation, data collection, target picking, and data analysis. I contributed to all aspects of electron microscopy experiments, including experimental design, preparing the samples, and data acquisition with Dr. Kaustuv Basu at the Facility for Electron Microscopy Research (FEMR) of McGill University, under the supervision of Dr. Elitza Tocheva. Together with Dr. Elitza Tocheva, we analyzed the collected data and prepared for the final images. I also contributed to the biochemistry experiments through sample preparation, and data collection and analysis in collaboration with my colleague Isabelle Morneau. I wrote the first drafts of the manuscript and reviewed and edited it. Polina and Dr. Tocheva finally revised and completed our work to submit the manuscript. Dr. Tocheva was the supervisor of the whole project. Dr. Nanci contributed to this article by supervision, funding, and project administration. The SEM and EDX experiments were performed in collaboration with Dainelys Guadarrama Bello, from Dr. Nanci’s lab, who operated the microscope at UdeM, where I was responsible for sample preparation, and data collection, picking targets, and data analysis. Furthermore, the whole lipidomic analysis experiment was done in collaboration with Dr. Huan at the University of British Columbia (UBC). The bioinformatics analysis of sporulation genes in *R. jhorii* was performed by Ameena Hashimi from the Tocheva lab at UBC.

The second manuscript entitled “Characterization of phase bright objects by cutting-edge microscopy techniques in *Mycobacterium Marinum*” is still in preparation. In this work we investigated the ability of *Mycobacterium Marinum* to form endospores. The *B. subtilis* was used as the control species as endospore former bacterium. In this project, I contributed to investigation,

sample preparation, data analysis, visualization, writing first draft, review and editing. This project was done in collaboration with Will dePass, Dr. Grant Jensen, and Dr. Dianne Newman, from the Division of Biology and Biological Engineering at California Institute of Technology. The project was initiated at Dr. Tocheva's lab by following the sample preparation and visualization protocols of *M. marinum* that were optimized by Will dePass. I prepared samples and worked on data visualization and analysis. I collected the EM data at the FEMR platform at McGill University with the microscope operator Dr. Kaustuv Basu and the supervision of Dr. Tocheva. I also performed CLEM and Biochemistry experiments at Université de Montréal.

Project II:

This project didn't yield any article. More investigation to be done for the analysis and characterization of Alp7A and its role in plasmid segregation. I participated in experimental design, investigation, data curation, and sample preparations. I did Alp7A purification and the generation of Alp7A-GFP-His construct with the help of Dr. Driss Lajoi from Dr. Tocheva's lab at UdeM. I also performed the experiment of conventional resin section in collaboration with Katia Ponce from Dr. Nanci's lab at UdeM; in these experiments I prepared the samples, collected data, and analysed the results. The mutant *B. subtilis* (Δ ponA) was kindly offered by Dr. Pogliano from University of California San Diego (UCSD). The three plasmid constructs, 3266, 3267, and 3268, were kindly offered by Dr. Derman at UCSD. Finally, the mass spectrometry experiments were performed in collaboration with Lisbeth-Carolina Aguilar at Oeffinger lab (IRCM).

6 References

1. Parker J. Bacteria. In: Brenner S, Miller JH, editors. Encyclopedia of Genetics. New York: Academic Press; 2001. p. 146-51.
2. Schroeder E, Wuertz S. 3 - Bacteria. In: Mara D, Horan N, editors. Handbook of Water and Wastewater Microbiology. London: Academic Press; 2003. p. 57-68.
3. Silhavy TJ, Kahne D, Walker S. The bacterial cell envelope. Cold Spring Harbor perspectives in biology. 2010;2(5):a000414-a.
4. Neuhaus FC, Baddiley J. A continuum of anionic charge: structures and functions of D-alanyl-teichoic acids in gram-positive bacteria. Microbiology and molecular biology reviews : MMBR. 2003;67(4):686-723.
5. van der Es D, Hogendorf WFJ, Overkleeft HS, van der Marel GA, Codée JDC. Teichoic acids: synthesis and applications. Chemical Society Reviews. 2017;46(5):1464-82.
6. Mikami K, Kimura M, Takahashi H. Influence of maternal bifidobacteria on the development of gut bifidobacteria in infants. Pharmaceuticals (Basel). 2012;5(6):629-42.
7. Kang SS, Sim JR, Yun CH, Han SH. Lipoteichoic acids as a major virulence factor causing inflammatory responses via Toll-like receptor 2. Arch Pharm Res. 2016;39(11):1519-29.
8. Love MJ, Bhandari D, Dobson RCJ, Billington C. Potential for Bacteriophage Endolysins to Supplement or Replace Antibiotics in Food Production and Clinical Care. Antibiotics (Basel). 2018;7(1).
9. Cano RJ, Borucki MK. Revival and identification of bacterial spores in 25- to 40-million-year-old Dominican amber. Science. 1995;268(5213):1060-4.
10. Kennedy MJ, Reader SL, Swierczynski LM. Preservation records of micro-organisms: evidence of the tenacity of life. Microbiology. 1994;140 (Pt 10):2513-29.
11. Vreeland RH, Rosenzweig WD, Powers DW. Isolation of a 250 million-year-old halotolerant bacterium from a primary salt crystal. Nature. 2000;407(6806):897-900.
12. Setlow P. I will survive: DNA protection in bacterial spores. Trends Microbiol. 2007;15(4):172-80.

13. Galperin MY, Mekhedov SL, Puigbo P, Smirnov S, Wolf YI, Rigden DJ. Genomic determinants of sporulation in Bacilli and Clostridia: towards the minimal set of sporulation-specific genes. *Environmental microbiology*. 2012;14(11):2870-90.
14. Nicholson WL, Munakata N, Horneck G, Melosh HJ, Setlow P. Resistance of *Bacillus* endospores to extreme terrestrial and extraterrestrial environments. *Microbiology and molecular biology reviews : MMBR*. 2000;64(3):548-72.
15. Tocheva EI, Ortega DR, Jensen GJ. Sporulation, bacterial cell envelopes and the origin of life. *Nat Rev Microbiol*. 2016;14(8):535-42.
16. Vaksman Z, Kaplan HB. *Myxococcus xanthus* Growth, Development, and Isolation. *Current protocols in microbiology*. 2015;39:7A 1 -7A 1 21.
17. Qinyuan L, Xiu C, Yi J, Chenglin J. Morphological Identification of Actinobacteria. In: Dharumadurai D, Yi J, editors. *Actinobacteria: IntechOpen*; 2016.
18. Bobek J, Šmídová K, Čihák M. A Waking Review: Old and Novel Insights into the Spore Germination in *Streptomyces*. *Frontiers in Microbiology*. 2017;8:2205.
19. Barka EA, Vatsa P, Sanchez L, Gaveau-Vaillant N, Jacquard C, Meier-Kolthoff JP, et al. Taxonomy, Physiology, and Natural Products of Actinobacteria. *Microbiology and molecular biology reviews : MMBR*. 2015;80(1):1-43.
20. Briza P, Breitenbach M, Ellinger A, Segall J. Isolation of two developmentally regulated genes involved in spore wall maturation in *Saccharomyces cerevisiae*. *Genes & development*. 1990;4(10):1775-89.
21. Ausmees N, Wahlstedt H, Bagchi S, Elliot MA, Buttner MJ, Flardh K. SmeA, a small membrane protein with multiple functions in *Streptomyces* sporulation including targeting of a SpoIIIE/FtsK-like protein to cell division septa. *Mol Microbiol*. 2007;65(6):1458-73.
22. Thaxter R. On the Myxobacteriaceae, a new order of Schizomycetes. *Bot Gaz*. 1892;17:389-406.
23. Kaiser D, Welch R. Dynamics of fruiting body morphogenesis. *Journal of bacteriology*. 2004;186(4):919-27.
24. Paredes CJ, Alsaker KV, Papoutsakis ET. A comparative genomic view of clostridial sporulation and physiology. *Nat Rev Microbiol*. 2005;3(12):969-78.

25. Kroos L. The *Bacillus* and *Myxococcus* developmental networks and their transcriptional regulators. *Annual review of genetics*. 2007;41:13-39.
26. de Hoon MJL, Eichenberger P, Vitkup D. Hierarchical evolution of the bacterial sporulation network. *Current biology : CB*. 2010;20(17):R735-R45.
27. Tocheva EI, Lopez-Garrido J, Hughes HV, Fredlund J, Kuru E, Vannieuwenhze MS, et al. Peptidoglycan transformations during *Bacillus subtilis* sporulation. *Mol Microbiol*. 2013;88(4):673-86.
28. Stragier P, Losick R. Molecular genetics of sporulation in *Bacillus subtilis*. *Annual review of genetics*. 1996;30:297-41.
29. Piggot PJ, Hilbert DW. Sporulation of *Bacillus subtilis*. *Curr Opin Microbiol*. 2004;7(6):579-86.
30. Errington J. Regulation of endospore formation in *Bacillus subtilis*. *Nat Rev Microbiol*. 2003;1(2):117-26.
31. Errington J. *Bacillus subtilis* sporulation: regulation of gene expression and control of morphogenesis. *Microbiol Rev*. 1993;57(1):1-33.
32. Stephens C. Bacterial sporulation: a question of commitment? *Curr Biol*. 1998;8(2):R45-8.
33. Abecasis AB, Serrano M, Alves R, Quintais L, Pereira-Leal JB, Henriques AO. A Genomic Signature and the Identification of New Sporulation Genes. *Journal of Bacteriology*. 2013;195(9):2101.
34. Ajithkumar B, Ajithkumar VP, Iriye R, Doi Y, Sakai T. Spore-forming *Serratia marcescens* subsp. *sakuensis* subsp. nov., isolated from a domestic wastewater treatment tank. *Int J Syst Evol Microbiol*. 2003;53(Pt 1):253-8.
35. Girija KR, Sasikala C, Ramana Ch V, Sproer C, Takaichi S, Thiel V, et al. *Rhodobacter johrii* sp. nov., an endospore-producing cryptic species isolated from semi-arid tropical soils. *Int J Syst Evol Microbiol*. 2010;60(Pt 9):2099-107.
36. Hejazi A, Falkiner FR. *Serratia marcescens*. *Journal of medical microbiology*. 1997;46(11):903-12.
37. Guentzel MN. *Escherichia*, *Klebsiella*, *Enterobacter*, *Serratia*, *Citrobacter*, and *Proteus*. In: *th*, Baron S, editors. *Medical Microbiology*. Galveston (TX)1996.

38. Hurrell E, Kucerova E, Loughlin M, Caubilla-Barron J, Hilton A, Armstrong R, et al. Neonatal enteral feeding tubes as loci for colonisation by members of the Enterobacteriaceae. *BMC infectious diseases*. 2009;9:146.
39. Matsumoto Y, Kinjo T, Motooka D, Nabeya D, Jung N, Uechi K, et al. Comprehensive subspecies identification of 175 *nontuberculous mycobacteria* species based on 7547 genomic profiles. *Emerg Microbes Infect*. 2019;8(1):1043-53.
40. Lopez-Varela E, Garcia-Basteiro AL, Santiago B, Wagner D, van Ingen J, Kampmann B. *Nontuberculous mycobacteria* in children: muddying the waters of tuberculosis diagnosis. *The Lancet Respiratory medicine*. 2015;3(3):244-56.
41. Sia JK, Rengarajan J. Immunology of *Mycobacterium tuberculosis* Infections. *Microbiol Spectr*. 2019;7(4).
42. Halstrom S, Price P, Thomson R. Review: Environmental mycobacteria as a cause of human infection. *International journal of mycobacteriology*. 2015;4(2):81-91.
43. Falkingham JO, 3rd. Environmental sources of nontuberculous *mycobacteria*. *Clinics in chest medicine*. 2015;36(1):35-41.
44. Chin KL, Sarmiento ME, Alvarez-Cabrera N, Norazmi MN, Acosta A. Pulmonary non-tuberculous mycobacterial infections: current state and future management. *European journal of clinical microbiology & infectious diseases* : official publication of the European Society of Clinical Microbiology. 2020;39(5):799-826.
45. Wayne LG, Sohaskey CD. Nonreplicating persistence of *mycobacterium tuberculosis*. *Annual review of microbiology*. 2001;55:139-63.
46. Podinovskaia M, Lee W, Caldwell S, Russell DG. Infection of macrophages with *Mycobacterium tuberculosis* induces global modifications to phagosomal function. *Cellular microbiology*. 2013;15(6):843-59.
47. Ghosh J, Larsson P, Singh B, Pettersson BM, Islam NM, Sarkar SN, et al. Sporulation in *mycobacteria*. *Proc Natl Acad Sci U S A*. 2009;106(26):10781-6.
48. Volkman HE, Clay H, Beery D, Chang JCW, Sherman DR, Ramakrishnan L. Tuberculous Granuloma Formation Is Enhanced by a *Mycobacterium* Virulence Determinant. *PLOS Biology*. 2004;2(11):e367.

49. Hashish E, Merwad A, Elgaml S, Amer A, Kamal H, Elsadek A, et al. *Mycobacterium marinum* infection in fish and man: epidemiology, pathophysiology and management; a review. *Vet Q.* 2018;38(1):35-46.
50. Aubry A, Mougari F, Reibel F, Cambau E. *Mycobacterium marinum*. *Microbiol Spectr.* 2017;5(2).
51. Lienard J, Carlsson F. Murine *Mycobacterium marinum* Infection as a Model for Tuberculosis. *Methods in molecular biology* (Clifton, NJ). 2017;1535:301-15.
52. Traag BA, Driks A, Stragier P, Bitter W, Broussard G, Hatfull G, et al. Do mycobacteria produce endospores? *Proc Natl Acad Sci U S A.* 2010;107(2):878-81.
53. Wältermann M, Steinbüchel A. Neutral Lipid Bodies in Prokaryotes: Recent Insights into Structure, Formation, and Relationship to Eukaryotic Lipid Depots. *Journal of bacteriology.* 2005;187(11):3607.
54. Anderson AJ, Dawes EA. Occurrence, metabolism, metabolic role, and industrial uses of bacterial polyhydroxyalkanoates. *Microbiological reviews.* 1990;54(4):450-72.
55. Lee GN, Na J. Future of microbial polyesters. *Microb Cell Fact.* 2013;12:54.
56. Seebach D, Brunner A, Bürger HM, Schneider J, Reusch RN. Isolation and ¹H-NMR spectroscopic identification of poly(3-hydroxybutanoate) from prokaryotic and eukaryotic organisms. Determination of the absolute configuration (R) of the monomeric unit 3-hydroxybutanoic acid from *Escherichia coli* and spinach. *European journal of biochemistry.* 1994;224(2):317-28.
57. Barksdale L, Kim KS. *Mycobacterium*. *Bacteriological reviews.* 1977;41(1):217-372.
58. Alvarez HM, Mayer F, Fabritius D, Steinbüchel A. Formation of intracytoplasmic lipid inclusions by *Rhodococcus opacus* strain PD630. *Archives of microbiology.* 1996;165(6):377-86.
59. Alvarez HM, Steinbüchel A. Triacylglycerols in prokaryotic microorganisms. *Applied microbiology and biotechnology.* 2002;60(4):367-76.
60. Gallagher IH. Occurrence of waxes in *Acinetobacter*. *Journal of general microbiology.* 1971;68(2):245-7.
61. Wang L, Takayama K, Goldman DS, Schnoes HK. Synthesis of alcohol and wax ester by a cell-free system in *Mycobacterium tuberculosis*. *Biochim Biophys Acta.* 1972;260(1):41-8.

62. Bredemeier R, Hulsch R, Metzger JO, Berthe-Corti L. Submersed culture production of extracellular wax esters by the marine bacterium *Fundibacter jadensis*. *Marine biotechnology* (New York, NY). 2003;5(6):579-83.
63. Burchard AC, Burchard RP, Kloetzel JA. Intracellular, periodic structures in the gliding bacterium *Myxococcus xanthus*. *Journal of bacteriology*. 1977;132(2):666-72.
64. Meng KE, Pfister RM. Intracellular structures of *Mycoplasma pneumoniae* revealed after membrane removal. *Journal of bacteriology*. 1980;144(1):390.
65. Bi EF, Lutkenhaus J. FtsZ ring structure associated with division in *Escherichia coli*. *Nature*. 1991;354(6349):161-4.
66. Jones LJ, Carballido-López R, Errington J. Control of cell shape in bacteria: helical, actin-like filaments in *Bacillus subtilis*. *Cell*. 2001;104(6):913-22.
67. Shih Y-L, Rothfield L. The Bacterial Cytoskeleton. *Microbiology and Molecular Biology Reviews*. 2006;70(3):729-54.
68. Devos DP, Reynaud EG. Evolution. Intermediate steps. *Science*. 2010;330(6008):1187-8.
69. Shih Y-L, Rothfield L. The bacterial cytoskeleton. *Microbiology and molecular biology reviews* : MMBR. 2006;70(3):729-54.
70. Wickstead B, Gull K. The evolution of the cytoskeleton. *The Journal of cell biology*. 2011;194(4):513-25.
71. Pilhofer M, Jensen GJ. The bacterial cytoskeleton: more than twisted filaments. *Current opinion in cell biology*. 2013;25(1):125-33.
72. Oakley BR. An abundance of tubulins. *Trends in cell biology*. 2000;10(12):537-42.
73. Findeisen P, Mühlhausen S, Dempewolf S, Hertzog J, Zietlow A, Carlomagno T, et al. Six subgroups and extensive recent duplications characterize the evolution of the eukaryotic tubulin protein family. *Genome biology and evolution*. 2014;6(9):2274-88.
74. Heald R, Nogales E. Microtubule dynamics. *Journal of cell science*. 2002;115(Pt 1):3-4.
75. Howard J, Hyman AA. Dynamics and mechanics of the microtubule plus end. *Nature*. 2003;422(6933):753-8.
76. Jordan MA, Wilson L. Microtubules as a target for anticancer drugs. *Nature reviews Cancer*. 2004;4(4):253-65.

77. Löwe J, Amos LA. Crystal structure of the bacterial cell-division protein FtsZ. *Nature*. 1998;391(6663):203-6.
78. Thanedar S, Margolin W. FtsZ exhibits rapid movement and oscillation waves in helix-like patterns in *Escherichia coli*. *Current biology : CB*. 2004;14(13):1167-73.
79. Erickson HP. Evolution of the cytoskeleton. *BioEssays : news and reviews in molecular, cellular and developmental biology*. 2007;29(7):668-77.
80. Nogales E, Wolf SG, Downing KH. Structure of the alpha beta tubulin dimer by electron crystallography. *Nature*. 1998;391(6663):199-203.
81. Löwe J, Amos LA. Evolution of cytomotive filaments: the cytoskeleton from prokaryotes to eukaryotes. *The international journal of biochemistry & cell biology*. 2009;41(2):323-9.
82. Larsen RA, Cusumano C, Fujioka A, Lim-Fong G, Patterson P, Pogliano J. Treadmilling of a prokaryotic tubulin-like protein, TubZ, required for plasmid stability in *Bacillus thuringiensis*. *Genes & development*. 2007;21(11):1340-52.
83. Tinsley E, Khan SA. A novel FtsZ-like protein is involved in replication of the anthrax toxin-encoding pXO1 plasmid in *Bacillus anthracis*. *Journal of bacteriology*. 2006;188(8):2829-35.
84. Ni L, Xu W, Kumaraswami M, Schumacher MA. Plasmid protein TubR uses a distinct mode of HTH-DNA binding and recruits the prokaryotic tubulin homolog TubZ to effect DNA partition. *Proc Natl Acad Sci U S A*. 2010;107(26):11763-8.
85. Aylett CH, Wang Q, Michie KA, Amos LA, Löwe J. Filament structure of bacterial tubulin homologue TubZ. *Proc Natl Acad Sci U S A*. 2010;107(46):19766-71.
86. Jenkins C, Samudrala R, Anderson I, Hedlund BP, Petroni G, Michailova N, et al. Genes for the cytoskeletal protein tubulin in the bacterial genus *Prostheco bacter*. *Proc Natl Acad Sci U S A*. 2002;99(26):17049-54.
87. Pilhofer M, Rosati G, Ludwig W, Schleifer KH, Petroni G. Coexistence of tubulins and ftsZ in different *Prostheco bacter* species. *Mol Biol Evol*. 2007;24(7):1439-42.
88. Schlieper D, Oliva MA, Andreu JM, Lowe J. Structure of bacterial tubulin BtubA/B: evidence for horizontal gene transfer. *Proc Natl Acad Sci U S A*. 2005;102(26):9170-5.
89. Sontag CA, Sage H, Erickson HP. BtubA-BtubB Heterodimer Is an Essential Intermediate in Protofilament Assembly. *PLoS ONE*. 2009;4(9):e7253.

90. Deng X, Fink G, Bharat TAM, He S, Kureisaite-Ciziene D, Löwe J. Four-stranded mini microtubules formed by *Prostheco bacter* BtubAB show dynamic instability. *Proc Natl Acad Sci U S A*. 2017;114(29):E5950-e8.
91. Fuchs E, Weber K. Intermediate filaments: structure, dynamics, function, and disease. *Annual review of biochemistry*. 1994;63:345-82.
92. Helfand BT, Chang L, Goldman RD. Intermediate filaments are dynamic and motile elements of cellular architecture. *Journal of cell science*. 2004;117(Pt 2):133-41.
93. Chang L, Goldman RD. Intermediate filaments mediate cytoskeletal crosstalk. *Nature reviews Molecular cell biology*. 2004;5(8):601-13.
94. Herrmann H, Aebi U. Intermediate filaments: molecular structure, assembly mechanism, and integration into functionally distinct intracellular Scaffolds. *Annual review of biochemistry*. 2004;73:749-89.
95. Coulombe PA, Wong P. Cytoplasmic intermediate filaments revealed as dynamic and multipurpose scaffolds. *Nature cell biology*. 2004;6(8):699-706.
96. IZARD J. Cytoskeletal cytoplasmic filament ribbon of *Treponema*: a member of an intermediate-like filament protein family. *Journal of molecular microbiology and biotechnology*. 2006;11(3-5):159-66.
97. Bagchi S, Tomenius H, Belova LM, Ausmees N. Intermediate filament-like proteins in bacteria and a cytoskeletal function in *Streptomyces*. *Molecular microbiology*. 2008;70(4):1037-50.
98. Ausmees N, Kuhn JR, Jacobs-Wagner C. The Bacterial Cytoskeleton: An Intermediate Filament-Like Function in Cell Shape. *Cell*. 2003;115(6):705-13.
99. Esue O, Rupprecht L, Sun SX, Wirtz D. Dynamics of the bacterial intermediate filament crescentin in vitro and in vivo. *PLoS one*. 2010;5(1):e8855-e.
100. Derman AI, Becker EC, Truong BD, Fujioka A, Tucey TM, Erb ML, et al. Phylogenetic analysis identifies many uncharacterized actin-like proteins (Alps) in bacteria: regulated polymerization, dynamic instability and treadmilling in Alp7A. *Mol Microbiol*. 2009;73(4):534-52.
101. Roeben A, Kofler C, Nagy I, Nickell S, Hartl FU, Bracher A. Crystal structure of an archaeal actin homolog. *Journal of molecular biology*. 2006;358(1):145-56.

102. Bork P, Sander C, Valencia A. An ATPase domain common to prokaryotic cell cycle proteins, sugar kinases, actin, and hsp70 heat shock proteins. *Proc Natl Acad Sci U S A*. 1992;89(16):7290-4.
103. dos Remedios CG, Chhabra D, Kekic M, Dedova IV, Tsubakihara M, Berry DA, et al. Actin binding proteins: regulation of cytoskeletal microfilaments. *Physiological reviews*. 2003;83(2):433-73.
104. Ozyamak E, Kollman JM, Komeili A. Bacterial actins and their diversity. *Biochemistry*. 2013;52(40):6928-39.
105. van den Ent F, Amos LA, Löwe J. Prokaryotic origin of the actin cytoskeleton. *Nature*. 2001;413(6851):39-44.
106. Esue O, Cordero M, Wirtz D, Tseng Y. The assembly of MreB, a prokaryotic homolog of actin. *J Biol Chem*. 2005;280(4):2628-35.
107. Komeili A, Li Z, Newman DK, Jensen GJ. Magnetosomes are cell membrane invaginations organized by the actin-like protein MamK. *Science*. 2006;311(5758):242-5.
108. Salje J, Löwe J. Bacterial actin: architecture of the ParMRC plasmid DNA partitioning complex. *The EMBO journal*. 2008;27(16):2230-8.
109. Ingerson-Mahar M, Gitai Z. A growing family: the expanding universe of the bacterial cytoskeleton. *FEMS microbiology reviews*. 2012;36(1):256-66.
110. Kühn J, Briegel A, Mörschel E, Kahnt J, Leser K, Wick S, et al. Bactofilins, a ubiquitous class of cytoskeletal proteins mediating polar localization of a cell wall synthase in *Caulobacter crescentus*. *The EMBO journal*. 2010;29(2):327-39.
111. diCenzo GC, Finan TM. The Divided Bacterial Genome: Structure, Function, and Evolution. *Microbiology and Molecular Biology Reviews*. 2017;81(3):e00019-17.
112. Kado CI. Historical Events That Spawned the Field of Plasmid Biology. *Microbiol Spectr*. 2014;2(5).
113. Aslam B, Wang W, Arshad MI, Khurshid M, Muzammil S, Rasool MH, et al. Antibiotic resistance: a rundown of a global crisis. *Infect Drug Resist*. 2018;11:1645-58.
114. Carattoli A. Plasmids and the spread of resistance. *International journal of medical microbiology : IJMM*. 2013;303(6-7):298-304.

115. Dionisio F, Zilhão R, Gama JA. Interactions between plasmids and other mobile genetic elements affect their transmission and persistence. *Plasmid*. 2019;102:29-36.
116. Casjens S, Palmer N, van Vugt R, Huang WM, Stevenson B, Rosa P, et al. A bacterial genome in flux: the twelve linear and nine circular extrachromosomal DNAs in an infectious isolate of the Lyme disease spirochete *Borrelia burgdorferi*. *Mol Microbiol*. 2000;35(3):490-516.
117. Novick RP. Plasmid incompatibility. *Microbiol Rev*. 1987;51(4):381-95.
118. Verma PS, Agarwal VK. *Genetics*. New Delhi: S. Chand; 2010.
119. Münch K, Münch R, Biedendieck R, Jahn D, Müller J. Evolutionary model for the unequal segregation of high copy plasmids. *PLoS computational biology*. 2019;15(3):e1006724.
120. Salje J, Gayathri P, Löwe J. The ParMRC system: molecular mechanisms of plasmid segregation by actin-like filaments. *Nat Rev Microbiol*. 2010;8(10):683-92.
121. Møller-Jensen J, Jensen RB, Löwe J, Gerdes K. Prokaryotic DNA segregation by an actin-like filament. *The EMBO journal*. 2002;21(12):3119-27.
122. Salje J, Zuber B, Löwe J. Electron cryomicroscopy of *E. coli* reveals filament bundles involved in plasmid DNA segregation. *Science*. 2009;323(5913):509-12.
123. Gayathri P, Fujii T, Møller-Jensen J, van den Ent F, Namba K, Löwe J. A bipolar spindle of antiparallel ParM filaments drives bacterial plasmid segregation. *Science*. 2012;338(6112):1334-7.
124. Møller-Jensen J, Ringgaard S, Mercogliano CP, Gerdes K, Löwe J. Structural analysis of the ParR/parC plasmid partition complex. *The EMBO journal*. 2007;26(20):4413-22.
125. Schumacher MA, Glover TC, Brzoska AJ, Jensen SO, Dunham TD, Skurray RA, et al. Segrosome structure revealed by a complex of ParR with centromere DNA. *Nature*. 2007;450(7173):1268-71.
126. Meijer WJ, de Boer AJ, van Tongeren S, Venema G, Bron S. Characterization of the replication region of the *Bacillus subtilis* plasmid pLS20: a novel type of replicon. *Nucleic acids research*. 1995;23(16):3214-23.
127. Tanaka T, Kuroda M, Sakaguchi K. Isolation and characterization of four plasmids from *Bacillus subtilis*. *Journal of bacteriology*. 1977;129(3):1487-94.

128. Koehler TM, Thorne CB. *Bacillus subtilis* (natto) plasmid pLS20 mediates interspecies plasmid transfer. *Journal of bacteriology*. 1987;169(11):5271-8.
129. Singh PK, Ramachandran G, Ramos-Ruiz R, Peiró-Pastor R, Abia D, Wu LJ, et al. Mobility of the native *Bacillus subtilis* conjugative plasmid pLS20 is regulated by intercellular signaling. *PLoS genetics*. 2013;9(10):e1003892.
130. Derman AI, Nonejuie P, Michel BC, Truong BD, Fujioka A, Erb ML, et al. Alp7R Regulates Expression of the Actin-Like Protein Alp7A in *Bacillus subtilis*. *Journal of bacteriology*. 2012;194(10):2715.
131. Garner EC, Campbell CS, Mullins RD. Dynamic instability in a DNA-segregating prokaryotic actin homolog. *Science*. 2004;306(5698):1021-5.
132. Zernike F, Stratton FJM. Diffraction Theory of the Knife-Edge Test and its Improved Form, The Phase-Contrast Method. *Monthly Notices of the Royal Astronomical Society*. 1934;94(5):377-84.
133. Tocheva EI, Li Z, Jensen GJ. Electron cryotomography. *Cold Spring Harbor perspectives in biology*. 2010;2(6):a003442-a.
134. Tivol WF, Briegel A, Jensen GJ. An improved cryogen for plunge freezing. *Microscopy and microanalysis : the official journal of Microscopy Society of America, Microbeam Analysis Society, Microscopical Society of Canada*. 2008;14(5):375-9.
135. McMullan G, Faruqi AR, Henderson R, Guerrini N, Turchetta R, Jacobs A, et al. Experimental observation of the improvement in MTF from backthinning a CMOS direct electron detector. *Ultramicroscopy*. 2009;109(9):1144-7.
136. Wan W, Briggs JA. Cryo-Electron Tomography and Subtomogram Averaging. *Methods Enzymol*. 2016;579:329-67.
137. Khan MSI, Oh S-W, Kim Y-J. Power of Scanning Electron Microscopy and Energy Dispersive X-Ray Analysis in Rapid Microbial Detection and Identification at the Single Cell Level. *Scientific Reports*. 2020;10(1):2368.
138. Boekema EJ, Folea M, Kouřil R. Single particle electron microscopy. *Photosynthesis research*. 2009;102(2-3):189-96.

139. Fan X, Wang J, Zhang X, Yang Z, Zhang J-C, Zhao L, et al. Single particle cryo-EM reconstruction of 52 kDa streptavidin at 3.2 Angstrom resolution. *Nature Communications*. 2019;10(1):2386.
140. Setlow P. Spores of *Bacillus subtilis*: their resistance to and killing by radiation, heat and chemicals. *J Appl Microbiol*. 2006;101(3):514-25.
141. Reynolds J, Moyes RB, Breakwell DP. Differential staining of bacteria: acid fast stain. *Curr Protoc Microbiol*. 2009;Appendix 3:Appendix 3H.
142. Eichenberger P, Fujita M, Jensen ST, Conlon EM, Rudner DZ, Wang ST, et al. The program of gene transcription for a single differentiating cell type during sporulation in *Bacillus subtilis*. *PLoS Biol*. 2004;2(10):e328.
143. Steil L, Serrano M, Henriques AO, Volker U. Genome-wide analysis of temporally regulated and compartment-specific gene expression in sporulating cells of *Bacillus subtilis*. *Microbiology*. 2005;151(Pt 2):399-420.
144. Chen S, McDowall A, Dobro MJ, Briegel A, Ladinsky M, Shi J, et al. Electron cryotomography of bacterial cells. *Journal of visualized experiments : JoVE*. 2010(39):1943.
145. Kremer JR, Mastronarde DN, McIntosh JR. Computer visualization of three-dimensional image data using IMOD. *J Struct Biol*. 1996;116(1):71-6.
146. Gunsolus IL, Hu D, Mihai C, Lohse SE, Lee C-s, Torelli MD, et al. Facile method to stain the bacterial cell surface for super-resolution fluorescence microscopy. *The Analyst*. 2014;139(12):3174-8.
147. Janssen FW, Lund AJ, Anderson LE. Colorimetric assay for dipicolinic acid in bacterial spores. *Science*. 1958;127(3288):26-7.
148. Chakrabarty K, Wu W, Booth JL, Duggan ES, Coggeshall KM, Metcalf JP. *Bacillus anthracis* spores stimulate cytokine and chemokine innate immune responses in human alveolar macrophages through multiple mitogen-activated protein kinase pathways. *Infection and immunity*. 2006;74(8):4430-8.
149. Gerhardt P. *Methods for general and molecular bacteriology*. Washington, D.C.: American Society for Microbiology; 1994.

150. Gerhardt P, American Society for M. Manual of methods for general bacteriology. Washington, D.C.: American Society for Microbiology; 1981.
151. Matyash V, Liebisch G, Kurzchalia TV, Shevchenko A, Schwudke D. Lipid extraction by methyl-tert-butyl ether for high-throughput lipidomics. *J Lipid Res.* 2008;49(5):1137-46.
152. Aramaki T, Blanc-Mathieu R, Endo H, Ohkubo K, Kanehisa M, Goto S, et al. KofamKOALA: KEGG Ortholog assignment based on profile HMM and adaptive score threshold. *Bioinformatics.* 2020;36(7):2251-2.
153. Haft DH, Selengut JD, White O. The TIGRFAMs database of protein families. *Nucleic Acids Res.* 2003;31(1):371-3.
154. Potter SC, Luciani A, Eddy SR, Park Y, Lopez R, Finn RD. HMMER web server: 2018 update. *Nucleic Acids Res.* 2018;46(W1):W200-w4.
155. Derman AI, Nonejuie P, Michel BC, Truong BD, Fujioka A, Erb ML, et al. Alp7R Regulates Expression of the Actin-Like Protein Alp7A in *Bacillus subtilis*. *Journal of Bacteriology.* 2012;194(10):2715.
156. Neuhoff V, Arold N, Taube D, Ehrhardt W. Improved staining of proteins in polyacrylamide gels including isoelectric focusing gels with clear background at nanogram sensitivity using Coomassie Brilliant Blue G-250 and R-250. *ELECTROPHORESIS.* 1988;9(6):255-62.
157. Mahmood T, Yang P-C. Western blot: technique, theory, and trouble shooting. *North American journal of medical sciences.* 2012;4(9):429-34.
158. Newman GR, Jasani B, Williams ED. A simple post-embedding system for the rapid demonstration of tissue antigens under the electron microscope. *The Histochemical Journal.* 1983;15(6):543-55.
159. Skepper JN, Powell JM. Immunogold Staining of London Resin (LR) White Sections for Transmission Electron Microscopy (TEM). *CSH Protoc.* 2008;2008:pdb.prot5016.
160. Chung CT, Miller RH. [43] Preparation and storage of competent Escherichia coli cells. In: Wu R, editor. *Methods in Enzymology.* 218: Academic Press; 1993. p. 621-7.
161. Froger A, Hall JE. Transformation of plasmid DNA into E. coli using the heat shock method. *Journal of visualized experiments : JoVE.* 2007(6):253-.

162. Beskrovnaya P, Fakih D, Morneau I, Hashimi A, Guadarrama Bello D, Xing S, et al. No Endospore Formation Confirmed in Members of the Phylum *Proteobacteria*. *Applied and Environmental Microbiology*. 2021;87(5):e02312-20.
163. Wahl A, Schuth N, Pfeiffer D, Nussberger S, Jendrossek D. PHB granules are attached to the nucleoid via PhaM in *Ralstonia eutropha*. *BMC Microbiology*. 2012;12(1):262.
164. Schaefer WB, Lewis CW, Jr. Effect of oleic acid on growth and cell structure of mycobacteria. *J Bacteriol*. 1965;90(5):1438-47.
165. Maurya RK, Bharti S, Krishnan MY. Triacylglycerols: Fuelling the Hibernating *Mycobacterium tuberculosis*. *Front Cell Infect Microbiol*. 2018;8:450.
166. Ryabova NA, Marchenkov VV, Marchenkova SY, Kotova NV, Semisotnov GV. Molecular chaperone GroEL/ES: Unfolding and refolding processes. *Biochemistry (Moscow)*. 2013;78(13):1405-14.
167. Wingfield PT. Overview of the purification of recombinant proteins. *Current protocols in protein science*. 2015;80:6.1.-6.1.35.
168. Huh S, Kanade T. Apoptosis detection for non-adherent cells in time-lapse phase contrast microscopy. *Med Image Comput Comput Assist Interv*. 2013;16(Pt 2):59-66.
169. Hitchins AD, Kahn AJ, Slepecky RA. Interference contrast and phase contrast microscopy of sporulation and germination of *Bacillus megaterium*. *J Bacteriol*. 1968;96(5):1811-7.
170. Garton NJ, Christensen H, Minnikin DE, Adegbola RA, Barer MR. Intracellular lipophilic inclusions of *mycobacteria* in vitro and in sputum. *Microbiology*. 2002;148(Pt 10):2951-8.
171. Alvarez HM, Kalscheuer R, Steinbuchel A. Accumulation and mobilization of storage lipids by *Rhodococcus opacus* PD630 and *Rhodococcus ruber* NCIMB 40126. *Applied microbiology and biotechnology*. 2000;54(2):218-23.
172. Shabtai Y. Isolation and characterization of a lipolytic bacterium capable of growing in a low-water-content oil-water emulsion. *Appl Environ Microbiol*. 1991;57(6):1740-5.
173. Santucci P, Johansen MD, Point V, Poncin I, Viljoen A, Cavalier JF, et al. Nitrogen deprivation induces triacylglycerol accumulation, drug tolerance and hypervirulence in mycobacteria. *Sci Rep*. 2019;9(1):8667.

174. Shi L, Derouiche A, Pandit S, Rahimi S, Kalantari A, Futo M, et al. Evolutionary analysis of the *Bacillus subtilis* genome reveals new genes involved in sporulation. *Mol Biol Evol.* 2020.
175. Veening JW, Murray H, Errington J. A mechanism for cell cycle regulation of sporulation initiation in *Bacillus subtilis*. *Genes & development.* 2009;23(16):1959-70.
176. Rigden DJ, Galperin MY. Sequence analysis of GerM and SpoVS, uncharacterized bacterial 'sporulation' proteins with widespread phylogenetic distribution. *Bioinformatics (Oxford, England).* 2008;24(16):1793-7.
177. Onyenwoke RU, Brill JA, Farahi K, Wiegel J. Sporulation genes in members of the low G+C Gram-type-positive phylogenetic branch (Firmicutes). *Archives of microbiology.* 2004;182(2-3):182-92.
178. Petek NA, Derman AI, Royal JA, Pogliano J, Mullins RD. Polymer dynamics of Alp7A reveals two 'critical' concentrations that govern dynamically unstable actin-like proteins. *bioRxiv.* 2017:098954.
179. Zhang J, Ji G, Huang X, Xu W, Sun F. An improved cryo-FIB method for fabrication of frozen hydrated lamella. *Journal of Structural Biology.* 2016;194(2):218-23.
180. Zachs T, Schertel A, Medeiros J, Weiss GL, Hugener J, Matos J, et al. Fully automated, sequential focused ion beam milling for cryo-electron tomography. *eLife.* 2020;9:e52286.

7 Annex




AMERICAN
SOCIETY FOR
MICROBIOLOGY

Applied and Environmental
Microbiology®

ENVIRONMENTAL MICROBIOLOGY



8 No Endospore Formation Confirmed in Members of the Phylum Proteobacteria

Polina Beskrovnaya,^a Doaa Fakh, ^b Isabelle Morneau, ^b Ameena Hashimi, ^a Dainelys Guadarrama Bello, ^b Shipei Xing, ^c Antonio Nanci, ^b Tao Huan, ^c  Elitza I. Tocheva^{a, b}

^aDepartment of Microbiology & Immunology, The University of British Columbia, Vancouver, British Columbia, Canada

^bDepartment of Stomatology, Université de Montréal, Montréal, Québec, Canada

^cDepartment of Chemistry, The University of British Columbia, Vancouver, British Columbia, Canada

Polina Beskrovnaya and Doaa Fakh contributed equally to this work. Author order was determined based on data and analysis contribution.

ABSTRACT Endospore formation is used by members of the phylum Firmicutes to withstand extreme environmental conditions. Several recent studies have proposed endospore formation in species outside Firmicutes, particularly in *Rhodobacter johrii* and *Serratia marcescens*, members of the phylum Proteobacteria. In this study, we aimed to investigate endospore formation in these two species by using advanced imaging and analytical approaches. Examination of the phase-bright structures observed in *R. johrii* and *S. marcescens* using cryo-electron tomography failed to identify endospores or stages of endospore formation. We determined that the phase-bright objects in *R. johrii* cells were triacylglycerol storage granules and those in *S. marcescens* were aggregates of cellular debris. In addition, *R. johrii* and *S. marcescens* containing phasebright objects do not possess phenotypic and genetic features of endospores, including enhanced resistance to heat, presence of dipicolinic acid, or the presence of many of the genes associated with endospore formation. Our results support the hypothesis that endospore formation is restricted to the phylum Firmicutes.

Citation Beskrovnaya P, Fakh D, Morneau I, Hashimi A, Guadarrama Bello D, Xing S, Nanci A, Huan T, Tocheva EI. 2021. No endospore formation confirmed in members

IMPORTANCE Bacterial endospore formation is an important process that allows the formation of dormant life forms called spores. Organisms able to sporulate can survive harsh environmental conditions for hundreds of years. Here, we follow up on previous claims that two members of Proteobacteria, *Serratia marcescens* and *Rhodobacter johrii*, are able to form spores. We conclude that those claims were incorrect and show that the putative spores in *R. johrii* and *S. marcescens* are storage granules and cellular debris, respectively. This study concludes that endospore formation is still unique to the phylum Firmicutes.

KEYWORDS endospores, Firmicutes, cryo-electron tomography, correlative light electron microscopy, whole-cell lipidomic analysis, EDX of storage granules, EDX analysis, *Rhodobacter johrii*, *Serratia marcescens*, correlative light and electron microscopy, storage granules

Spores represent a dormant state of bacteria that can persist for many years (1–3).

Bacterial sporulation encompasses diverse modes; however, it is typically triggered by starvation and ultimately results in the production of metabolically inactive cells displaying increased resilience to stressors. For example, low nitrogen or carbon availability in Firmicutes can stimulate formation of endospores resistant to UV radiation, extreme pH, high temperature, and pressure (4–6). Similarly, exospore formation in Actinobacteria and fruiting-body production in *Myxococcus* have also been linked to nutrient limitation and can serve for preservation of genetic material under unfavorable environmental conditions (7–9). Despite the apparent similarities between these

Applied and Environmental Microbiology

different types of sporulation, the underlying transformations are morphologically distinct and encoded by nonhomologous pathways (10).

Endospore formation begins with asymmetric cell division, with the septum placed near one pole of the cell, and produces two cells with different fates (11–13). Upon septation, the smaller compartment becomes engulfed through a phagocytosis-like mechanism, yielding a prespore bound by two lipid membranes in the cytoplasm of the mother cell. Subsequent endospore maturation involves the synthesis of protective layers, such as the peptidoglycan-based cortex and proteinaceous coat. Metabolic inactivation is achieved by gradual dehydration of the core through replacement of water with dipicolinic acid (DPA) and calcium ions and compaction of DNA with DNA-binding proteins. Together, these modifications account for the resistance properties of endospores (14). Ultimately, the spore is released upon lysis of the mother cell (15). In contrast, other modes of sporulation, such as those observed in Actinobacteria and *Myxococcus*, produce spores through morphological differentiation and cell division without engulfment.

Several studies in the past decade have reported, but not proven, formation of endospores in Proteobacteria (16, 17). While endosporulation has recently been confirmed in some Gram-negative bacteria, all of the identified organisms still belong to the phylum Firmicutes, highlighting the question of evolutionary origins of the bacterial outer membrane (18). Additionally, sporulation involves tight cooperation of hundreds of genes distributed across the chromosome, hindering acquisition of this pathway through horizontal gene transfer (10, 19, 20). Therefore, if confirmed, the ability to form endospores across distantly related bacterial phyla suggests an ancient nature of the process and can provide clues to the characteristics of the last bacterial common ancestor (10). In this study, we investigated two articles attributing sporulation to members of Proteobacteria (16, 17). Briefly, Girija et al. (17) described endospore production in the purple, nonsulfur bacterium *Rhodobacter johrii*, strain JA192(T), a close relative of the model organism for bacterial photosynthesis *Rhodobacter sphaeroides*. The second study, by Ajithkumar et al. (16), reported endospore formation in *Serratia marcescens* subsp. *sakuensis* (strain no. 9; KRED^T), a pathogenic bacterium that infects humans and causes bacteremia, urinary tract

of the phylum Proteobacteria. Appl Environ
Microbiol 87:e02312-20.
<https://doi.org/10.1128/AEM>

.02312-20.

Editor Emma R. Master, University
of Toronto

Copyright © 2021 Beskrovnaya
et al. This is an

open-access article distributed
under the terms of the [Creative Commons
Attribution 4.0](#)

[International license.](#)

Address correspondence to Elitza I.
Tocheva,

elitza.tocheva@ubc.ca.

Received 20 September 2020

Accepted 27 November 2020

Accepted manuscript posted online

18

December 2020

Published 12 February 2021

infection, and wound infections (21). Thus, confirmation and further characterization of endospore formation in these organisms can bring valuable insight into the physiology of these species and the role of endospore formation in diversification and speciation of modern phyla.

In this study, we employed cutting-edge structural biology techniques, such as cryo-electron tomography (cryo-ET), correlative light and electron microscopy (CLEM), and energy-dispersive X-ray spectroscopy (EDX), as well as biochemical and microbiological approaches, to characterize endospore formation in *R. johrii* and *S. marcescens*. Our results showed that *R. johrii* and *S. marcescens* were unable to form endospores as previously reported (16, 17). Further analyses indicated that the putative spores in *R. johrii* were lipid storage granules (SGs) rich in triacylglycerols (TAGs) and that the phase-bright objects in *S. marcescens* were aggregates of cellular debris. Overall, our observations contradict the previously published studies by Girija et al. and Ajithkumar et al. and support the observation that these members of Proteobacteria are unable to form endospores.

RESULTS AND DISCUSSION

Prolonged incubation induces formation of phase-bright objects in *R. johrii* and *S. marcescens*. For initial assessment of the previously reported endospore formation, we cultivated *R. johrii* and *S. marcescens* according to the published conditions and examined the cultures with phase-contrast light microscopy (LM) (Fig. 1). Vegetative *R. johrii* cells appeared phase-dark (Fig. 1A); however, after 7 s incubation, phase-bright objects were observed either at one pole or mid-cell (Fig. 1B, black arrows). Vegetative *S. marcescens* cells also appeared phase-dark (Fig. 1C). Although phase-bright objects were occasionally visible at mid-cell following a 65-day incubation (Fig. 1D, black arrows), the majority of culture was dead and appeared as “ghost” cells (Fig. 1D, white arrows).

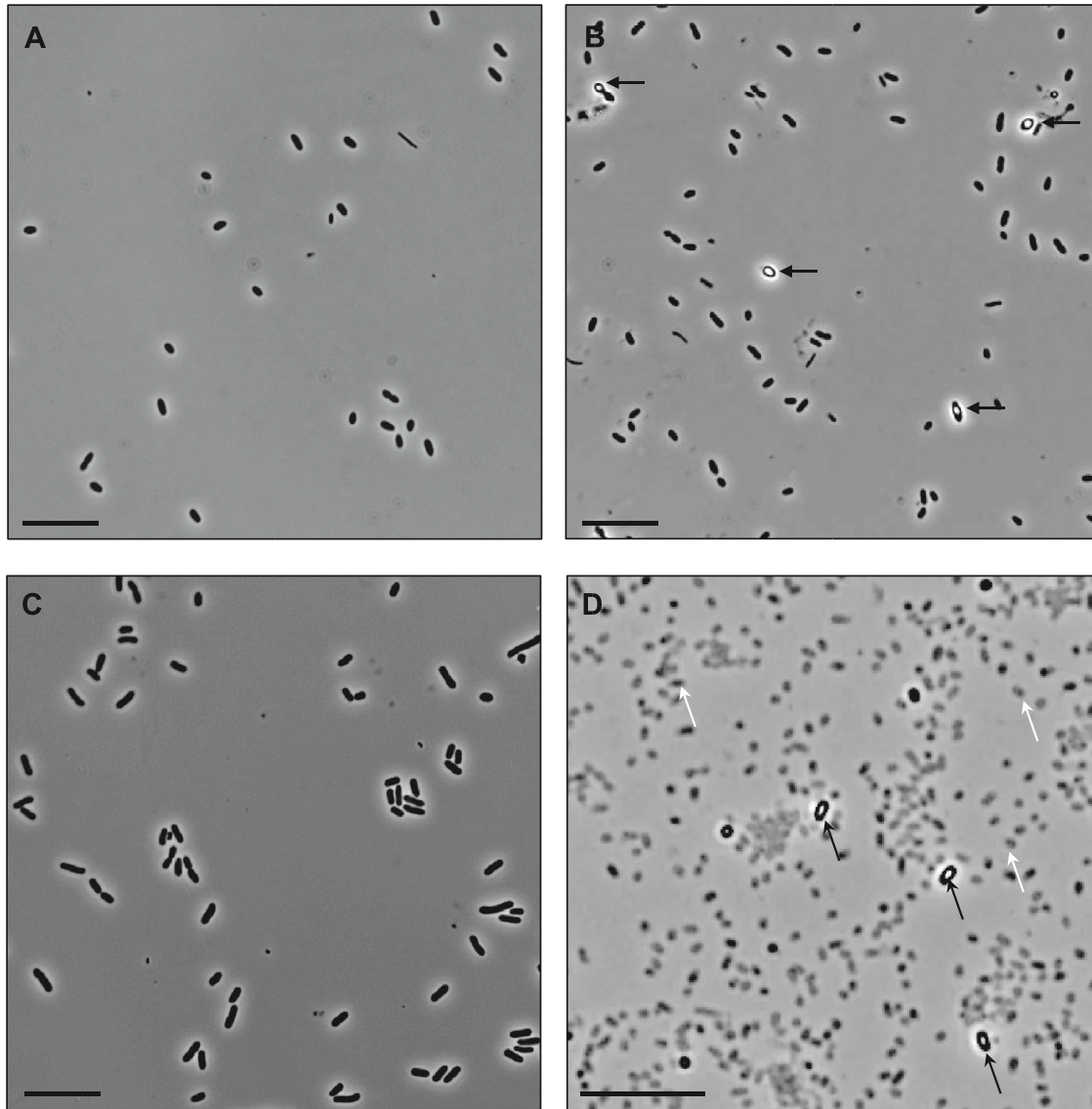


FIG 1 Phase-contrast light microscopy of *R. johrii* and *S. marcescens* cells. (A) Two-day-old *R. johrii* cells lack phase-bright objects. (B) Seven-day-old *R. johrii* cells show phase-bright objects (black arrows). (C) Seven-day-old *S. marcescens* cells lack phase-bright objects. (D) After 65 days, *S. marcescens* cells show two kinds of cell morphologies: phase-bright (black arrows) and ghost cells (white arrows). Scale bar, 10mm.

Altogether, our results recapitulate reports of formation of phase-bright objects in *R. johrii* and *S. marcescens* following extended incubation under nutrient-limited conditions.

Characterization of phase-bright objects in *R. johrii*. To further characterize the phase-bright objects observed in *R. johrii*, we performed correlative LM and cryo-ET experiments on phase-bright and phase-dark cells following extended incubation (Fig. 2). Tomograms of *R. johrii* cells with phase-bright objects revealed the presence of intracellular granules, which were highly sensitive to the electron beam, as represented by the sample damage (Fig. 2A). Beam sensitivity was detected regardless of the total dose used (25 to 150 electrons $[e^-]/\text{Å}^2$), suggesting that the granules were rich in lipids. Further, the spherical nature of the granules resembled previously characterized storage granules (SG) in bacterial cells (22). No evidence of sporulation-associated morphological changes, such as engulfing membranes or the presence of immature or mature spores in the sample ($n = 40$),

was observed, indicating that the phase-bright objects were not endospores. Finally, cells with phase-bright objects always displayed 1 to 3 of

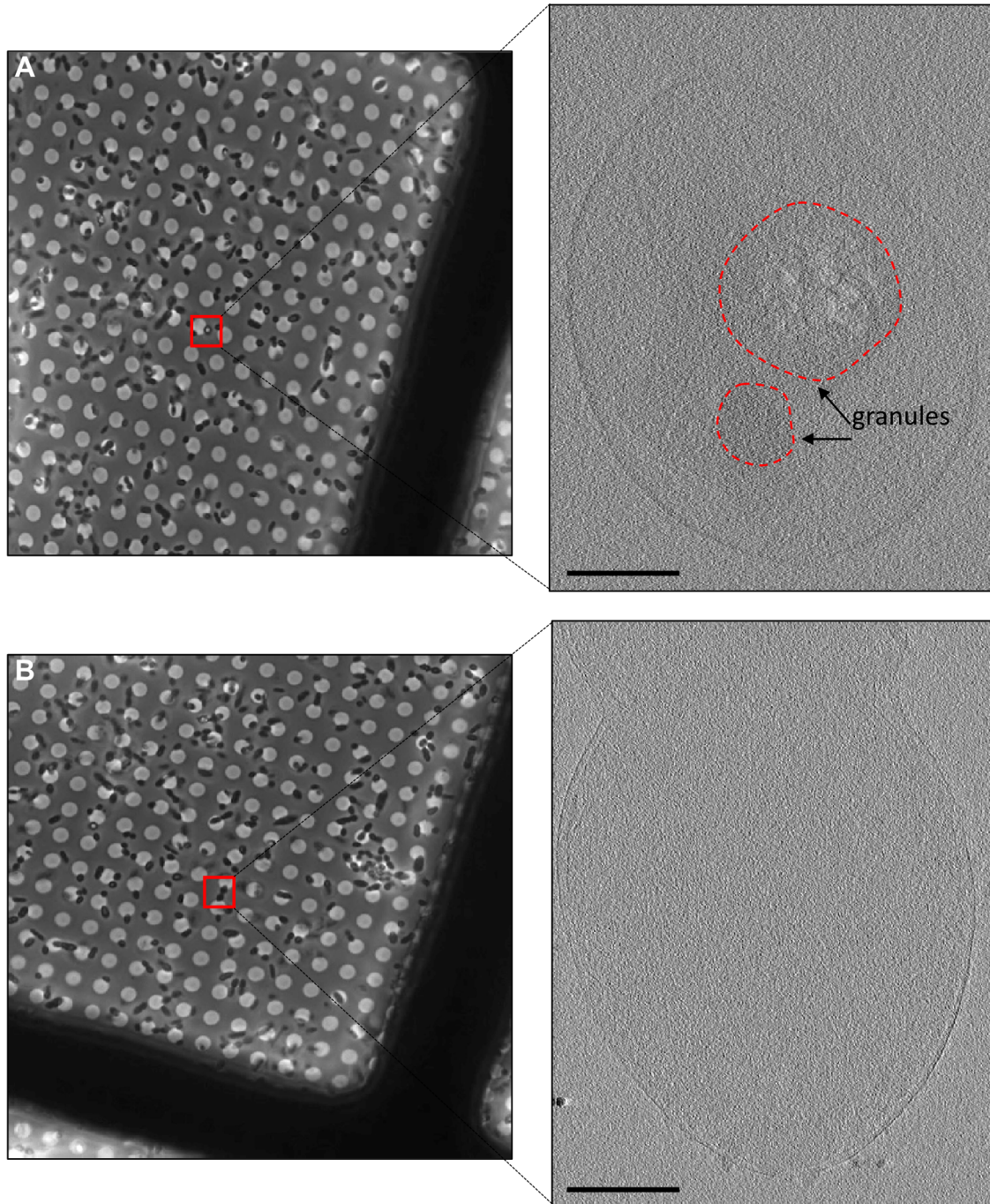


FIG 2 Correlative light and cryo-ET of *R. johrii*. (A) (Left) Phase-contrast microscopy image of an *R. johrii* cell (boxed) displaying a phase-bright object. (Right) Tomographic slice of the same cell showing two granular structures. (B) (Left) Phase-contrast microscopy image of *R. johrii* cells (boxed) lacking phase-bright objects. (Right) Tomographic slice of the same cell showing lack of subcellular structures. Scale bar, 200 nm.

the 100- to 250-nm-diameter granules (Fig. 2A), whereas the phase-dark cells lacked the presence of granules (Fig. 2B). Thus, our observations suggest that the phasebright objects were likely lipid-containing SGs.

To determine the composition of the storage granules, we performed correlative LM and scanning electron microscopy (SEM) in combination with EDX compositional analysis.

Cells possessing the putative storage granules were identified with phasecontrast microscopy (Fig. 3A) and examined at higher resolution with SEM (Fig. 3B).

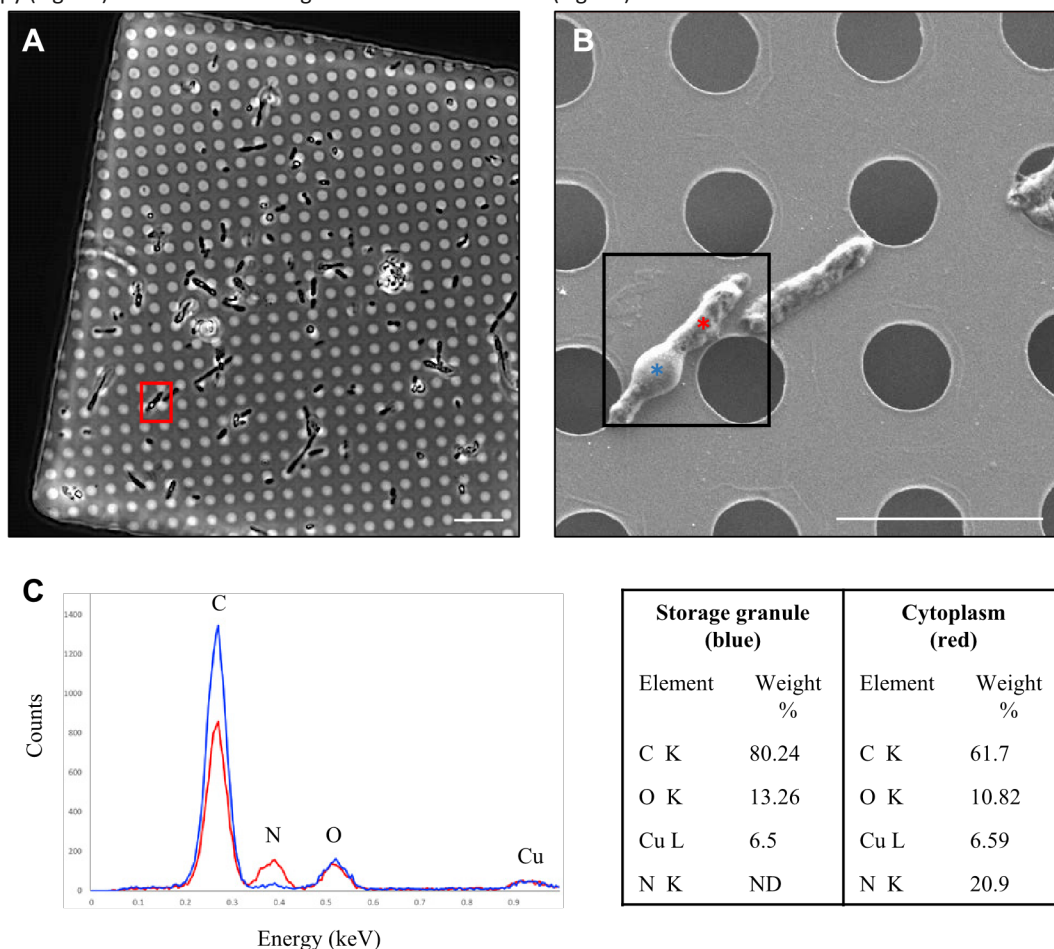


FIG 3 Correlative LM and SEM of *R. johrii* for storage granule characterization with EDX. (A) An LM image of *R. johrii* shows the presence of storage granules (phase-bright objects) inside a cell (red square). (B) The same cell as in panel A imaged with SEM. Areas corresponding to the storage granule and cytoplasm are depicted by blue and red asterisks, respectively. (C) Elemental composition of the storage granule (blue) and cytoplasm (red) using EDX semiquantitative analysis. Major peaks are assigned and data are summarized in a table format. Scale bars, 10mm (A) and 5mm (B). ND, nondetected.

Correlative LM and SEM were then used to guide EDX analysis, so that spectra were collected from a region containing the putative storage granules and a cytoplasmic region lacking the storage granules (Fig. 3C). Elemental analysis of the storage granule (blue spectrum) revealed counts for carbon (C) of 80.24%, oxygen (O) of 13.26%, and copper (Cu) of 6.5% (due to the copper of the EM grid). Cytoplasmic analysis (red spectrum) revealed lower counts for carbon (61.7%) and oxygen (10.82%), copper at 6.59%, and elevated counts for nitrogen (N; 20.9%) (Fig. 3C).

Based on the cryo-ET and EDX data, we hypothesized that the granules observed in *R. johrii* were composed of lipids, as lipids are enriched in carbon and oxygen atoms. To characterize the nature of the granular composition, we performed whole-cell lipidomic analysis of *R. johrii* 7-day-old cultures expressing phase-bright objects (granules) against *R. johrii* cultures grown for 2 days and lacking phase-bright objects as the negative control. Cultures producing putative storage granules were enriched in several lipids, the most abundant of which were triacylglycerols (TAGs) and phosphatidylethanolamines (PEs) (Table 1). Because PEs are typical membrane lipids, the increased levels observed under starvation conditions suggested that cells remodel their membrane composition to account for the environmental changes. TAGs are nonpolar, occur as insoluble inclusions in bacteria,

and are considered a major source of energy (23, 24). TAGs have been shown to accumulate in actinobacteria and mycobacteria either as

TABLE1 Lipidomic analysis of whole *R. johrii* cells

Lipid ^a	Lipid class(+)/R.j (2)	Fold change, ^b R.j	P value
PE 33:1; PE 16:0-17:1 ^c	PE	147.84	4.71E209
TAG 58:1; TAG 16:0- 24:0-18:1	TAG	93.81	1.81E208
TAG 52:3; TAG 16:0- 18:1-18:2	TAG	67.19	1.24E208
TAG 54:5; TAG 18:1- 18:2-18:2	TAG	60.41	1.37E206
TAG 52:2; TAG 18:0- 16:1-18:1	TAG	57.72	1.93E207
TAG 54:4; TAG 18:1- 18:1-18:2	TAG	54.46	2.37E208
TAG 52:1; TAG 16:0- 18:0-18:1	TAG	49.15	1.22E210
TAG 56:2; TAG 16:0- 18:1-22:1	TAG	48.89	5.37E209
TAG 50:1; TAG 16:0- 16:0-18:1	TAG	46.43	7.39E209
TAG 54:2; TAG 18:0- 18:1-18:1	TAG	44.82	2.37E209
TAG 58:2; TAG 16:0- 18:1-24:1	TAG	42.04	9.59E209
TAG 52:2; TAG 16:0- 18:1-18:1	TAG	41.06	5.93E209
TAG 56:1; TAG 16:0- 22:0-18:1	TAG	39.72	8.65E210
TAG 54:1; TAG 18:0- 18:0-18:1	TAG	39.35	1.15E208
TAG 54:3; TAG 18:0- 18:1-18:2	TAG	17.15	3.93E208
TAG 50:2; TAG 16:0- 16:1-18:1	TAG	12.30	1.90E208
PE 32:0; PE 16:0-16:0	PE	11.55	1.73E206
PC 39:3	PC	10.77	1.06E208
PE 32:1; PE 16:0-16:1	PE	7.68	3.84E207
TAG 48:1; TAG 14:0- 16:0-18:1	TAG	4.94	2.00E205
PE 35:2; PE 17:1-18:1	PE	3.09	6.92E206

No Endospores in Proteobacteria				
PC 36:4	PC	3.03		4.93E206
TAG 48:1; TAG 16:0-	TAG	2.52		4.51E203
16:0-16:1				
PC 32:1	PC	2.18		4.46E207
PC 34:1; PC 16:0-18:1	PC	2.15		6.50E208
DAG 36:2; DAG 18:1-	DAG	2.08		5.34E208
18:1				
PC 34:2; PC 16:1-18:1	PC	2.02		1.57E206

^aAbbreviations: PE, phosphatidyl ethanolamine; TAG, triacylglycerol; PC, phosphatidylcholine; DAG, diglyceride. ^bThe total lipid composition of *R. johrii* expressing storage granules [R.j (1)] was compared to that of a fresh *R. johrii* culture lacking storage granules [R.j (2)].

^cPE is a lipid class with two acyl chains. PE 16:0-17:1 indicates that the chain lengths are 16 carbons and 17 carbons and the saturation degrees are 0 and 1, respectively. PE 33:1 is the simpler form of PE 16:0-17:1.

peripheral deposits associated with the cell envelope or as inclusion bodies in the cytoplasm (25). Previously, *in vitro* studies showed that mycobacteria accumulated TAG and wax ester when subjected to stresses, such as low oxygen, high CO₂, low nutrients, and low pH (25–27). Similarly, we observed an increased propensity to form phasebright objects in *R. johrii* cells incubated under low-nitrogen conditions in defined media. Therefore, it is likely that *R. johrii* utilizes TAG storage as an adaptive strategy in response to starvation, allowing cells to enter stationary phase and survive for longer periods. We thus conclude that the granules observed as phase-bright objects in *R. johrii* were storage granules enriched in TAGs.

Characterization of phase-bright objects in *S. marcescens*. Tomograms of *S. marcescens* were collected for 2-day and 65-day-old cultures (Fig. 4). At 2 days, we observed regular morphology of vegetative cells, displaying cell envelope architecture typical for Gram-negative bacteria (Fig. 4A). *S. marcescens* grown for 65 days revealed the presence of two kinds of morphologies: cells packed with cellular debris (black asterisk in Fig. 4B) and cells void of any cellular material (white asterisks in Fig. 4B), likely correlating to cells containing phase-bright objects and ghost cells identified using LM, respectively. Extensive survey of the sample ($n = 80$) did not reveal any cells possessing intracellular membranes or morphologies suggestive of engulfing membranes or stages of sporulation. Neither of the two identified morphologies displayed any features similar to a cortex or proteinaceous spore coat characteristic of mature endospores. Additionally, we did not observe accumulation of storage granules within cells. Together, these results suggest that the appearance of phase-bright objects in *S. marcescens* was the result of accumulation of cellular debris and dehydration.

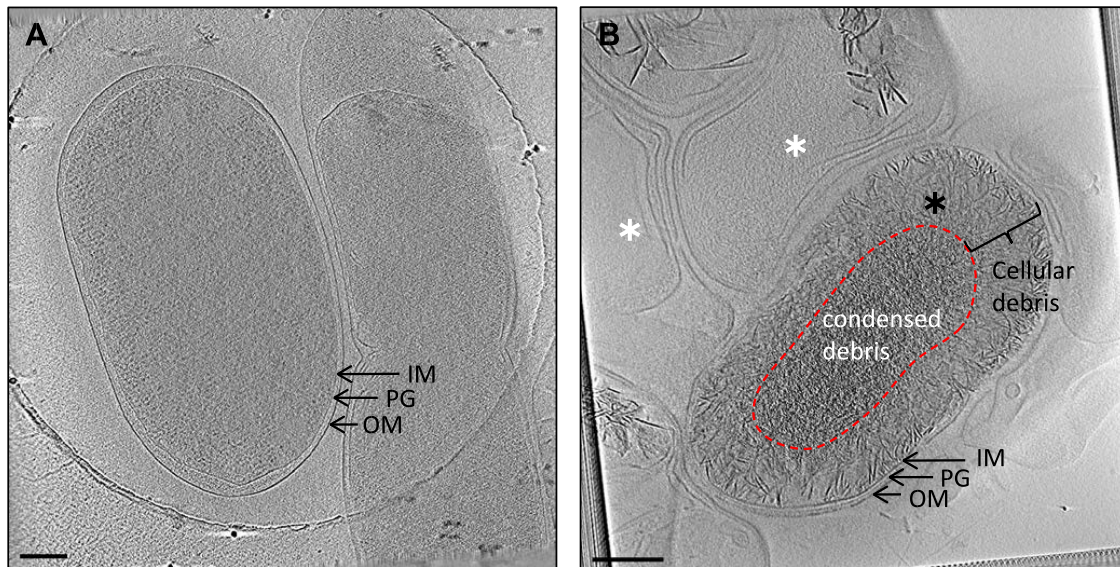
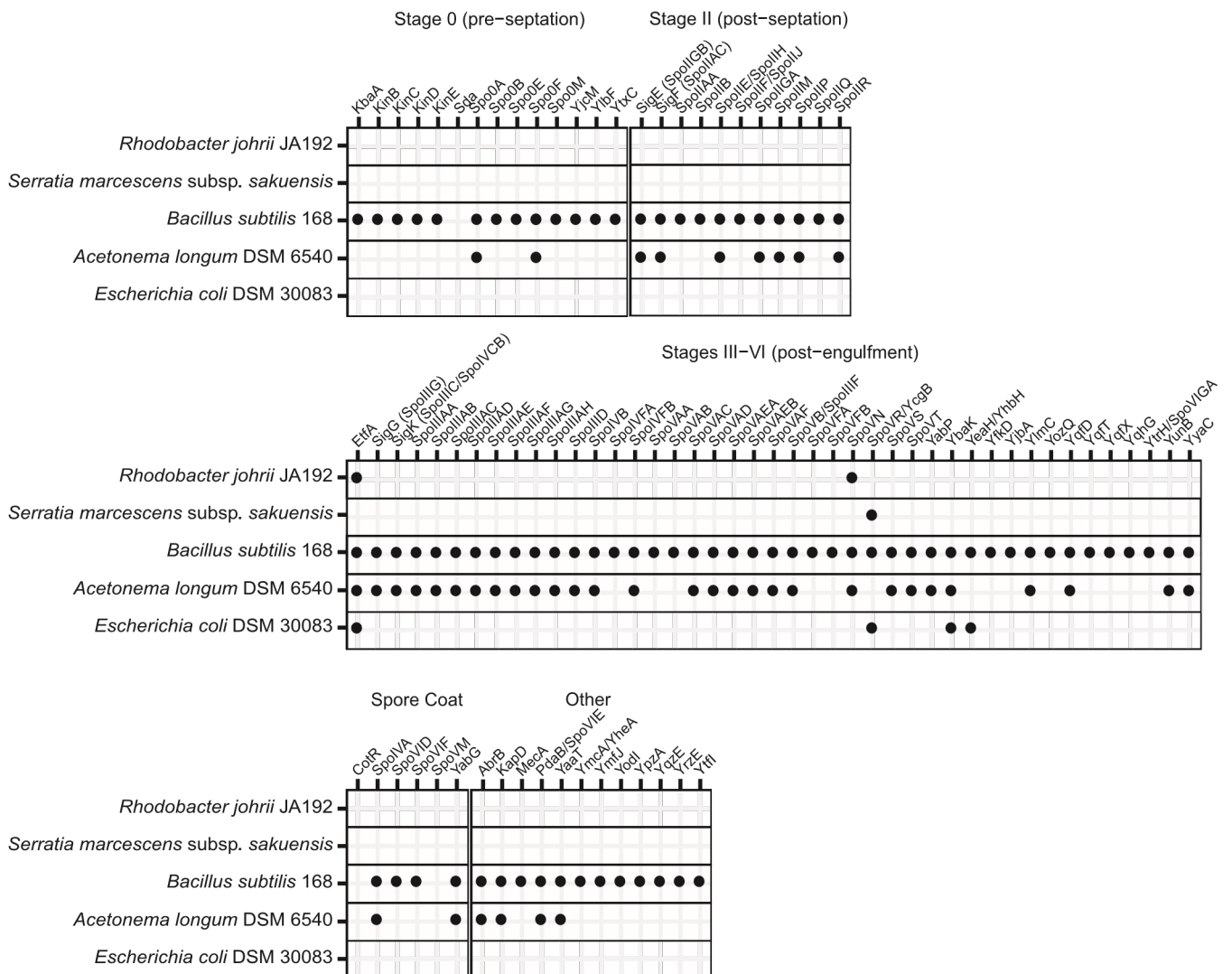


FIG 4 Cryo-ET of *S. marcescens*. Tomographic slices through the following are shown: vegetative cells from a 2-day-old culture (A) and cells from a 65-day-old culture showing phase-bright objects (B). Panel B shows two cell types: cells with accumulated cellular debris (black asterisk) and ghost cells void of cellular material (white asterisks). Scale bar, 200 nm. IM, inner membrane; PG, peptidoglycan; OM, outer membrane.

Proteobacteria do not possess features of endospores following extended incubation. Independent of imaging-based methods, endospores have traditionally been identified in samples through heat resistance and increased concentration of intracellular DPA. To verify the results of our cryo-ET experiments, we first investigated the heat resistance properties of *R. johrii* and *S. marcescens* following prolonged incubation and subsequent exposure to high temperatures. Despite an extended recovery period (7 days), no viable *R. johrii* cells were observed on solid media following 15, 30, and 60 min of incubation at 80°C. Similarly, viable cells were not isolated from *S. marcescens* cultures incubated at 60°C for 15, 30, and 60 min. In contrast, *Bacillus subtilis* cultures producing endospores and treated at 80°C for 15, 30, and 60 min yielded viable growth on solid media after a 24-h recovery period. Thus, we were unable to replicate the results of Girija et al. and Ajithkumar et al., who found viable cells following heat treatment of *R. johrii* at 80°C for 20 min and *S. marcescens* at 60°C for 15 min, respectively. Additionally, we quantitatively analyzed the presence of DPA in cultures of *R. johrii* and *S. marcescens* displaying phase-bright objects using a colorimetric method. Whereas the purified endospores of *B. subtilis* contained 6.74mg/ml of DPA, no detectable amounts of DPA were observed in *R. johrii* or *S. marcescens* after prolonged cultivation. Collectively, these results indicate that *R. johrii* and *S. marcescens* cells do not possess the classic phenotypic features that are associated with endospore formation.

Minimal subset of genes required for endospore formation not conserved in *R. johrii* and *S. marcescens*. Endospore formation relies on expression of hundreds of conserved genes in a highly regulated manner (20, 28–30). For example, over 500 genes have been previously implicated in sporulation in the model firmicute *B. subtilis* (28). However, establishment of the minimal subset of genes required for endospore formation remains elusive, as many of the identified targets carry out redundant functions, e.g., histidine kinases, or are part of general pathways loosely associated with sporulation, such as iron uptake and DNA repair proteins (31). Consistently, several homologs to genes linked to sporulation have been detected in other phyla, including Proteobacteria, but have been shown to play regulatory roles in distinct processes, such as cell division and development (32, 33). Hence, possession of genes annotated as sporulative should not be considered concrete evidence to support sporulation capacity in a given species (5). Nevertheless, we investigated the genomes of *R. johrii* TABLE2 Analysis for presence of endospore formation



Downloaded from <http://aem.asm.org/> on February 24, 2021 by guest

genes in *R. johrii* and *S. marcescens* and *S. marcescens* for presence of genes that are conserved among all spore-forming bacilli and clostridia based on the COGs database and

have been shown to play pivotal roles in endospore formation through functional studies (Table 2) (5, 34, 35). Our analysis showed that both *R. johrii* and *S. marcescens* completely lack the SpoIIDMP peptidoglycan remodeling complex required for spore cortex formation, the SpoIIQ-SpoIIIAAH channel complex involved in communication between the mother cell and the prespore and facilitating regulation of endospore maturation, and the major protein coat assembly components, such as SpoIVA (12, 14, 36). Further, the master regulator of sporulation encoded by all endospore formers, SpoOA, is absent in *R. johrii* and *S. marcescens*. Both strains also lack homologs to all five sporulation sigma factors, SigE, SigF, SigG, SigH, and SigK. Finally, *R. johrii* and *S. marcescens* do not possess DapB, required for production of dipicolinic acid in Bacilli, which plays a major role in dehydration of the spore core and, therefore, resistance and dormancy (14). A homolog of *etfA* (a gene associated with DPA synthesis in some Clostridia), however, was identified in *R. johrii* and *Escherichia coli* but not in *S. marcescens* (Table 2). The role of this gene in Proteobacteria has not been characterized, and it could encode an electron transfer flavoprotein. Overall, our analysis confirms the lack of the major structural and regulatory sporulation genes in the genomes of *R. johrii* and *S. marcescens*. In addition, Ajithkumar et al. were also unable to detect genes related to endospore formation in *S. marcescens* (16).

Concluding remarks. Although endospore formation is considered a hallmark of the Firmicutes phylum (4, 5, 37), endospore production had been reported outside Firmicutes, particularly for two members of the phylum Proteobacteria (16, 17). These findings may affect our understanding of the evolutionary events surrounding outer membrane biogenesis and the significance of endospore formation in cell differentiation. In this study, using cutting-edge microscopy techniques and biochemical, microbiological, and bioinformatics approaches, we showed that the phase-bright objects observed in *R. johrii* and *S. marcescens* are storage granules and cellular debris, respectively. We did not observe mature spores or stages of endospore formation in vivo, and we failed to detect the pivotal biochemical and genomic features of endospore-producing bacteria in these organisms. Our findings thus demonstrate that *R. johrii* and *S. marcescens* are unable to form true endospores, which is in contrast to the results described by Girija et al. (17) and Ajithkumar et al. (16). Since we used the most advanced imaging techniques currently available to study whole-cell bacteria and their ultrastructure, previous results could be due to the presence of contamination with spore-forming bacteria or misinterpretation of methodology artifacts.

MATERIALS AND METHODS

Bacterial strains and growth conditions. *R. johrii* and *S. marcescens* cells were purchased from the Leibniz-Institut DSMZ bacterial strain collection. *R. johrii* JA192 cells (DSMZ 18678) were cultivated as previously described by Girija et al. (17). Briefly, cells were grown aerobically at room temperature in *R. sphaeroides* solid and liquid media comprising 4 mM KH_2PO_4 , 1 mM $\text{MgCl}_2 \cdot 6\text{H}_2\text{O}$, 7 mM NaCl, 22 mM NH_4Cl , 0.04 mM $\text{CaCl}_2 \cdot 2\text{H}_2\text{O}$, 17 mM sorbitol, 28 mM sodium pyruvate, 1.5 mM yeast extract, 1 liter distilled water (pH 7.0), 1 ml of trace element solution SL7, and 20 ng of vitamin B₁₂ solution for 2 days for vegetative cells or 7 days to induce production of phase-bright objects. Additionally, cells were grown in Luria-Bertani (LB) broth at 30°C with agitation for 2 days and either harvested as the vegetative growth control or subsequently inoculated 1:100 into modified M9 medium for an additional 7 days to induce formation of phase-bright objects. The modified M9 medium contained 47.8 mM Na_2HPO_4 , 22 mM KH_2PO_4 , 8.56 mM NaCl, 18.7 mM (3.74 mM for limited nitrogen) NH_4Cl , 1 mM MgSO_4 , 0.3 mM CaCl_2 , 0.4% (wt/vol) glucose, 1mg/liter of biotin, 1mg/liter of thiamine, 31mM $\text{FeCl}_3 \cdot 6\text{H}_2\text{O}$, 12.5mM ZnCl_2 , 2.5mM $\text{CuCl}_2 \cdot 2\text{H}_2\text{O}$, 2.5mM $\text{CoCl}_2 \cdot 2\text{H}_2\text{O}$, 5mM $\text{MnCl}_2 \cdot 4\text{H}_2\text{O}$, and 2.5mM $\text{Na}_2\text{MoO}_4 \cdot 2\text{H}_2\text{O}$. *S. marcescens* cells (DSMZ 30121) were cultivated in LB broth at 32°C with shaking at 200 rpm, as previously described by Ajithkumar et al. (16), for 7 days for vegetative growth or 65 days to induce formation of phase-bright objects. *B. subtilis* strain PY79 was chosen as the positive control for endospore formation, and cells were cultivated in LB broth at 37°C with shaking at 200 rpm overnight for vegetative growth or for 3 days to induce sporulation. LB agar was used for cultivation on plates for *S. marcescens* and *B. subtilis*.

Detection of phase-bright objects using phase-contrast light microscopy. *R. johrii* and *S. marcescens* cultures were pelleted and washed with 1 phosphate-buffered saline (PBS; pH 7.4) composed of 137 mM NaCl, 27 mM KCl, 10 mM Na_2HPO_4 , and 1.8 mM KH_2PO_4 . Cells were imaged with an upright Zeiss Axio Imager M2 microscope (Carl Zeiss, Oberkochen, Germany) equipped with a 506 monochrome camera and a 100 oil lens objective with a numerical aperture (NA) of 1.46.

Sample preparation for correlative light and cryo-electron tomography. *R. johrii* cells were lightly fixed using 2.5% paraformaldehyde in 30 mM phosphate buffer for 15 min, washed twice, and resuspended in 150 mM phosphate buffer. Bacterial cells were loaded onto Cu Finder R 2/2 EM grids (Electron Microscopy Sciences, Hatfield, PA), coated with 1 mg/ml of poly-L-lysine, and subsequently imaged at room temperature as described above. Following room temperature light microscopy, 20-nm colloidal gold particles (UMC Utrecht, Netherlands) were added and samples were plunge-frozen into liquid ethane-propane mix cooled at liquid nitrogen temperatures with a Mark IV Vitrobot (Thermo Fisher Scientific), maintained at room temperature and 70% humidity. Cryo-ET was conducted on cells with phase-bright signal as described below. For standalone cryo-ET experiments, samples were directly mixed with 20-nm colloidal gold particles, loaded onto glow-discharged carbon grids (R2/2; Quantifoil), and plunge-frozen as described above.

Cryo-ET data collection. For both standalone cryo-ET and CLEM experiments, tilt series were collected on a 300-kV Titan Krios transmission electron microscope (Thermo Fisher Scientific) equipped with a Falcon 2 camera. Tilt series were collected at nominal magnifications of 14,000 to 18,000, 1- to 3-degree oscillations, and a final dose of 30 to 150 e²/Å². Three-dimensional reconstructions were calculated with IMOD software package using the weighted back projection method (38).

Correlative LM and SEM with EDX analysis. *R. johrii* cells were fixed with 12.5% paraformaldehyde in 150 mM sodium phosphate buffer (73.6 mM K₂HPO₄, 26.4 mM KH₂PO₄; pH 7.5) and then washed three times with 150 mM sodium phosphate buffer (39). Glow-discharged Cu R2/2 grids were coated with poly-L-lysine hydrobromide solution (1 mg/ml) and dried for 30 min at 60°C. Fixed cells were loaded onto the grids and immediately imaged with LM in 1 PBS to identify phase-bright objects. The grids were subsequently air dried, and regions of interest identified with LM were examined with SEM using a JSM-7400F field emission scanning electron microscope (JEOL Ltd., Tokyo, Japan) operated at 5 kV without any coating. EDX analysis with a silicon drift detector (Octane, EDAX Inc., Mahwah, NJ) at 10 kV was used for semiquantitative elemental analysis of regions of interest.

Whole-cell lipidomic analysis of *R. johrii*. *R. johrii* cells displaying phase-bright properties were cultivated as described above, harvested by centrifugation (20 min at 5,000 rpm), and washed twice in sterile H₂O. Cell pellets were then lyophilized overnight and stored at room temperature for up to 7 days. *R. johrii* cultures grown in LB for 2 days and lacking phase-bright objects were chosen as the negative control. Sample normalization between samples of *R. johrii* expressing storage granules [R.j (1)] and *R. johrii* lacking storage granules [R.j (2)] was achieved by their culture weights. For R.j (1) samples, 4.0 mg of cells (wet weight) was used; for R.j (2) samples, 2.5 mg was used. The lipidomic results were normalized according to culture weights. For the whole-cell lipidomic analysis, a methyl tert-butyl ether (MTBE)-based membrane lipid extraction protocol was used, with modifications (40). Briefly, samples in 1.5-ml Eppendorf vials were first mixed with 300 μl of ice-cold methanol and 10-ml internal standards. The mixture was then sonicated in icewater bath for 15 min for protein precipitation. One milliliter of MTBE was added to the mixture, followed by vortex mixing for 20 min at room temperature for thorough lipid extraction. Next, 200 μl of liquid chromatography-mass spectrometry (LC-MS)-grade water was added to induce phase separation, and the samples were further mixed for 30 s. After settling for 10 min, the upper layer, containing the lipids, was transferred to new Eppendorf vials. To dry the lipid samples, the solvent was evaporated using a vacuum concentrator at 4°C. A total of 100 μl of isopropanol/acetonitrile (1:1, vol/vol) was added to reconstitute the dried residue. The reconstituted solution was vortexed for 30 s and centrifuged at 14,000 rpm at 4°C for 15 min. The resulting supernatants were transferred to glass inserts for LC-tandem MS (LC-MS/MS) analysis. Only lipids above the noise level (1,000 average intensity) were considered in the analysis. A cutoff value of at least 2 increase in average intensity and a P value threshold of 0.01 were used to determine significant increase in lipid species.

Heat inactivation and counting of endospores. After induction of the phase-bright objects in *R. johrii*, *S. marcescens*, and *B. subtilis* as described above, cells were washed with sterile, deionized water, spun at 10,000 g for 10 min, and resuspended in chilled water. Suspensions of *R. johrii* and *B. subtilis* were heated to 80°C, and *S. marcescens* to 60°C, for 15 min, 30 min, and 1 h, as described previously (16, 17). After the heat treatment, the samples were centrifuged for 10 min at 10,000 g. The pellets were washed five times to remove cellular debris and then plated onto solid media. *R. johrii* was incubated at 30°C for 7 days, *S. marcescens* was incubated at 32°C for 7 days, and *B. subtilis* was incubated at 37°C overnight, and plates were subsequently examined for viable growth.

DPA detection. Following the detection of phase-bright objects, dipicolinic acid (DPA) was detected as previously described (41). Briefly, 5-ml cultures of *R. johrii*, *S. marcescens*, and *B. subtilis* containing ;10 mg of cells (dry weight) were autoclaved for 15 min at 15 lb/in². The suspensions were cooled to ambient temperature, acidified with 0.1 ml of 1.0 N acetic acid, and incubated for 1 h to cluster the insoluble material. To remove cellular debris, the suspensions were centrifuged at 1,500 g for 10 min. To each 4 ml of supernatant, 1 ml of 1% Fe(NH₄)₂(SO₄)₂·6H₂O and 1% ascorbic acid in 0.5 M acetate buffer (pH 5.5) was added. Colorimetric shift at 440 nm was compared to a standard curve prepared with pure DPA (Sigma-Aldrich, Oakville, Canada).

Detection of genes required for endospore production. We assessed the genomes of *S. marcescens* subsp. *sakuensis* KRED^T and *Rhodobacter johrii* JA192—the two strains originally described by Giriya et al. and Ajithkumar et al., respectively (16, 17)—for endospore formation genes. Using the recently updated COGs database, we compiled a list of genes associated with sporulation (5, 42). Corresponding KEGG and TIGRFAM hidden Markov models (HMMs) were used to assess the genomes for the presence of these genes using HMMER 3.2.1 (<http://hmmmer.org/>) (43, 44). Genes without representative HMMs were identified using local alignment against sequences from *B. subtilis* 168 and *Clostridium perfringens* SM101 using a minimum

percent identity of 30% and an E value of $1E225$. *B. subtilis* 168 (monoderm sporulator), *Acetoneema longum* DSM 6540 (diderm sporulator), and *Escherichia coli* DSM 30083 (diderm nonsporulator) were included as sporulating and nonsporulating controls.

ACKNOWLEDGMENTS

We thank Kaustuv Basu at the Facility for Electron Microscopy Research (FEMR) of McGill University and Claire Atkinson at the High Resolution Macromolecular CryoElectron Microscopy Facility at the University of British Columbia for help with microscope operation and data collection.

Work in the EIT lab was supported by a Natural Sciences and Engineering
Research

REFERENCES

- Cano RJ, Borucki MK. 1995. Revival and identification of bacterial spores in 25- to 40-million-year-old Dominican amber. *Science* 268:1060–1064. <https://doi.org/10.1126/science.7538699>.
- Kennedy MJ, Reader SL, Swierczynski LM. 1994. Preservation records of microorganisms: evidence of the tenacity of life. *Microbiology* 140:2513–2529. <https://doi.org/10.1099/00221287-140-10-2513>.
- Vreeland RH, Rosenzweig WD, Powers DW. 2000. Isolation of a 250 million-year-old halotolerant bacterium from a primary salt crystal. *Nature* 407:897–900. <https://doi.org/10.1038/35038060>.
- Setlow P. 2007. I will survive: DNA protection in bacterial spores. *Trends Microbiol* 15:172–180. <https://doi.org/10.1016/j.tim.2007.02.004>.
- Galperin MY, Mekhedov SL, Puigbo P, Smirnov S, Wolf YI, Rigden DJ. 2012. Genomic determinants of sporulation in Bacilli and Clostridia: towards the minimal set of sporulation-specific genes. *Environ Microbiol* 14:2870–2890. <https://doi.org/10.1111/j.1462-2920.2012.02841.x>.
- Nicholson WL, Munakata N, Horneck G, Melosh HJ, Setlow P. 2000. Resistance of Bacillus endospores to extreme terrestrial and extraterrestrial environments. *Microbiol Mol Biol Rev* 64:548–572. <https://doi.org/10.1128/mmr.64.3.548-572.2000>.
- Vaksmann Z, Kaplan HB. 2015. Myxococcus xanthus growth, development, and isolation. *Curr Protoc Microbiol* 39:7A.1.1–7A.1.21. <https://doi.org/10.1002/9780471729259.mc07a01s39>.
- Qinyuan L, Xiu C, Yi J, Chenglin J. 2016. Morphological identification of actinobacteria. In Dharumadurai D, Yi J (ed), *Actinobacteria—basics and biotechnological applications*. IntechOpen, Rijeka, Croatia. <https://doi.org/10.5772/61461>.
- Bobek J, Šmidová K, Cihák M. 2017. A waking review: old and novel insights into the spore germination in Streptomyces. *Front Microbiol* 8:2205. <https://doi.org/10.3389/fmicb.2017.02205>.
- Tocheva EI, Ortega DR, Jensen GJ. 2016. Sporulation, bacterial cell envelopes and the origin of life. *Nat Rev Microbiol* 14:535–542. <https://doi.org/10.1038/nrmicro.2016.85>.
- Stragier P, Losick R. 1996. Molecular genetics of sporulation in Bacillus subtilis. *Annu Rev Genet* 30:297–341. <https://doi.org/10.1146/annurev.genet.30.1.297>.
- Piggot PJ, Hilbert DW. 2004. Sporulation of Bacillus subtilis. *Curr Opin Microbiol* 7:579–586. <https://doi.org/10.1016/j.mib.2004.10.001>.
- Errington J. 2003. Regulation of endospore formation in Bacillus subtilis. *Nat Rev Microbiol* 1:117–126. <https://doi.org/10.1038/nrmicro750>.
- Errington J. 1993. Bacillus subtilis sporulation: regulation of gene expression and control of morphogenesis. *Microbiol Rev* 57:1–33. <https://doi.org/10.1128/MR.57.1.1-33.1993>.
- Tocheva EI, Lopez-Garrido J, Hughes HV, Fredlund J, Kuru E, VannieuwenhzeMS, Brun YV, Pogliano K, Jensen GJ. 2013. Peptidoglycan transformations during Bacillus subtilis sporulation. *Mol Microbiol* 88:673–686. <https://doi.org/10.1111/mmi.12201>.
- Ajithkumar B, Ajithkumar VP, Iriye R, Doi Y, Sakai T. 2003. Spore-forming Serratia marcescens subsp. sakuensis subsp. nov., isolated from a domestic wastewater treatment tank. *Int J Syst Evol Microbiol* 53:253–258. <https://doi.org/10.1099/ijs.0.02158-0>.
- Girija KR, Sasikala C, Ramana CV, Sproer C, Takaichi S, Thiel V, Imhoff JF. 2010. Rhodobacter johrii sp. nov., an endospore-producing cryptic species isolated from semi-arid tropical soils. *Int J Syst Evol Microbiol* 60:2099–2107. <https://doi.org/10.1099/ijs.0.011718-0>.
- Galperin MY. 2013. Genome diversity of spore-forming Firmicutes. *Microbiol Spectr* 1:TBS-0015-2012. <https://doi.org/10.1128/microbiolspectrum.TBS-0015-2012>.
- Eichenberger P, Fujita M, Jensen ST, Conlon EM, Rudner DZ, Wang ST, Ferguson C, Haga K, Sato T, Liu JS, Losick R. 2004. The program of gene transcription for a single differentiating cell type during sporulation in Bacillus subtilis. *PLoS Biol* 2:e328. <https://doi.org/10.1371/journal.pbio.0020328>.
- Steil L, Serrano M, Henriques AO, Volker U. 2005. Genome-wide analysis of temporally regulated and compartment-specific gene expression in sporulating cells of Bacillus subtilis. *Microbiology (Reading)* 151:399–420. <https://doi.org/10.1099/mic.0.27493-0>.
- Hejazi A, Falkner FR. 1997. Serratia marcescens. *J Med Microbiol* 46:903–912. <https://doi.org/10.1099/00222615-46-11-903>.
- Wahl A, Schuth N, Pfeiffer D, Nussberger S, Jendrossek D. 2012. PHB granules are attached to the nucleoid via PhaM in Ralstonia eutropha. *BMC Microbiol* 12:262. <https://doi.org/10.1186/1471-2180-12-262>.
- Alvarez HM, Kalscheuer R, Steinbuechel A. 2000. Accumulation and mobilization of storage lipids by Rhodococcus opacus PD630 and Rhodococcus ruber NCIMB 40126. *Appl Microbiol Biotechnol* 54:218–223. <https://doi.org/10.1007/s002530000395>.
- Alvarez HM, Steinbuechel A. 2002. Triacylglycerols in prokaryotic microorganisms. *Appl Microbiol Biotechnol* 60:367–376. <https://doi.org/10.1007/s00253-002-1135-0>.
- Maurya RK, Bharti S, Krishnan MY. 2018. Triacylglycerols: fuelling the hibernating Mycobacterium tuberculosis. *Front Cell Infect Microbiol* 8:450. <https://doi.org/10.3389/fcimb.2018.00450>.
- Shabtai Y. 1991. Isolation and characterization of a lipolytic bacterium capable of growing in a low-water-content oil-water emulsion. *Appl Environ Microbiol* 57:1740–1745. <https://doi.org/10.1128/AEM.57.6.1740-1745.1991>.
- Santucci P, Johansen MD, Point V, Poncin I, Viljoen A, Cavalier JF, Kremer L, Canaan S. 2019. Nitrogen deprivation induces triacylglycerol accumulation, drug tolerance and hypervirulence in mycobacteria. *Sci Rep* 9:8667. <https://doi.org/10.1038/s41598-019-45164-5>.
- Shi L, Derouiche A, Pandit S, Rahimi S, Kalantari A, Futo M, Ravikumar V, JersC, Mokkaapati V, Vlahovicek K, Mijakovic I. 2020. Evolutionary analysis of the Bacillus subtilis genome reveals new genes involved in sporulation. *Mol Biol Evol* 37:1667–1678. <https://doi.org/10.1093/molbev/msaa035>.
- Veening JW, Murray H, Errington J. 2009. A mechanism for cell cycle regulation of sporulation initiation in Bacillus subtilis. *Genes Dev* 23:1959–1970. <https://doi.org/10.1101/gad.528209>.
- de Hoon MJ, Eichenberger P, Vitkup D. 2010. Hierarchical evolution of the bacterial sporulation network. *Curr Biol* 20:R735–R745. <https://doi.org/10.1016/j.cub.2010.06.031>.
- Dembek M, Barquist L, Boinett CJ, Cain AK, Mayho M, Lawley TD, Fairweather NF, Fagan RP. 2015. High-throughput analysis of gene essentiality and sporulation in Clostridium difficile. *mBio* 6:e02383-14. <https://doi.org/10.1128/mBio.02383-14>.

32. Rigden DJ, Galperin MY. 2008. Sequence analysis of GerM and SpoVS, uncharacterized bacterial “sporulation” proteins with widespread phylogenetic distribution. *Bioinformatics* 24:1793–1797. <https://doi.org/10.1093/bioinformatics/btn314>.
33. Onyenwoke RU, Brill JA, Farahi K, Wiegel J. 2004. Sporulation genes in members of the low G1C Gram-type-positive phylogenetic branch (Firmicutes). *Arch Microbiol* 182:182–192. <https://doi.org/10.1007/s00203-004-0696-y>.
34. Meeske AJ, Rodrigues CD, Brady J, Lim HC, Bernhardt TG, Rudner DZ. 2016. High-throughput genetic screens identify a large and diverse collection of new sporulation genes in *Bacillus subtilis*. *PLoS Biol* 14:e1002341. <https://doi.org/10.1371/journal.pbio.1002341>.
35. Abecasis AB, Serrano M, Alves R, Quintais L, Pereira-Leal JB, Henriques AO. 2013. A genomic signature and the identification of new sporulation genes. *J Bacteriol* 195:2101–2115. <https://doi.org/10.1128/JB.02110-12>.
36. Rodrigues CD, Henry X, Neumann E, Kurauskas V, Bellard L, Fichou Y, Schanda P, Schoehn G, Rudner DZ, Morlot C. 2016. A ring-shaped conduit connects the mother cell and forespore during sporulation in *Bacillus subtilis*. *Proc Natl Acad Sci U S A* 113:11585–11590. <https://doi.org/10.1073/pnas.1609604113>.
37. Paredes CJ, Alsaker KV, Papoutsakis ET. 2005. A comparative genomic view of clostridial sporulation and physiology. *Nat Rev Microbiol* 3:969–978. <https://doi.org/10.1038/nrmicro1288>.
38. Kremer JR, Mastrorade DN, McIntosh JR. 1996. Computer visualization of three-dimensional image data using IMOD. *J Struct Biol* 116:71–76. <https://doi.org/10.1006/jsbi.1996.0013>.
39. Gunsolus IL, Hu D, Mihai C, Lohse SE, Lee C-s, Torelli MD, Hamers RJ, Murphy CJ, Orr G, Haynes CL. 2014. Facile method to stain the bacterial cell surface for super-resolution fluorescence microscopy. *Analyst* 139:3174–3178. <https://doi.org/10.1039/c4an00574k>.
40. Matyash V, Liebisch G, Kurzchalia TV, Shevchenko A, Schwudke D. 2008. Lipid extraction by methyl-tert-butyl ether for high-throughput lipidomics. *J Lipid Res* 49:1137–1146. <https://doi.org/10.1194/jlr.D700041-JLR200>.
41. Janssen FW, Lund AJ, Anderson LE. 1958. Colorimetric assay for dipicolinic acid in bacterial spores. *Science* 127:26–27. <https://doi.org/10.1126/science.127.3288.26>.
42. Galperin MY, Wolf YI, Makarova KS, Vera Alvarez R, Landsman D, Koonin EV. 2020. COG database update: focus on microbial diversity, model organisms, and widespread pathogens. *Nucleic Acids Res* <https://doi.org/10.1093/nar/gkaa1018>.
43. Aramaki T, Blanc-Mathieu R, Endo H, Ohkubo K, Kanehisa M, Goto S, Ogata H. 2020. KofamKOALA: KEGG ortholog assignment based on profile HMM and adaptive score threshold. *Bioinformatics* 36:2251–2252. <https://doi.org/10.1093/bioinformatics/bt2859>.
44. Haft DH, Selengut JD, White O. 2003. The TIGRFAMs database of protein families. *Nucleic Acids Res* 31:371–373. <https://doi.org/10.1093/nar/gkg128>.